EVALUATION OF A LOW REYNOLDS NUMBER CORRECTION TO THE $K - \epsilon$ TWO EQUATION COMPRESSIBLE TURBULENCE MODEL
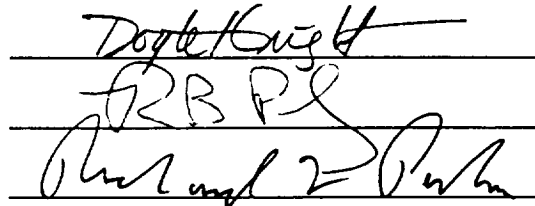
BY ROBERT J. BECHT

A thesis submitted to the

Graduate School—New Brunswick

Rutgers, The State University of New Jersey

in partial fulfillment of the requirements

for the degree of

Master of Science

Graduate Program in Mechanical and Aerospace Engineering

Written under the direction of

Dr. Doyle D. Knight

and approved by

New Brunswick, New Jersey

January, 1995

ABSTRACT OF THE THESIS

Evaluation of a Low Reynolds Number Correction to the $k - \epsilon$ Two Equation Compressible Turbulence Model

by Robert J. Becht, M.S.

Thesis Director: Dr. Doyle D. Knight

The objective of the current research is the development of an improved $k - \epsilon$ two-equation compressible turbulence model for turbulent boundary layer flows experiencing strong viscous-inviscid interactions. The development of an improved model is important in the design of hypersonic vehicles such as the National Aerospace Plane (NASP) and the High Speed Civil Transport (HSCT).

Improvements have been made to the low Reynolds number functions in the eddy viscosity and dissipation of solenoidal dissipation of the $k - \epsilon$ turbulence model. These corrections offer easily applicable modifications that may be utilized for more complex geometries. The low Reynolds number corrections are functions of the turbulent Reynolds number and are therefore independent of the coordinate system. The proposed model offers advantages over some current models which are based upon the physical distance from the wall, modify the constants of the standard model or make more corrections than are necessary to the governing equations.

The code has been developed to solve the Favre averaged, boundary layer equations for mass, momentum, energy, turbulence kinetic energy, and dissipation of solenoidal dissipation using Keller's box scheme and the Newton spatial marching method. The code has been validated by removing the turbulent terms and comparing the solution

with the Blasius solution; and by comparing the turbulent solution with an existing $k - \epsilon$ model code using wall function boundary conditions. Excellent agreement is seen between the computed solution and the Blasius solution, and between the two codes.

The model has been tested for both subsonic and supersonic flat-plate turbulent boundary layer flow by comparing the computed skin friction with the Van Driest II theory, and the experimental data of Weighardt; by comparing the transformed velocity profile with the data of Weighardt, and the Law of the Wall and the Law of the Wake; and by comparing the computed results of an adverse pressure gradient with the experimental data of Fernando and Smits. Good agreement is obtained with the experimental correlations for all flow conditions.

Acknowledgements

I would like to express my sincere and deep appreciation to Dr. Doyle D. Knight, my academic advisor, for his concern, guidance, patience, and most especially his encouragement during the course of this work and my graduate studies. I also want to thank Dr. Richard Pelz and Dr. Richard Peskin, my thesis committee members, for their review of this work.

I am very gratefull to my officemates, Pushkar, Hin, Mariana, Fred, Gecheng, and Vijay for their support, expertise and good nature; and their combined ability to make my studies as enjoyable as possible.

I thank the department staff Ann Cunningham and Dawn Deto for being able to solve almost any problem brought on by the Rutgers bureaucracy. I would also like to thank the technical support staff Rick Thomas and Bill Kish for their support and help, especially for keeping the computers in D115A operational.

Very special thanks go to my friends, both in school and out of school, who maintained confidence in my abilities even when I was not sure myself. If it were not for their encouragement this effort would not have been possible.

Dedication

This document and the work contained within is dedicated to my wife, Kristin Becht. Without her support, patience and understanding this work would not have been possible. If the encouragement she has shown me towards this effort is any indication of the support to be received in my future career, there will be no obstacles I will be unable to overcome, nor any task that I will be unable to accomplish.

Table of Contents

List of Tables

List of Figures

List of Abbreviations

Roman Characters

A	Adiabatic Term in the Van Driest Velocity Transformation
a	Derivative of ϵ_v with Respect to y
B	Additive Constant in the Law of the Wall Heat Transfer Term in the Van Driest Velocity Transformation
B_j^n	Numerical Diffusion of k
C_f	Skin Friction Based on Edge Velocity, $\frac{\tau_{wall}}{\frac{1}{2}\rho_e U_e^2}$
$C_{f\infty}$	Skin Friction Based on Conditions at ∞, $\frac{\tau_{wall}}{\frac{1}{2}\rho_\infty U_\infty^2}$
C_h	Heat Transfer Coefficient
C_y	Grid Stretching Parameter
b	Derivative of q with Respect to y
c	Derivative of T with Respect to y
$C_{\epsilon 1}$	Constant in the Production of ϵ_v
$C_{\epsilon 2}$	Constant in the Dissipation of ϵ_v
$C_{\epsilon 3}$	Constant in Low Reynolds Number Correction to D_{ϵ_v}
C_μ	Constant in Turbulent Eddy Viscosity
C_p	Specific Heat at Constant Pressure
C_v	Specific Heat at Constant Volume
D_k	Dissipation of k
D_{ϵ_v}	Dissipation of ϵ_v
Di_k	Diffusion of k
Di_{ϵ_v}	Diffusion of ϵ_v
e	Total Energy per Unit Mass
$\vec{F}$	System of Governing Equations

f_2	Low Reynolds Number Correction to D_{ϵ_v}
f_μ	Low Reynolds Number Correction to the Eddy Viscosity
h	Derivative of u with Respect to y
$\vec{J}$	Jacobian
j	Grid Point Perpendicular to the Plate
$jsbegin$	Grid Number to Begin Stretching
$jsend$	Grid Number to End Stretching
jl	Number of Grid Points in the Computational Domain
k	Turbulent Kinetic Energy
$kiso$	Control Parameter for Determination of BC on T at the Wall
$kvvel$	Control Parameter for Determination of BC on v at $j = 1$
$kwall$	Control Parameter for Determination of BC at $j = 1$
$kgrad$	Control Parameter for Determination of BC at e
l_{mfp}	Molecular Mean Free Path
l_{mix}	Mixing Length
M	Local Mach Number
M_∞	Mach Number at ∞
M_t	Turbulent Mach Number, $\sqrt{2k^2/\sqrt{\gamma R T}}$
n	Grid Point Parallel to the Plate
p	Pressure
P_k	Production of k
P_{ϵ_v}	Production of ϵ_v
Pr	Molecular Prandtl Number
Pr_T	Turbulent Prandtl Number
Q	Molecular Heat Flux
Q_{wall}	Heat Flux at the Wall
q	Square Root of k
R	Gas Constant
R_t	Turbulent Reynolds Number, $R_t = \rho k^2/\mu\epsilon$

Re_{δ_o}	Reynolds Number Based on Initial Boundary Layer Height, $Re_{\delta_o} = \rho_\infty U_\infty \delta_o / \mu_\infty$
Re_θ	Reynolds Number Based on Momentum Thickness, $Re_\theta = \rho_e U_e \theta / \mu_e$
Re_ψ	Reynolds Number Based on Displacement Thickness, $Re_\psi = \rho_e U_e \psi / \mu_e$
T	Local Temperature
T_0	Total Temperature
T_{ref}	Reference Temperature in Sutherland's Law
T_s	Static Temperature
t	time
U	Specified u Velocity
u	Velocity Parallel to the Plate
u_i	Velocity Vector in Einstein Notation
u_τ	Friction Velocity, $\sqrt{\frac{\tau_{wall}}{\rho_{wall}}}$
u^+	u-Velocity Non-dimensionalized by u_τ
v	Velocity Perpendicular to the Plate
v_{mix}	Mixing Velocity
v_{th}	Molecular Thermal Velocity
$\vec{w}$	Vector of Unknown Independent Variables
x	Direction Parallel to the Plate and Bulk Flow
y	Direction Perpendicular to the Plate and Bulk Flow
z	Direction Parallel to the Plate and Perpendicular to the Bulk Flow

Greek Characters

α_j^n	Ratio of Grid Spacing
β	Pressure Gradient Term
γ	Ratio of Specific Heats
Δy_j	Grid Spacing Perpendicular to the Plate
Δx^n	Grid Spacing Parallel to the Plate
δ	Local Boundary Layer Height as Defined in Chapter 4
δ_o	Initial Boundary Layer Height

δ_{ik}	Kronecker Delta
$\delta \vec{w}^i$	Increment for Newton's Method
ϵ	Total Dissipation of k
ϵ_d	Dilatational Dissipation of k
ϵ_v	Solenoidal Dissipation of k
η	Variable Transformation for Blasius Solution, Levy-Lees Grid Transformation for y
θ	Momentum Thickness, $\int_0^\delta \frac{\rho u}{\rho_e U_e}(1 - \frac{u}{U_e})dy$
κ	Karman Constant
μ	Molecular Viscosity
μ_T	Turbulent Eddy Viscosity
ν	Molecular Kinematic Viscosity
ψ	Displacement Thickness, $\int_0^\delta (1 - \frac{\rho u}{\rho_e U_e})dy$
Π	Wake Strength Parameter in the Law of the Wake
ρ	Density
σ_ϵ	Turbulent Schmidt Number for ϵ_v
σ_k	Turbulent Schmidt Number for k
τ_{ik}	Viscous Stress Tensor
τ_{xy}	Shear Stress
τ_{wall}	Wall Shear Stress
ξ	Levy-Lees Grid Transformation for x
ω	Vorticity

Superscripts

$+$	Viscous Sublayer Scaled Parameter
$*$	Dimensional Parameter
$\tilde{}$	Favre Averaged Quantity
$\bar{}$	Reynolds Averaged Quantity
$''$	Favre Fluctuating Quantity
$'$	Reynolds Fluctuating Quantity

i	Iteration Number
$molec$	Molecular Quantity
n	Node Location in x Direction
$turb$	Turbulent Quantity

Subscripts

∞	Parameter Evaluated at ∞
0	Stagnation Value
e	Parameter Evaluated at the Edge of the Boundary Layer
end	Conditions at the End of the Numerical Calculation
i, j, k	Component in i, j, k Directions for Einstein Notation
j	Node Location in y Direction
$wall$	Parameter Evaluated at the Wall

Chapter 1

INTRODUCTION

1.1 Motivation

The standard equations governing fluid motion are the conservation of mass, conservation of momentum and conservation of energy. However, it is widely known that there exist only a few conditions under which these equations may be analytically solved. The majority of other fluid flow cases need to either be determined experimentally or solved computationally. The advent of supersonic aircraft and the corresponding expense of wind tunnel testing has made computational fluid dynamics the desirable first step in design, and in the case of high hypersonic aircraft often the only viable option.

There are limitations associated with the computational methods of solving the equations of motion. These manifest themselves as limitations on computer resources and the physics of the fluid flow problem. Limitations on computer resources include computer memory and execution time. The advent of larger and faster computers, such as the Cray C-90 and massively parallel machines, has increased the domain of computational effectiveness, but has yet to encompass the entire spectrum of fluid flow problems. These include typical fluid flow problems dealing with aircraft design. The majority of aircraft flow design problems deal with motion that is turbulent in nature. Turbulent flow problems have historically proven the most demanding and difficult to solve and until recently solutions were almost entirely dependent upon experimental correlations.

The complex nature of turbulent flow, due its chaotic behavior and the multitude of scales and frequencies present, has made its analytical solution impossible and its computational solution extremely difficult. Because of the limitations associated with current computers it requires more than simply discretizing the quations of motion to

computationally solve these problems. An attempt to numerically solve the equations of motion, for the range of practical problems, in an exact sense for all frequencies and length scales inherent in the problem requires more computer resource than are available with current supercomputers. To solve this problem the equations of motion are not solved exactly, but are solved in an average sense, with assumptions being made about certain length scales. This averaging is termed Reynolds averaging. By averaging the Navier Stokes equations a closure problem results with the formation of the Reynolds stress tensor. In 1972 Jones and Launder proposed the $k - \epsilon$ two equation closure model [20], [21] for the Reynolds stress based upon the eddy viscosity introduced in the Boussinesq approximation [42]. This model relates the turbulence length scales to the turbulence kinetic energy and the dissipation of turbulence kinetic energy. It must be emphasized that Jones' and Launder's solution to the Reynolds averaged Navier Stokes equations is only a model and is not exact.

Since its inception there have been numerous changes to Jones' and Launder's original model [5], [9], [13], [15], [33], [34], [38], [40], [47], [49], [55] and [57]. These have primarily taken the form of modifications to the low Reynolds number correction and boundary conditions needed to accurately predict the fluid flow in the viscous sublayer of wall bounded flows. Typically these models have incorporated complicated damping functions for modifying the eddy viscosity, the production of solenoidal dissipation and the dissipation of solenoidal dissipation; have made these corrections dependent upon the physical distance from the wall; and have employed *ad hoc* boundary conditions at the wall for the solenoidal dissipation. The current research attempts to undertake a more fundamental examination of the low Reynolds number modifications that need to be employed when integrating through the viscous sublayer.

1.2 $k - \epsilon$ Two Equation Turbulence Modeling

Algebraic, one equation and two equation turbulence models usually utilize the Boussinesq approximation in modeling the Reynolds stress. In analogy to the molecular theory of gases the Reynolds stress is modeled by a mixing coefficient times the gradient of the velocity [42]. This mixing coefficient is termed the eddy viscosity. In 1925 Prandtl took

the Boussinesq approximation one step further when he postulated his mixing length theory [51].

Assuming two dimensional, shear flow and a Newtonian fluid the molecular shear stress may be approximated by a known coefficient, μ, times the derivative of the velocity

$$\tau_{xy}^{molec} = \mu \frac{du}{dy} \tag{1.1}$$

where the molecular viscosity is defined by

$$\mu = \frac{1}{2} \rho v_{th} l_{mfp} \tag{1.2}$$

v_{th} is the average molecular velocity and l_{mfp} is the mean free path of the molecules. Using this analogy the Boussinesq approximation says that

$$\tau_{xy}^{turb} = \mu_T \frac{d\bar{u}}{dy} \tag{1.3}$$

where $\bar{u}$ is the mean velocity and the eddy viscosity is defined by

$$\mu_T = C_1 v_{mix} l_{mix} \tag{1.4}$$

In Prandtl's mixing length theory v_{mix} and l_{mix} replace v_{th} and l_{mfp} respectively in the molecular theory of gases [54]. v_{mix} is the characteristic velocity of the turbulence and l_{mix} is the characteristic length scale of the turbulence. However, unlike v_{th} and l_{mfp} which are properties of the fluid, v_{mix} and l_{mix} are properties of the flow and are not known a priori. v_{mix} and l_{mix} typically vary greatly within the flow field. Using a momentum transport analysis Prandtl further hypothesized that v_{mix} is a function of the mixing length and the gradient of the mean velocity

$$v_{mix} = l_{mix} \frac{d\bar{u}}{dy} \tag{1.5}$$

Utilizing this approximation it is sufficient to close the system of governing equations if l_{mix} can be specified. Algebraic models specify l_{mix} as a function of the type of flow begin examined. For wake flow and wall bounded flows l_{mix} will be different. This limits the applicability of algebraic models, especially for three dimensional, complex flows in which more than one type of flow is encountered.

Unlike algebraic turbulence models, two equation turbulence models are developed such that they are independent of the flow geometry being examined. This has the advantage of being applicable over a wider range of geometrical configurations. The $k - \epsilon$ model works by specifying v_{mix} and l_{mix}. The characteristic velocity scale of the turbulence is based on the assumption that it is related to the turbulent kinetic energy, k,

$$k = \frac{1}{2}\overline{(u'^2 + v'^2 + w'^2)} \tag{1.6}$$

where $'$ denotes the turbulent fluctuations from the mean and $^-$ denotes Reynolds averaging. The mixing velocity is taken to be equal to $\sqrt{k}$. This leaves the mixing length to be specified. It is necessary to formulate the mixing length based upon the physics of the flow. To do this the mixing length is related to the turbulence kinetic energy and the rate of dissipation of turbulence kinetic energy. Purely on dimensional grounds this yields

$$l_{mix} \sim \frac{k^{\frac{3}{2}}}{\epsilon} \tag{1.7}$$

where ϵ is the rate of dissipation of turbulence kinetic energy. Therefore in the standard $k - \epsilon$ model the eddy viscosity is specified by

$$\mu_T = \frac{\rho C_\mu k^2}{\epsilon} \tag{1.8}$$

and the system is closed, provided equations are known for k and ϵ. The model proposed by Jones and Launder [20], [21] provides approximate equations for k and ϵ such that the system is closed. These equations and the closure coefficients proposed by Launder and Spalding [35] make up the standard $k - \epsilon$ turbulence model.

1.3 Present Research

The ability of the standard $k - \epsilon$ turbulence model to handle all types of fluid flow problems is limited. The standard model cannot be integrated fully to the surface, requiring the use of wall function boundary conditions which are not universally applicable (See Chapter 2). To extend the $k - \epsilon$ model to the surface, modifications need to be made to the governing equations through damping functions that only become

important in regions near a solid surface. These modifications are termed low Reynolds number corrections.

The objective of the current research is the development of a low Reynolds correction that is as simple as possible and which may easily be applied to more complicated, three dimensional flows. To keep the model simple the fewest number of modifications are made to the governing equations. Speziale *et al* have shown that it is sufficient to modify only the eddy viscosity and the dissipation of solenoidal dissipation terms in the governing equations [47]. For this reason, the current model only modifies these terms. For applicability to more complex geometries, it is necessary that the corrections be independent of the coordinate system. Many models utilize the physical distance from the wall and the wall friction velocity in defining the low Reynolds number modification. Such models may have problems; for example, in the vicinity of a corner where the distance from the wall may be defined by two independent surfaces; or in a two dimensional flow where the friction velocity is zero at separation. The current model assumes the low Reynolds number modifications are functions of the turbulent Reynolds number, $R_t = \rho k^2/\mu\epsilon$, thereby avoiding the problems associated with employing the physical distance from the wall and the friction velocity. Many models also utilize *ad hoc* boundary conditions for the dissipation rate or introduce a pseudo-dissipation rate for numerical reasons. It is found that this is not necessary and the physical boundary condition for the dissipation may be employed.

In summary, the current model avoids many of the limitations of previous models in that it makes as few modifications to the governing equations as are required, makes these corrections functions of the flow properties, and properly implements the boundary condition for the dissipation.

Chapter 2

GOVERNING EQUATIONS

2.1 Equations Governing Mass, Momentum and Energy

The instantaneous equations governing fluid motion in Einstein notation are given as:

- **Conservation of Mass (Continuity)**

$$\frac{\partial \rho}{\partial t} + \frac{\partial(\rho u_k)}{\partial x_k} = 0 \tag{2.1}$$

- **Conservation of Momentum**

$$\frac{\partial(\rho u_k)}{\partial t} + \frac{\partial(\rho u_i u_k)}{\partial x_k} = -\frac{\partial p}{\partial x_i} + \frac{\partial(\tau_{ik})}{\partial x_k} \tag{2.2}$$

- **Conservation of Energy**

$$\frac{\partial(\rho e)}{\partial t} + \frac{\partial[u_k(\rho e + p)]}{\partial x_k} = -\frac{\partial Q_k}{\partial x_k} + \frac{\partial(u_i \tau_{ik})}{\partial x_k} \tag{2.3}$$

where the equations are written in dimensional form.

However, as already stated, it is currently impossible to solve these equations numerically for most turbulent flow applications. Therefore these equations are not solved instantaneously, but are solved in an average sense utilizing Favre and Reynolds averaging. This is accomplished by introducing mass averaged and ensemble averaged variables in place of the instantaneous variables and then averaging the equations of motion. The ensemble average is defined as:

$$\bar{f} = \lim_{n \to \infty} \frac{1}{n} \sum_{i=1}^{n} f_i \tag{2.4}$$

and the mass average is defined as the density weighted ensemble average:

$$\tilde{f} = \frac{1}{\bar{\rho}} \lim_{n \to \infty} \frac{1}{n} \sum_{i=1}^{n} (\rho f_i) \tag{2.5}$$

The f_i are the individual realizations of the variable $f(x_i, t)$. The dependent variables may now be written as the sum of an average part and a fluctuating part. For mass averaging this is written as:

$$f = \tilde{f} + f''$$ (2.6)

and for ensemble averaging it is written as:

$$f = \bar{f} + f'$$ (2.7)

where $''$ and $'$ represent the fluctuating variables in the mass-averaged and unweighted expansions respectively.

If the sum of the average and fluctuating parts of the instantaneous variables are substituted into equations 2.1 - 2.3 and the equations are averaged, the resulting system are the Reynolds mass averaged conservation equations of mass, momentum, and energy:

- **Reynolds Averaged Conservation of Mass**

$$\frac{\partial \bar{\rho}}{\partial t} + \frac{\partial (\bar{\rho} \tilde{u}_k)}{\partial x_k} = 0$$ (2.8)

- **Reynolds Averaged Conservation of Momentum**

$$\frac{\partial (\bar{\rho} \tilde{u}_k)}{\partial t} + \frac{\partial (\bar{\rho} \tilde{u}_i \tilde{u}_k)}{\partial x_k} = -\frac{\partial \bar{p}}{\partial x_i} + \frac{\partial_k (-\overline{\rho u_i'' u_k''} + \bar{\tau}_{ik})}{\partial x_k}$$ (2.9)

- **Reynolds Averaged Conservation of Energy**

$$\frac{\partial (\bar{\rho} \tilde{e})}{\partial t} + \frac{\partial [\tilde{u}_k (\bar{\rho} \tilde{e} + \bar{p})]}{\partial x_k} = \frac{\partial (C_p \overline{\rho T'' u_k''} - \bar{Q}_k)}{\partial x_k} +$$
$$\frac{\partial}{\partial x_k} \left(-\overline{\rho u_j'' u_k'' \tilde{u}_j} - \frac{1}{2} \overline{\rho u_j'' u_j'' u_k''} + \overline{\tilde{u}_j \bar{\tau}_{jk}} + \overline{u_j'' \tau_{jk}} \right)$$ (2.10)

In equations 2.8 - 2.10, $\bar{\rho}$ is the mean density, $\tilde{u}_k$ is the mass-averaged velocity, $\bar{p}$ is the mean pressure, and $\tilde{e}$ is the mass-averaged total energy per unit mass given by:

$$\tilde{e} = C_v \tilde{T} + \frac{1}{2} \tilde{u}_k \tilde{u}_k + \tilde{k}$$ (2.11)

where C_v is the specific heat at constant volume and $\tilde{k}$ is the mass-averaged turbulent kinetic energy defined by:

$$\bar{\rho} \tilde{k} = \frac{1}{2} \overline{\rho u_k'' u_k''}$$ (2.12)

In order to close the system of equations defined by 2.8-2.10 it is necessary to specify expressions for the mass-averaged Reynolds stress, $\overline{\rho u_i'' u_k''}$, and the molecular viscous stress, $\bar{\tau}_{ik}$, in the Reynolds averaged conservation of momentum equation 2.9; and expressions for the molecular heat flux, $\bar{Q}_k$, the turbulent heat flux, $C_p \overline{\rho T'' u_k''}$, the triple velocity-density correlation, $\frac{1}{2} \overline{\rho u_j'' u_j'' u_k''}$, and the velocity-molecular shear stress correlation, $\overline{u_j'' \tau_{jk}}$, in the mean energy equation 2.10.

The molecular viscous stress, $\bar{\tau}_{ik}$, is approximated by assuming a Newtonian fluid

$$\bar{\tau}_{ik} = \tilde{\mu}\left(\frac{\partial \tilde{u}_k}{\partial x_i} + \frac{\partial \tilde{u}_i}{\partial x_k}\right) - \frac{2}{3}\tilde{\mu}\frac{\partial \tilde{u}_j}{\partial x_j}\delta_{ik} \tag{2.13}$$

where $\tilde{\mu} = \tilde{\mu}(\tilde{T})$ is the molecular dynamic viscosity as function of the mass-averaged temperature, approximated by Sutherlands law [4]

$$\frac{\tilde{\mu}}{\mu_\infty} = \left(\frac{\tilde{T}}{T_\infty}\right)^{\frac{3}{2}} \frac{T_\infty + T_{ref}}{\tilde{T} + T_{ref}} \tag{2.14}$$

T_{ref} is the reference temperature given for air as $198.6°R$.

The molecular heat flux, $\bar{Q}_k$, is approximated by assuming the Fourier heat law

$$\bar{Q}_k = -\frac{C_p\tilde{\mu}}{Pr}\frac{\partial \tilde{T}}{\partial x_k} \tag{2.15}$$

where Pr is the molecular Prandtl number and C_p is the specific heat at constant pressure.

2.2 Standard $k - \epsilon$ Model

Expressions need to be found for the remaining terms in equations 2.9 and 2.10. This is the classical problem of closure associated with solving turbulent flow problems. The current research utilizes the $k - \epsilon$ two equation turbulence model to close the equations of motion. The $k - \epsilon$ model is calibrated not only for wall bounded flows, but also for free shear flows. In order to assure acceptable agreement in those regions where the low Reynolds number modification is not required, it is necessary to utilize those model constants which have been shown and accepted to accurately predict this type of flow behavior. For this reason the standard $k - \epsilon$ model coefficients as given by Launder and Spalding [35] are used.

The standard $k - \epsilon$ model and nearly all two equation models utilize the Boussinesq approximation to approximate the Reynolds stress. In analogy to the kinetic theory of gases the Reynolds stress is approximated by an eddy viscosity that is dependent upon the characteristic lengths of the turbulence. An approximation to the Reynolds stress is therefore given as:

$$- \overline{\rho u_i'' u_k''} = \mu_T \left(\frac{\partial \tilde{u}_k}{\partial x_i} + \frac{\partial \tilde{u}_i}{\partial x_k} - \frac{2}{3} \frac{\partial \tilde{u}_j}{\partial x_j} \delta_{ik} \right) - \frac{2}{3} \bar{\rho} \tilde{k} \delta_{ik} \qquad (2.16)$$

where δ_{ik} is the kronecker delta function and μ_T is the eddy viscosity defined for the $k - \epsilon$ model as

$$\mu_T = \bar{\rho} C_\mu \frac{\tilde{k}^2}{\tilde{\epsilon}} \qquad (2.17)$$

C_μ is a closure coefficient and $\tilde{\epsilon}$ is the rate of dissipation of turbulent kinetic energy defined as

$$\bar{\rho}\tilde{\epsilon} \equiv \overline{\tau_{ik} \frac{\partial u_i''}{\partial x_k}} \qquad (2.18)$$

In analogy to the molecular transport of heat the turbulent heat flux, $-C_p \overline{\rho T'' u_k''}$, is modeled according to

$$C_p \overline{\rho T'' u_k''} = \frac{C_p \mu_T}{Pr_T} \frac{\partial \tilde{T}}{\partial x_k} \qquad (2.19)$$

where Pr_T is the turbulent Prandtl number.

The triple velocity-density correlation, $\frac{1}{2} \overline{\rho u_j'' u_j'' u_k''}$, appearing in the energy equation 2.10 is small compared to $\overline{\rho u_j'' u_k''} \tilde{u}_j$ and maybe ignored [25]. The velocity-molecular shear correlation, $\overline{u_j'' \tau_{jk}}$, appearing in equation 2.10 is also small and may also be ignored [25]. These approximations may be carried into the supersonic range, but lose their validity if they are carried into the hypersonic range [54].

The introduction of the eddy viscosity into the equations of motion has added two more unknowns to the system, $\tilde{k}$ and $\tilde{\epsilon}$. This necessitates including two more equations of motion. The first is the equation for the transport of turbulence kinetic energy, equation 2.20, and the second is the equation for the transport of solenoidal dissipation, equation 2.24. Utilizing the standard $k - \epsilon$ model approximations these equations are

- **Transport of Turbulence Kinetic Energy**

$$\frac{\partial \bar{\rho}\tilde{k}}{\partial t} + \frac{\partial \bar{\rho}\tilde{k}\tilde{u}_k}{\partial x_k} = - \overline{\rho u_j'' u_k''}\frac{\partial \tilde{u}_j}{\partial x_k}$$

$$+ \frac{\partial}{\partial x_k}\left[\frac{\mu_T}{\bar{\rho}\sigma_k}\frac{\partial(\bar{\rho}\tilde{k})}{\partial x_k} + \tilde{\mu}\frac{\partial \tilde{k}}{\partial x_k}\right]$$

$$- \bar{\rho}\tilde{\epsilon} \tag{2.20}$$

where the production of turbulent kinetic energy is defined by;

$$P_k \equiv -\overline{\rho u_j'' u_k''}\frac{\partial \tilde{u}_j}{\partial x_k} \tag{2.21}$$

the dissipation of turbulent kinetic energy is defined by;

$$D_k \equiv -\bar{\rho}\tilde{\epsilon} \tag{2.22}$$

and the diffusion of turbulent kinetic energy is defined by

$$Di_k \equiv \frac{\partial}{\partial x_k}\left[\frac{\mu_T}{\bar{\rho}\sigma_k}\frac{\partial(\bar{\rho}\tilde{k})}{\partial x_k} + \tilde{\mu}\frac{\partial \tilde{k}}{\partial x_k}\right] \tag{2.23}$$

- **Transport of Solenoidal Dissipation**

$$\frac{\partial \bar{\rho}\tilde{\epsilon}_v}{\partial t} + \frac{\partial \bar{\rho}\tilde{u}_k\tilde{\epsilon}_v}{\partial x_k} = -C_{\epsilon 1}\frac{\tilde{\epsilon}_v}{\tilde{k}}\overline{\rho u_j'' u_k''}\frac{\partial \tilde{u}_j}{\partial x_k} - C_{\epsilon 2}\bar{\rho}\frac{\tilde{\epsilon}_v^2}{\tilde{k}} + \frac{\partial}{\partial x_k}\left[\left(\frac{\mu_T}{\sigma_\epsilon} + \tilde{\mu}\right)\frac{\partial \tilde{\epsilon}_v}{\partial x_k}\right] \tag{2.24}$$

where the production of dissipation is defined by;

$$P_{\epsilon_v} \equiv -C_{\epsilon 1}\frac{\tilde{\epsilon}_v}{\tilde{k}}\overline{\rho u_j'' u_k''}\frac{\partial \tilde{u}_j}{\partial x_k} \tag{2.25}$$

the dissipation of dissipation is defined by;

$$D_{\epsilon_v} \equiv -C_{\epsilon 2}\bar{\rho}\frac{\tilde{\epsilon}_v^2}{\tilde{k}} \tag{2.26}$$

and the diffusion of dissipation is defined by;

$$Di_{\epsilon_v} \equiv \frac{\partial}{\partial x_k}\left[\left(\frac{\mu_T}{\sigma_\epsilon} + \tilde{\mu}\right)\frac{\partial \tilde{\epsilon}_v}{\partial x_k}\right] \tag{2.27}$$

In the above equations σ_k, σ_ϵ, $C_{\epsilon 1}$, and $C_{\epsilon 2}$ are closure coefficients found by correlating with results from different flows [54].

The transport of solenoidal dissipation is not necessarily equivalent to the transport of dissipation. The total dissipation, $\tilde{\epsilon}$, is comprised of two parts; (1) the solenoidal dissipation, $\tilde{\epsilon}_v$, and (2) the dilatational dissipation, $\tilde{\epsilon}_d$, such that

$$\tilde{\epsilon} = \tilde{\epsilon}_v + \tilde{\epsilon}_d \tag{2.28}$$

The solenoidal dissipation is that part of the dissipation that is associated with vorticity fluctuations

$$\bar{\rho}\tilde{\epsilon}_v = 2\bar{\nu}\overline{\rho(\omega_i'')^2} \tag{2.29}$$

and the dilatational dissipation is the part of the dissipation that for high Reynolds number, inhomogenous turbulence may be approximated by the divergence of the fluctuating velocity

$$\bar{\rho}\tilde{\epsilon}_d = \frac{4}{3}\bar{\nu}\rho\overline{\left(\frac{\partial u_i''}{\partial x_i}\right)^2} \tag{2.30}$$

which is only present in compressible flows [54].

To account for the dilatational dissipation, corrections have been proposed by Sarkar et al [41] and Zeman [56]. These corrections postulate that the dilatational dissipation may be modeled as a function of the solenoidal dissipation and the turbulent Mach number:

$$\tilde{\epsilon}_d = C_k F(\tilde{\epsilon}_v, M_t) \tag{2.31}$$

where

$$M_t = \sqrt{\frac{2\bar{\rho}\tilde{k}}{\gamma R\tilde{T}}} \tag{2.32}$$

The corrections proposed by Sarkar and Zeman were first calibrated for compressible mixing layers and their application to compressible wall bounded flows is suspect as shown by Huang et al [17]. It was found by Huang et al that the baseline $k - \epsilon$ model behaves better in predicting the compressible Law of the Wall than models which incorporate the corrections of Sarkar or Zeman. For this reason they are not tested, although the code has been constructed with the Sarkar formulation built in. This formulation assumes the total dissipation to be a function of the solenoidal dissipation and turbulent Mach number as seen in equation 2.33.

$$\tilde{\epsilon} = \tilde{\epsilon}_v\left(1 + C_k M_t^2\right) \tag{2.33}$$

All cases currently run assume $C_k = 0$ making $\check{\epsilon} = \check{\epsilon}_v$. For the cases examined the maximum of the turbulence Mach number is .09. This corresponds to the dilatational dissipation being less than 9% of the solenoidal dissipation everywhere.

To close the system of equations an equation of state needs to be specified. This equation is the ideal gas law

$$\bar{p} = \bar{\rho}R\tilde{T} \tag{2.34}$$

where R is the gas constant given for air as $1716 \ ft^2/(s^{2\circ}R)$.

2.3 Boundary Layer Approximations

The model proposed is validated and tested for steady flow over a flat plate at varying Mach numbers and pressure gradients. Because of the geometry of the flow high Reynolds number boundary layer approximations are made to the governing equations 2.8 - 2.24, yielding equations 2.35 - 2.43.

- **Continuity**

$$\frac{\partial \bar{\rho}\tilde{u}}{\partial x} + \frac{\partial \bar{\rho}\tilde{v}}{\partial y} = 0 \tag{2.35}$$

- **x-Momentum**

$$\bar{\rho}\tilde{u}\frac{\partial \tilde{u}}{\partial x} + \bar{\rho}\tilde{v}\frac{\partial \tilde{u}}{\partial y} = -\frac{\partial \bar{p}}{\partial x} + \frac{\partial}{\partial y}\left[(\mu_T + \bar{\mu})\frac{\partial \tilde{u}}{\partial y}\right] \tag{2.36}$$

where the eddy viscosity is

$$\mu_T = \frac{\bar{\rho}C_\mu \tilde{k}^2}{\tilde{\epsilon}} \tag{2.37}$$

and the pressure gradient is

$$\frac{\partial \bar{p}}{\partial x} = -\rho_e U_e \frac{dU_e}{dx} \tag{2.38}$$

- **Mean Energy**

$$\frac{\partial}{\partial x}\left[(C_p\tilde{T} + \tilde{k})\bar{\rho}\tilde{u}\right] + \frac{\partial}{\partial y}\left[(C_p\tilde{T} + \tilde{k})\bar{\rho}\tilde{v}\right] =$$
$$\frac{\partial}{\partial y}\left[-C_p\overline{\rho T''v''} - \bar{Q}_y\right] + \tilde{u}\frac{\partial \bar{p}}{\partial x} + (-\overline{\rho u''v''} + \bar{\tau}_{xy})\frac{\partial \tilde{u}}{\partial y} \tag{2.39}$$

where

$$-\bar{Q}_y = \frac{C_p \tilde{\mu}}{Pr} \frac{\partial \tilde{T}}{\partial y} \tag{2.40}$$

$$-C_p \overline{\rho T'' v''} = \frac{C_p \mu_T}{Pr_T} \frac{\partial \tilde{T}}{\partial y} \tag{2.41}$$

- **Transport of Turbulence Kinetic Energy**

$$\bar{\rho} \tilde{u} \frac{\partial \tilde{k}}{\partial x} + \bar{\rho} \tilde{v} \frac{\partial \tilde{k}}{\partial y} = \mu_T \left(\frac{\partial \tilde{u}}{\partial y} \right)^2 - \bar{\rho} \tilde{\epsilon} + \frac{\partial}{\partial y} \left[\left(\frac{\mu_T}{\sigma_k} + \tilde{\mu} \right) \frac{\partial \tilde{k}}{\partial y} + \frac{\mu_T \tilde{k}}{\sigma_k \bar{\rho}} \frac{\partial \bar{\rho}}{\partial y} \right] \tag{2.42}$$

- **Transport of Solenoidal Dissipation**

$$\bar{\rho} \tilde{u} \frac{\partial \tilde{\epsilon}_v}{\partial x} + \bar{\rho} \tilde{v} \frac{\partial \tilde{\epsilon}_v}{\partial y} = C_{\epsilon 1} \mu_T \left(\frac{\partial \tilde{u}}{\partial y} \right)^2 \frac{\tilde{\epsilon}_v}{\tilde{k}} - C_{\epsilon 2} \bar{\rho} \frac{\tilde{\epsilon}_v{}^2}{\tilde{k}} + \frac{\partial}{\partial y} \left[\left(\frac{\mu_T}{\sigma_\epsilon} + \tilde{\mu} \right) \frac{\partial \tilde{\epsilon}_v}{\partial y} \right] \tag{2.43}$$

2.4   Low Reynolds Number Correction

In order to successfully integrate the equations of motion through the viscous sublayer to the wall surface it is necessary to modify the eddy viscosity of equation 2.37 and the dissipation term in the dissipation of turbulence kinetic energy equation 2.43. These modifications take the form of dimensionless functions that are multiplied to the existing terms. Both of these functions are functions of only the turbulent Reynolds number and are described in Chapter 3. The resulting modifications to the equations of motion may now be described by

$$\mu_T = \frac{\bar{\rho} C_\mu f_\mu \tilde{k}^2}{\tilde{\epsilon}} \tag{2.44}$$

and

$$D_\epsilon = \frac{\bar{\rho} f_2 \tilde{\epsilon}_v{}^2}{\tilde{k}} \tag{2.45}$$

where f_μ and f_2 are the low Reynolds number terms.

2.5   Boundary Conditions

There are two types of boundary conditions employed near the wall to solve for the flow over a flat plate. The first are wall functions and the second are the boundary conditions associated with integrating to the wall.

Boundary Conditions in Wall Layer
$\tilde{u} = \frac{u_\tau}{\kappa} \ln(\frac{u_\tau y}{\nu}) + B u_\tau$
$\tilde{v} = -y \frac{\tilde{u}}{u_\tau} \frac{du_\tau}{dx}$
$\tilde{\epsilon} = \frac{u_\tau^3}{\kappa y}$
$\tilde{k} = \frac{u_\tau^2}{\sqrt{C_\mu}}$

Table 2.1: Incompressible Wall Function Boundary Conditions

2.5.1 Wall Function Boundary Conditions

The wall function boundary conditions are given in Table 2.1 assuming an incompressible flow [54]. These boundary conditions do not require the use of a low Reynolds number correction and therefore only the standard $k - \epsilon$ model equations need be employed. These boundary conditions are currently used to verify that the code is properly solving turbulent flow problems, by comparing the current code with an existing standard $k - \epsilon$ model code.

These boundary conditions are found from the equations governing fluid flow in the wall layer. The wall layer is defined as the area between the viscous sublayer and the defect layer in which convection, pressure gradient, and molecular diffusion are negligible. The resulting governing equations for momentum, dissipation and turbulent kinetic energy are respectively

$$\frac{\partial}{\partial y}\left[\mu_T \frac{\partial \tilde{u}}{\partial y}\right] = 0 \tag{2.46}$$

$$\mu_T \left(\frac{\partial \tilde{u}}{\partial y}\right)^2 - \bar{\rho}\tilde{\epsilon} + \frac{\partial}{\partial y}\left[\frac{\mu_T}{\sigma_k}\frac{\partial \tilde{k}}{\partial y}\right] = 0 \tag{2.47}$$

$$C_{\epsilon 1}\bar{\rho}C_\mu \tilde{k}\left(\frac{\partial \tilde{u}}{\partial y}\right)^2 - C_{\epsilon 2}\bar{\rho}\frac{\tilde{\epsilon}_v}{\tilde{k}} + \frac{\partial}{\partial y}\left[\frac{\mu_T}{\sigma_\epsilon}\frac{\partial \tilde{\epsilon}}{\partial y}\right] = 0 \tag{2.48}$$

where

$$\mu_T = \frac{\bar{\rho}C_\mu \tilde{k}^2}{\tilde{\epsilon}} \tag{2.49}$$

The solution to these equations is specified in Table 2.1. The constants κ and B are found from experimental correlation [6], and are given as $\kappa = .41$ and $B = 5.0$.

The boundary condition for $\tilde{v}$ is a result of satisfying the continuity equation at the first grid point.

The introduction of these boundary conditions necessitates the inclusion of an additional equation for the friction velocity, u_τ, where

$$u_\tau = \sqrt{\frac{\tau_{wall}}{\rho_{wall}}} \tag{2.50}$$

and τ_{wall} is the wall shear stress. This additional equation is found from the momentum equation by assuming that in the viscous sublayer there is no convection and no pressure gradient.

$$\frac{\partial}{\partial y}\left[(\bar{\mu} + \mu_T)\frac{\partial \tilde{u}}{\partial y}\right] = 0 \tag{2.51}$$

Integrating this equation yields

$$(\bar{\mu} + \mu_T)\frac{\partial \tilde{u}}{\partial y} = \tau_{wall} \tag{2.52}$$

In the limit as y enters the wall layer $\bar{\mu}$ becomes much smaller than μ_T and may therefore be neglected. The resulting equation gives the wall shear stress in terms of the eddy viscosity and the local velocity gradient

$$\mu_T\frac{\partial \tilde{u}}{\partial y} = \tau_{wall} = \bar{\rho}_{wall}u_\tau^2 \tag{2.53}$$

There are also wall function boundary conditions applicable for compressible flows. The compressible boundary conditions for $\bar{k}$ and $\bar{\epsilon}$, shown in Table 2.2, have been derived by Knight [28] for adiabatic walls. The compressible boundary condition for $\tilde{u}$ arises from the compressible Law of the Wall [53] and the boundary condition for $\tilde{T}$ assumes an adiabatic boundary condition with constant total temperature through the boundary layer. The boundary condition for $\tilde{v}$ is approximate. In the present research, the compressible wall functions boundary conditions are utilized only to find an accurate first guess for the independent variables in the wall layer and wake region at the first x station in the calculation.

There are limitations on the applicability of both the compressible and incompressible wall functions. Wall functions are only valid for high Reynolds number flows where the molecular viscosity is negligible and for flows where $y^+ = yu_\tau/\nu_{wall}$ is well defined. Flows with complex three dimensional geometries or flows in which separation occurs may not be handled with wall functions. As these cases comprise a large portion of the

Boundary Conditions in Wall Layer
$\frac{1}{A}\sin^{-1}A\tilde{u} = \frac{u_\tau}{\kappa}\ln\left(\frac{u_\tau y}{\nu_{wall}}\right) + Bu_\tau$ where $A = \frac{\gamma-1}{2}Pr_T\frac{T_\infty}{T_{wall}}M_\infty$
$\tilde{v} = 0$
$\tilde{\epsilon} = \frac{u_\tau^3}{\kappa y}\left(\frac{\rho_{wall}}{\rho}\right)^{\frac{1}{4}}$
$\tilde{k} = \frac{u_\tau^2}{\sqrt{C_\mu}}\left(\frac{\rho_{wall}}{\rho}\right)$
$\frac{\partial \tilde{T}}{\partial y} + \frac{Pr_T\tilde{u}}{C_p}\frac{\partial \tilde{u}}{\partial y} = 0$

Table 2.2: Compressible Adiabatic Wall Function Boundary Conditions

relevant engineering problems that need to be studied, it is necessary to formulate and validate low Reynolds number modifications.

2.5.2 Integration to the Wall

When the low Reynolds number correction is utilized boundary conditions are needed at the wall surface. These are shown in Table 2.3.

Boundary Conditions at Wall Surface
$\tilde{u} = 0$
$\tilde{v} = 0$
$\frac{\partial \tilde{T}}{\partial y} = 0$ or $\tilde{T} = T_{wall}$
$\tilde{\epsilon} = 2\nu_{wall}\left(\frac{\partial\sqrt{k}}{\partial y}\right)^2$
$\tilde{k} = 0$

Table 2.3: Wall Surface Boundary Conditions

The boundary conditions for $\tilde{u}$, $\tilde{v}$, and $\tilde{k}$ are found from the no slip condition. The boundary condition for $\tilde{T}$ depends on whether the wall is adiabatic or if the wall temperature is specified. The boundary condition for $\tilde{\epsilon}$ arises from the turbulence kinetic energy equation being applied at the wall. At the wall surface the dissipation of turbulence kinetic energy is equal to the diffusion

$$\tilde{\epsilon} = \tilde{\nu}_{wall}\frac{\partial^2\tilde{k}}{\partial y^2} \qquad (2.54)$$

However, it is difficult to apply a second derivative as a boundary condition. Equation

2.54 is therefore rewritten and applied as the numerically equivalent boundary condition

$$\tilde{\epsilon} = 2\tilde{\nu}_{wall} \left(\frac{\partial \sqrt{\tilde{k}}}{\partial y} \right)^2 \tag{2.55}$$

2.5.3 Boundary Conditions at the Edge of Computational Domain

The boundary conditions at the edge of the computational domain are given in Table 2.4 where the subscript e refers to the conditions in the free stream at that x location.

Boundary Conditions at Edge of Domain
$\tilde{u} = U_e$
$\tilde{\epsilon} = \epsilon_e$ or $\frac{\partial \tilde{\epsilon}}{\partial y} = 0$
$\tilde{k} = k_e$ or $\frac{\partial \tilde{k}}{\partial y} = 0$
$\tilde{T} = T_e$

Table 2.4: Boundary Conditions at the Edge of the Computational Domain

The condition for U_e is specified according to the pressure gradient that is applied, and is known *a priori*, as is the condition for T_e. The conditions for k_e and ϵ_e are found from the equations governing the decay of freestream turbulence. An initial value for k_e and ϵ_e is specified and subsequent values are found from the solutions to equations 2.56 and 2.57 which describe the decay of freestream turbulence.

$$U_e \frac{\partial \tilde{k}_e}{\partial x} = -\tilde{\epsilon}_e \tag{2.56}$$

$$U_e \frac{\partial \tilde{\epsilon}_e}{\partial x} = -C_{\epsilon 2} f_2 \frac{\tilde{\epsilon}_e^2}{\tilde{k}_e} \tag{2.57}$$

The exact analytical solution for the above equations is known for $f_2 = 1$ and constant U_e (See Equations 2.60-2.61), however these equations are solved separately by the same method as the governing equations to achieve consistency with the equations of motion in the boundary layer.

2.6 Closure Coefficients

To assure results for flows in which no wall interaction is encountered, the standard $k - \epsilon$ model closure coefficients are utilized [39]. These are given in Table 2.5. The

closure coefficients for the $k - \epsilon$ model are found by correlating with the experimental results of different flow fields, including the far wake, mixing layer and jet [54].

Symbol	Source	Value
C_μ	Turbulent Eddy Viscosity	.09
$C_{\epsilon 1}$	Production of Dissipation	1.44
$C_{\epsilon 2}$	Dissipation of Dissipation	1.92
C_k	Dilatational Dissipation	0.0
Pr_T	Turbulent Prandtl Number	0.9
σ_k	Turbulent Schmidt Number for k	1.0
σ_ϵ	Turbulent Schmidt Number for $\tilde{\epsilon}_v$	1.3

Table 2.5: $k - \epsilon$ Model Coefficients

The choice of these coefficients yields certain properties of different flows. The decay of isotropic turbulence for incompressible flow is governed by equations 2.58 and 2.59, where the spatial gradients are assumed to be equal to 0.

$$\frac{\partial \bar{\rho} \tilde{k}}{\partial t} = -\bar{\rho} \tilde{\epsilon}_v \tag{2.58}$$

and

$$\frac{\partial \bar{\rho} \tilde{\epsilon}_v}{\partial t} = -C_{\epsilon 2} \bar{\rho} \frac{\tilde{\epsilon}_v^2}{\tilde{k}} \tag{2.59}$$

The solution to this system of equations is

$$\tilde{k} = \tilde{k}_o [1 + (C_{\epsilon 2} - 1)\tilde{\epsilon}_{vo} t / \tilde{k}_o]^{-1/(C_{\epsilon 2}-1)} \tag{2.60}$$

$$\tilde{\epsilon}_v = \tilde{\epsilon}_{vo} [1 + (C_{\epsilon 2} - 1)\tilde{\epsilon}_{vo} t / \tilde{k}_o]^{-C_{\epsilon 2}/(C_{\epsilon 2}-1)} \tag{2.61}$$

Where k_o and ϵ_{vo} are values for the turbulence kinetic energy and dissipation at $t = 0$. By substituting $C_{\epsilon 2} = 1.92$ it is observed that

$$\tilde{k} \sim t^{-1.087} \tag{2.62}$$

while experimental data [7] shows that

$$\tilde{k} \sim t^{-1.25} \tag{2.63}$$

The solution to the $k - \epsilon$ model also yields a slightly different value for the constant κ in the Law of the Wall. Substituting the wall functions into equation 2.48, and using

the standard $k - \epsilon$ model constants yields $\kappa = \sqrt{\sqrt{C_\mu}(C_{\epsilon 2} - C_{\epsilon 1})\sigma_\epsilon} = .43$. This value is slightly higher than the value of $\kappa = .41$ found from correlation with experiment [6], and is used to compare the computed results with the Law of the Wall.

Chapter 3

LOW REYNOLDS NUMBER CORRECTION

3.1 The Need for a Low Reynolds Number Correction

In order to integrate the $k - \epsilon$ model through the viscous sublayer it is necessary to incorporate a low Reynolds number correction to the model. The need for this correction arises from an asymptotic analysis of the fluctuating components of the velocity as $y \to 0$. If a Taylor series expansion is performed on the fluctuating components of the velocity, for a two dimensional boundary layer flow it may be shown that

$$u' \sim A_x(x,t) + B_x(x,t)y + C_x(x,t)y^2 + \dots.$$

$$v' \sim A_y(x,t) + B_y(x,t)y + C_y(x,t)y^2 + \dots.$$

As $y \to 0$, $A_x = A_y = 0$ by the no-slip condition and $B_y = 0$ by the continuity equation. Therefore $u' \to y$ and $v' \to y^2$ as $y \to 0$.[1] This means the Reynolds stress, $-\overline{\rho u'v'}$, should behave like y^3, the turbulent kinetic energy, k, should behave like y^2, and the dissipation, ϵ, should behave like $2\nu \overline{B_x^2}$ as $y \to 0$.

However, an examination of the eddy viscosity, $\mu_T = \frac{\rho C_\mu k^2}{\epsilon}$, shows that the Reynolds stress, $\mu_T \frac{\partial \bar{u}}{\partial y}$, goes like y^4 as $y \to 0$ without a low Reynolds number correction. In order to obtain asymptotic consistency it is necessary to multiply the eddy viscosity by a function, f_μ, that goes as y^{-1}.

Similarly the dissipation term in the transport of solenoidal dissipation equation,

$$D_\epsilon = C_{\epsilon 2} \frac{\tilde{\epsilon}_v}{\tilde{k}} \tag{3.1}$$

goes like y^{-2} as $y \to 0$. To maintain asymptotic consistency a second damping function, f_2, which $\to y^2$ as $y \to 0$ must be multiplied to this dissipation term.

---

[1] It is assumed that the acoustic mode of turbulence is negligible near the wall and that the temperature and hence density fluctuations at the wall may be neglected [45].

As shown by Speziale *et al* [48] it is sufficient in the formulation of a correction to the $k - \epsilon$ model to introduce only two damping functions, f_μ and f_2, if these terms are of $O(y^{-1})$ and $O(y^2)$ respectively near the wall and approach unity outside of the viscous sublayer. Models that do not incorporate this asymptotic consistency have to add additional damping terms to the dissipation equation. These terms usually modify the production of dissipation, P_ϵ, and are symbolized as the function f_1.

3.2 Current Model

The purpose of the current research is the development and validation of a low Reynolds number correction to the standard $k - \epsilon$ turbulence model that may be easily applied to more complicated three dimensional flow fields. In order to maintain this simplicity it is desired to make as few corrections to the governing equations as needed, and to make these corrections independent of the coordinate system. These corrections should also become negligible outside of the viscous sublayer. It is also desired that the proper limiting form of the physical properties be maintained as $y \to 0$. Following these guidelines only two corrections are made to the governing equations. These are the inclusion of the damping functions f_μ and f_2. The functional form of these equations are chosen such that they are asymptotically correct and they are assumed to be functions of only the turbulent Reynolds number, $R_t = \frac{\rho k^2}{\mu \epsilon}$. By making the corrections functions of only R_t the damping functions become independent of the physical coordinate. This is important in three dimensional applications where the height from the wall is ill defined, such as that encountered by a corner [32], or when dealing with rows of turbine or compressor blades [8].

The function f_2 is chosen to be

$$f_2 = 1. - exp(-C_{\epsilon 3}\sqrt{R_t}) \tag{3.2}$$

which has the proper limiting form $f_2 \to y^2$ as $y \to 0$, and rapidly approaches unity as $R_t \to \infty$. This function is chosen solely because it behaves properly both in the limit as $y \to 0$ and $R_t \to \infty$, as is seen in Figure 3.1. Other functions could have been chosen, but these would alter the form of f_μ found.

The functional form of f_μ is found by solving the equations of motion for the incompressible constant stress layer. The functional form obtained for f_μ is then applied without modification to both compressible flows, and flows that experience an adverse pressure gradient.

The equations for the incompressible constant stress layer, non-dimensionalized by the friction velocity, u_τ, and the kinematic viscosity, ν, are

- **Momentum Equation**

$$\frac{\partial}{\partial y^+}\left[(C_\mu f_\mu \frac{k^{+2}}{\epsilon^+} + 1)\frac{\partial u^+}{\partial y^+}\right] = 0 \tag{3.3}$$

- **Turbulence Kinetic Energy Equation**

$$C_\mu f_\mu \frac{k^{+2}}{\epsilon^+}\left(\frac{\partial u^+}{\partial y^+}\right)^2 - \epsilon^+ + \frac{\partial}{\partial y^+}\left[(\frac{C_\mu f_\mu}{\sigma_k}\frac{k^{+2}}{\epsilon^+} + 1)\frac{\partial k^+}{\partial y^+}\right] = 0 \tag{3.4}$$

- **Dissipation Equation**

$$C_{\epsilon 1}C_\mu f_\mu k^+\left(\frac{\partial u^+}{\partial y^+}\right)^2 - C_{\epsilon 2}f_2\frac{\epsilon^{+2}}{k^+} + \frac{\partial}{\partial y^+}\left[(\frac{C_\mu f_\mu}{\sigma_\epsilon}\frac{k^{+2}}{\epsilon^+} + 1)\frac{\partial \epsilon^+}{\partial y^+}\right] = 0 \tag{3.5}$$

where the definitions of the variables are given in Table 3.1.

Non-Dimensionalization
$y^+ = \frac{yu_\tau}{\nu}$
$u^+ = \frac{u}{u_\tau}$
$k^+ = \frac{k}{u_\tau^2}$
$\epsilon^+ = \frac{\nu\epsilon}{u_\tau^4}$
$\mu_T^+ = \frac{\mu_T}{\rho\nu} = \frac{\rho C_\mu f_\mu k^{+2}}{\epsilon^+}$

Table 3.1: Non-dimensional Parameters Employed in Solving for f_μ

The boundary conditions are chosen such that in the limit as $y \to \infty$ the boundary conditions approach the wall functions (See Table 2.1) and when $y = 0$ the boundary conditions are those associated with a solid surface (See Table 2.3).

The solution sought is a functional form for f_μ versus the turbulent Reynolds number. This is accomplished by solving equations 3.3 - 3.5, in conjunction with specifying the eddy viscosity. It is emphasized that the eddy viscosity is specified (as described

below) only for the incompressible constant stress layer. By doing this the system becomes closed and f_μ may be found.

For the incompressible constant stress layer, the eddy viscosity is specified by assuming Prandtl's mixing length hypothesis. Prandtl's mixing length hypothesis, equation 1.5, says that the eddy viscosity is dependent upon the gradient of the mean velocity and some mixing length, l_{mix}, that is a property of the flow [42]. In wall bounded flows the mixing length is said to be proportional to the distance from the wall [54]. This allows the specification of the mixing length based upon the distance from the wall. In the wall layer the eddy viscosity is specified from the Law of the Wall. Using equation 2.53 and assuming the velocity profile is equal to the Law of the Wall, it may be shown that

$$l^2_{mix} = \frac{1}{\frac{du^+}{dy}\frac{du^+}{dy}} = (\kappa y)^2 \tag{3.6}$$

and

$$\mu_T^+ = \kappa y^+ \tag{3.7}$$

This formulation for the mixing length is only valid in the wall layer and not in the viscous sublayer. Therefore another formulation for the eddy viscosity needs to be specified in this area. This is done by approximating the eddy viscosity by the polynomial

$$\mu_T^+ = \alpha y^{+3} + \beta y^{+5} \tag{3.8}$$

The α term arises because of the limiting form of μ_T as $y \to 0$, and the β term arises because it is necessary to maintain consistency in the first derivative at the matching point between the eddy viscosity in the viscous sublayer and in the wall layer.

At some point, y_m^+, the eddy viscosity and its first derivative match in the viscous sublayer and in the wall layer. This is the transition point between the two viscosities. At this point $\alpha = 2\kappa/y_m^{+2}$ and $\beta = -\kappa/y_m^{+4}$. The choice for y_m^+ is made to maintain $B = 5.0$ in the Law of the Wall. This value corresponds to $y_m^+ = 33.0$. By specifying the eddy viscosity the system has now been closed, and the equations may be solved to find the function f_μ as a function of the turbulent Reynolds number. f_μ is found from

the definition of the eddy viscosity for the $k - \epsilon$ model

$$f_\mu = \mu_T^+ \frac{\epsilon^+}{\rho C_\mu k^{+2}} \tag{3.9}$$

and is tabulated in Appendix A and displayed in Figure 3.1. The tabulated function f_μ in Appendix A does not behave as y^{-1} as $y \to 0$. The tabulated function $f_\mu \to .0314$ as $y \to 0$. The reason for this discrepancy in the behavior of f_μ is that there is no appreciable difference in the computed solution when the behavior of f_μ is y^{-1} as opposed to approaching the finite value. The value $f_\mu = .0314$ is the minimum value obtained by f_μ before it begins to increase as $y \to 0$. The reason there is no appreciable difference between the solutions utilizing the correct assymptotic behavior for f_μ and the applied behavior is that in this region the contribution by the eddy viscosity is minimal compared to the contribution of the molecular viscosity. Having f_μ approach a finite value is computationally easier to apply than to have $f_\mu \to y^{-1}$.

The value of the constant $C_{\epsilon 3}$ in equation 3.2 is chosen so that the correct value of ϵ_{wall}^+ is maintained. The correct value of ϵ_{wall}^+ is found from the DNS data of Spalart [46] and is equal to 26. It is found that in order to maintain this value for ϵ_{wall}^+ it is necessary to choose $C_{\epsilon 3} = 0.17$.
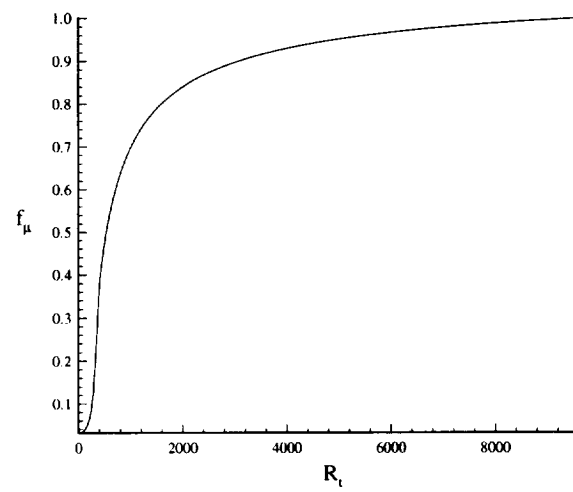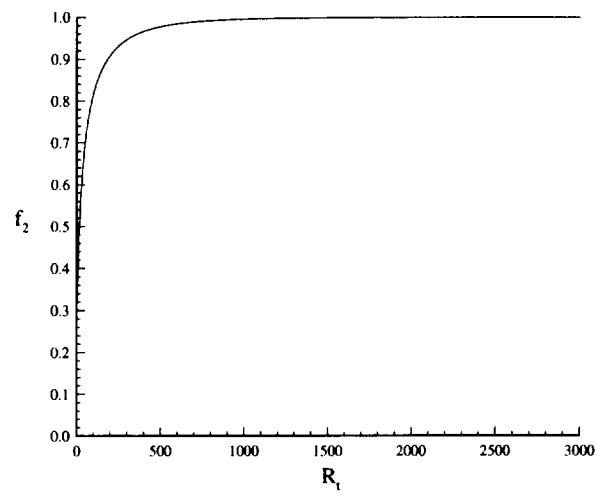
Figure 3.1: Damping Functions vs. Turbulent Reynolds Number a) f_2 vs. R_t, and b) f_μ vs. R_t

Chapter 4

NUMERICAL ALGORITHM

The algorithm has been developed to solve equations 2.35 - 2.43 on a structured, nonuniform grid. The resulting boundary layer equations are parabolic in nature and permit a spatial marching scheme in x. Keller's Box Scheme is chosen to discretize the equations of motion [4], [22], [23], [24]. This method is second order accurate in both Δx and Δy. Geometric grid stretching is employed in y to allow better resolution of the viscous sublayer. A regridding algorithm has been developed to resolve the turbulent non-turbulent interface and to allow for the growth of the boundary layer.

4.1 Nondimensionalization

The solution of the system of equations defined by equations 2.35 - 2.43 is facilitated if the variables are non-dimensionalized. The non-dimensionalization employed is given in Table 4.1 where $*$ denotes a dimensional parameter. The boundary condition for $\epsilon_{wall} = 2\nu_{wall}\left(\partial\sqrt{\bar{k}}/\partial y\right)^2$ necessitates changing the independent variable for the turbulence kinetic energy in the governing equations from $\bar{k}$ to $\sqrt{\bar{k}}$. The variable $\tilde{q}$ is introduced and defined as $\sqrt{\bar{k}}$.

The resulting system of equations utilizing nondimensional parameters is

- **Continuity Equation**

$$\frac{\partial\left(\frac{\rho_e T_e}{\bar{T}}\tilde{u}\right)}{\partial x} + \rho_e T_e \frac{\partial\left(\frac{\tilde{v}}{\bar{T}}\right)}{\partial y} = 0 \qquad (4.1)$$

where the subscript e denotes evaluation at the edge of the boundary layer.

- **Transport of Momentum Equation**

$$\rho_e T_e \frac{\tilde{u}}{\bar{T}}\frac{\partial\tilde{u}}{\partial x} + \rho_e T_e \frac{\tilde{v}}{\bar{T}}\frac{\partial\tilde{u}}{\partial y} = \beta + \frac{1}{Re_{\delta_o}}\frac{\partial}{\partial y}\left[(\mu_T + \tilde{\mu})\frac{\partial\tilde{u}}{\partial y}\right] \qquad (4.2)$$

Variable	Non-Dimensionalization	Variable	Non-Dimensionalization
x	$x^* = x\delta_o^*$	y	$y^* = y\delta_o^*$
$\tilde{u}$	$\tilde{u}^* = \tilde{u}U_\infty^*$	$\tilde{v}$	$\tilde{v}^* = \tilde{v}U_\infty^*$
$\bar{\rho}$	$\bar{\rho}^* = \bar{\rho}\rho_\infty^*$	$\bar{p}$	$\bar{p}^* = \bar{p}\rho_\infty^* U_\infty^{*2}$
$\tilde{\mu}$	$\tilde{\mu}^* = \tilde{\mu}\mu_\infty^*$	μ_T	$\mu_T^* = \mu_T\mu_\infty^*$
$\tilde{\epsilon}_v$	$\tilde{\epsilon}_v^* = \tilde{\epsilon}_v\frac{U_\infty^{*3}}{\delta_o^*}$	$\tilde{q}$	$\tilde{q}^* = \tilde{q}U_\infty^*$
$\tilde{T}$	$\tilde{T}^* = \tilde{T}T_\infty^*$	u_τ	$u_\tau^* = u_\tau U_\infty^*$
Q_{wall}	$Q_{wall}^* = Q_{wall}U_\infty^{*3}\rho_\infty^*$	T_{wall}	$T_{wall}^* = T_{wall}T_\infty^*$

Table 4.1: Non-dimensional Parameters Employed in the Present Code

where

$$Re_{\delta_o} = \frac{\rho_\infty^* U_\infty^* \delta_o^*}{\mu_\infty^*} \tag{4.3}$$

$$\mu_T = Re_{\delta_o}\rho_e T_e C_\mu f_\mu \frac{\tilde{q}^4}{\tilde{T}\tilde{\epsilon}} \tag{4.4}$$

f_μ is a Tabulated Function vs. Turbulent Reynolds Number given in Appendix A

$$\beta = \rho_e U_e \frac{dU_e}{dx} \tag{4.5}$$

Since pressure is assumed constant across the boundary layer, the ideal gas law, equation 2.34, yields

$$\rho T = \rho_e T_e \tag{4.6}$$

- **Mean Energy Equation**

$$\frac{1}{M_\infty^2(\gamma-1)}\rho_e T_e \left[\frac{\tilde{u}}{\tilde{T}}\frac{\partial \tilde{T}}{\partial x} + \frac{\tilde{v}}{\tilde{T}}\frac{\partial \tilde{T}}{\partial y}\right] + 2\rho_e T_e\frac{\tilde{q}}{\tilde{T}}\left[\tilde{u}\frac{\partial \tilde{q}}{\partial x} + \tilde{v}\frac{\partial \tilde{q}}{\partial y}\right] =$$

$$\frac{1}{M_\infty^2(\gamma-1)Re_{\delta_o}}\frac{\partial}{\partial y}\left[\left(\frac{\mu_T}{Pr_T} + \frac{\tilde{\mu}}{Pr}\right)\frac{\partial \tilde{T}}{\partial y}\right] - \tilde{u}\beta + \frac{1}{Re_{\delta_o}}(\mu_T + \tilde{\mu})\frac{\partial \tilde{u}}{\partial y}\frac{\partial \tilde{u}}{\partial y} \tag{4.7}$$

- **Transport of Turbulence Kinetic Energy Equation**

$$2\rho_e T_e\frac{\tilde{u}\tilde{q}}{\tilde{T}}\frac{\partial \tilde{q}}{\partial x} + 2\rho_e T_e\frac{\tilde{v}\tilde{q}}{\tilde{T}}\frac{\partial \tilde{q}}{\partial y} = \frac{\mu_T}{Re_{\delta_o}}\left(\frac{\partial \tilde{u}}{\partial y}\right)^2 +$$

$$\frac{1}{Re_{\delta_o}}\frac{\partial}{\partial y}\left[\left(\frac{\mu_T}{\sigma_k} + \tilde{\mu}\right)2\tilde{q}\frac{\partial \tilde{q}}{\partial y} - \frac{\mu_T\tilde{q}^2}{\tilde{T}\sigma_k}\frac{\partial \tilde{T}}{\partial y}\right] - \rho_e T_e\frac{\tilde{\epsilon}}{\tilde{T}} \tag{4.8}$$

- **Dissipation of Solenoidal Dissipation Equation**

$$\rho_e T_e\frac{\tilde{u}}{\tilde{T}}\frac{\partial \tilde{\epsilon}_v}{\partial x} + \rho_e T_e\frac{\tilde{v}}{\tilde{T}}\frac{\partial \tilde{\epsilon}_v}{\partial y} = +C_{\epsilon_1}\frac{\mu_T}{Re_{\delta_o}}\frac{\tilde{\epsilon}_v}{\tilde{q}^2}\left(\frac{\partial \tilde{u}}{\partial y}\right)^2$$

$$-C_{\epsilon_2}\rho_e T_e\frac{f_2}{q^2}\frac{\tilde{\epsilon}_v^2}{\tilde{T}} + \frac{1}{Re_{\delta_o}}\frac{\partial}{\partial y}\left[\left(\frac{\mu_T}{\sigma_\epsilon} + \tilde{\mu}\right)\frac{\partial \tilde{\epsilon}_v}{\partial y}\right] \tag{4.9}$$

where

$$f_2 = 1. - e^{-C_{\epsilon_3}\sqrt{R_t}} \tag{4.10}$$

$$R_t = Re_{\delta_o}\rho_e T_e \frac{q^4}{\tilde{\mu}\tilde{T}\epsilon} \tag{4.11}$$

$$\tilde{\epsilon} = \tilde{\epsilon}_v + \tilde{\epsilon}_d \tag{4.12}$$

The code has been adapted to incorporate the the modification proposed by Sarkar [41] which makes $\tilde{\epsilon}_d = C_k F(\tilde{\epsilon}_v, M_t^2)$. However, the effect of this modification has not yet been examined. Therefore for all results obtained $C_k = 0$ and $\tilde{\epsilon} = \tilde{\epsilon}_v$.

4.2 Keller's Box Scheme

To solve the equations of motion described in equations 4.1 - 4.9 by Keller's Box Scheme they must first be transformed into a system of first order, coupled, partial differential equations. This is accomplished by defining the variables $h,a,b,$ and c as the partial derivatives with respect to y of $\tilde{u},\tilde{\epsilon}$, $\sqrt{\tilde{k}}$ and $\tilde{T}$ respectively. The resulting system of equations becomes

- **Continuity Equation**

$$\frac{\partial\left(\frac{\rho_e T_e}{\tilde{T}}\tilde{u}\right)}{\partial x} + \rho_e T_e \frac{\partial\left(\frac{\tilde{v}}{\tilde{T}}\right)}{\partial y} = 0 \tag{4.13}$$

- **Transport of Momentum Equation**

$$\rho_e T_e \frac{\tilde{u}}{\tilde{T}}\frac{\partial\tilde{u}}{\partial x} + \rho_e T_e \frac{\tilde{v}}{\tilde{T}}\frac{\partial\tilde{u}}{\partial y} = \beta + \frac{1}{Re_{\delta_o}}\frac{\partial}{\partial y}\left[(\mu_T + \tilde{\mu})h\right] \tag{4.14}$$

- **Definition of $\partial\tilde{u}/\partial y$**

$$h = \frac{\partial\tilde{u}}{\partial y} \tag{4.15}$$

- **Dissipation of Solenoidal Dissipation Equation**

$$\rho_e T_e \frac{\tilde{u}}{\tilde{T}}\frac{\partial\tilde{\epsilon}_v}{\partial x} + \rho_e T_e \frac{\tilde{v}}{\tilde{T}}a = +C_{\epsilon_1}\frac{\mu_T}{Re_{\delta_o}}\frac{\tilde{\epsilon}_v}{\tilde{q}^2}h^2$$
$$-C_{\epsilon_2}\rho_e T_e \frac{f_2}{\tilde{q}^2}\frac{\tilde{\epsilon}_v^2}{\tilde{T}} + \frac{1}{Re_{\delta_o}}\frac{\partial}{\partial y}\left[(\frac{\mu_T}{\sigma_\epsilon} + \tilde{\mu})a\right] \tag{4.16}$$

- **Definition of $\partial \tilde{\epsilon}_v / \partial y$**

$$a = \frac{\partial \tilde{\epsilon}_v}{\partial y} \qquad (4.17)$$

- **Transport of Turbulent Kinetic Energy**

$$2\rho_e T_e \frac{\tilde{u}\tilde{q}}{\tilde{T}} \frac{\partial \tilde{q}}{\partial x} + 2\rho_e T_e \frac{\tilde{v}\tilde{q}}{\tilde{T}} b = \frac{\mu_T}{Re_{\delta_o}} h^2$$

$$\frac{1}{Re_{\delta_o}} \frac{\partial}{\partial y} \left[\left(\frac{\mu_T}{\sigma_k} + \tilde{\mu} \right) 2\tilde{q}b - \frac{\mu_T \tilde{q}^2}{\tilde{T}\sigma_k} c \right] - \rho_e T_e \frac{\tilde{\epsilon}}{\tilde{T}} \qquad (4.18)$$

- **Definition of $\partial \tilde{q} / \partial y$**

$$b = \frac{\partial \tilde{q}}{\partial y} \qquad (4.19)$$

- **Mean Energy Equation**

$$\frac{1}{M_\infty^2(\gamma-1)} \rho_e T_e \left[\frac{\tilde{u}}{\tilde{T}} \frac{\partial \tilde{T}}{\partial x} + \frac{\tilde{v}}{\tilde{T}} c \right] + 2\rho_e T_e \frac{\tilde{q}}{\tilde{T}} \left[\tilde{u} \frac{\partial \tilde{q}}{\partial x} + \tilde{v}b \right] =$$

$$\frac{1}{M_\infty^2(\gamma-1)Re_{\delta_o}} \frac{\partial}{\partial y} \left[\left(\frac{\mu_T}{Pr_T} + \frac{\tilde{\mu}}{Pr} \right) c \right] - \tilde{u}\beta + \frac{1}{Re_{\delta_o}} (\mu_T + \tilde{\mu}) h^2 \qquad (4.20)$$

- **Definition of $\partial \tilde{T} / \partial y$**

$$c = \frac{\partial \tilde{T}}{\partial y} \qquad (4.21)$$

The use of Keller's Box scheme necessitates creating a computational mesh over which the equations may be discretized. The grid spacing is constructed such that there is geometrical grid stretching in Δy to allow for more points in the viscous sublayer. A larger number of points is required near the wall to obtain the necessary accuracy [4]. The grid is found from the following formulation where $jsbegin$ and $jsend$ are chosen to allow for the geometric stretching and jl is the number of points in the computational domain:

$$\Delta y^j \;=\; \Delta y^1 \qquad 2 < j < jsbegin$$

$$\Delta y^j \;=\; C_y \Delta y^{j-1} \qquad jsbegin \leq j \leq jsend$$

$$\Delta y^j \;=\; \Delta y^{jsend} \qquad jsend < j \leq jl$$

$$y_j \;=\; y_{j-1} + \Delta y^j \qquad 2 \leq j \leq jl$$

C_y is the grid stretching parameter and is typically chosen between 1.01 and 1.2; y_1 is set equal to zero when integrating to the wall, and is chosen such that y_1 is in the wall

layer when using wall function boundary conditions. Typically y_1^+ is chosen between 50 and 100 when using wall functions. The solution is independent of this initial value as seen from the solution obtained in Chapter 4 comparing two different codes, using two different values of y_1^+. A large number of points is used in the computational domain; jl is typically between 300 and 1000 points, and grid resolution studies have been performed to show that each solution is independent of the number of points chosen. Variable grid spacing in x is also employed. In the area near the initial guess required for solving by the Newton's method, large changes in the independent variables occur. If the grid spacing in x is too large, these changes cause numerical oscillations that grow causing the solution to become unphysical. In areas far from the initial guess, where the flow is well developed, these drastic changes in the independent variables do not occur and a larger Δx may be chosen.

A typical computational cell is seen in Figure 4.1. Keller's Box scheme works by discretizing the equations of motion about the center of the computational cell [22]. Equations 4.13 - 4.21 are discretized by using central differencing and averaging about the cell center. The discretized equations are given in Appendix B. This method of discretization may be shown [4] to be second order accurate in both Δy and Δx, and may be increased to $O(\Delta y^4, \Delta x^4)$ if Richardson extrapolation is used. However, Richardson extrapolation is not employed because of the regridding scheme utilized.

4.3   Newton's Method

Newton's method is employed to solve the system of nonlinear algebraic equations resulting from Keller's Box Scheme. Newton's method requires the solution to be known at the $n-1$ grid location. This necessitates an initial guess at $n = 1$. The initial guesses for the independent variables are made based upon the physics of the flow field being tested. In the typical computational problem the initial transient region associated with the initial guess for the independent variables manifests itself as an unphysical change in the skin friction as the solution marches downstream. There is typically a sharp drop in the skin friction followed by a slow growth, culminating in a maximum at approximately 50 initial boundary layer lengths downstream. Following this maximum

the skin friction behaves in the physically expected manner. From this behavior and the subsequent behavior of the skin friction after this maximum, it is concluded that the transient region associated with the initial guess is of the order $50\delta_o$ and that the solution after $50\delta_o$ is physically correct.

The system of equations defined by the discretized equations B.25 - B.34 is denoted by $\vec{F}$, and the solution vector for the independent variables is denoted by $\vec{w}$. Both $\vec{F}$ and $\vec{w}$ are given in Appendix B. Newton's Method works by iterating

$$\frac{\partial \vec{F}^{i-1}}{\partial \vec{w}^{i-1}} \delta \vec{w}^i = -\vec{F}^{i-1} \tag{4.22}$$

$$\vec{w}^i = \vec{w}^{i-1} + \delta \vec{w}^i \tag{4.23}$$

until some convergence criteria on $\delta \vec{w}^i$ is met [18]. The parameter $\partial \vec{F}^{i-1}/\partial \vec{w}^{i-1}$ is termed the Jacobian, $\vec{J}$, and is detailed in Appendix C, while an explanation of the convergence criteria is given in Appendix D. The vector $\delta \vec{w}^i$ is the change in the solution matrix for the current iteration. If the initial guess for the solution matrix is close to the correct solution, Newton's method will converge quadratically causing $\delta \vec{w}^i$ to become smaller with each iteration.

Newton's method is implemented by making an initial guess for the independent variables at n. If $n = 1$ then the initial guess is based upon the physics of the flow problem; if $n > 1$ then the initial guess is the value of the independent variables found at $n - 1$. The ordering of the equations is made such that the Jacobian of equation 4.22 is a 9×9 block tridiagonal matrix as seen in Figure C.1. This allows for a faster computational solution over a nonbanded matrix. The method of solving the resulting system of equations given by equation 4.22 is accomplished by using the LINPACK solver created by Cleve Moler [36]. The LINPACK solver works by taking the Jacobian in banded form and factoring it by Gauss elimination. The factored matrix is then solved to yield the solution matrix $\delta \vec{w}^i$. The old solution is then updated by $\delta \vec{w}^i$ and the method is repeated until the desired convergence criteria is met, with the Jacobian being updated after each iteration.

4.4 Regridding

It is known from the Blasius solution that laminar boundary layers grow like $\sqrt{x}$, and with a proper grid transformation the computational grid can also be made to expand as such. However, this transformation or a similar grid transformation will not work with the current turbulent boundary layer model, as there is no universal grid transformation for the rate of growth or decay of the turbulent boundary layer in the presence of an arbitrary pressure gradient. Two possible solutions exist to solve this problem. The first is to apply a grid transformation such as the Levy-Lees transformation [14] which grows as the $\sqrt{x}$ and include enough points in the free stream to allow for the increased growth over the $\sqrt{x}$, and as the boundary layer grows to add more points in the free stream. This is a simple solution and a typically applied option. However, turbulent boundary layers with molecular viscosity also experience strong gradients at the turbulent non-turbulent (TNT) interface. The method of transformation given above does not guarantee adequate numerical resolution of these gradients. If these gradients are not properly resolved, Keller's box scheme creates $2\Delta y$ numerical oscillations which grow causing the numerical solution to become unphysical. To alleviate this problem it is necessary to apply a regridding scheme that guarantees sufficient points within the TNT interface to resolve these gradients. This regridding scheme also matches any growth in the height of the boundary layer.

The TNT interface is numerically defined as the region between the minimum of the derivative of the turbulence kinetic energy with respect to y and the point that is equal to 10% of this value closer to the edge of the computational domain. It is established that sufficient resolution is achieved if there are 30 points within this TNT interface. The edge of the boundary layer is defined as the point on the plot of b vs. y where the line tangent to the maximum of $\partial b/\partial y$ in the TNT interface intersects $b = 0$. The application of the regridding scheme allows the use of non-transformed coordinates in the computation. Linear interpolation is employed to match the values of the independent variables at the old grid locations to the new grid locations.
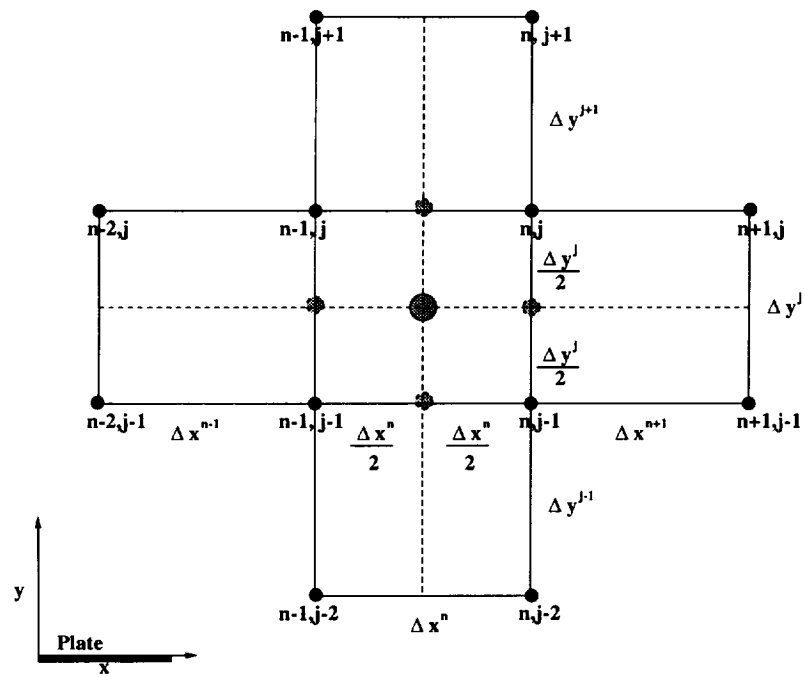
Figure 4.1: Typical Computational Cell at x^n and y^j

Chapter 5

VALIDATION

The code has been validated by comparing the computed laminar solution to the Blasius solution and by comparing the computed turbulent solution to an existing standard $k-\epsilon$ model code.

5.1 Laminar Solution

In order to validate the numerical algorithm, it is preferred to compare the resulting numerical solution with an exact analytical solution. However, no such solutions exist for turbulent boundary layer flow. Solutions do exist for laminar boundary flow. If the turbulent terms are removed from the governing equations, the resulting equations for continuity, momentum and energy revert back to their laminar form, and the analytical solution becomes the well known Blasius solution for flow over a flat plate [53] where

$$
\begin{aligned}
\eta &= y^* \sqrt{\frac{Re_{\delta o}}{2\mu_\infty x^*}} \\
\frac{df}{d\eta} = f' &= \frac{u^*}{U_\infty} \\
f''' + ff'' &= 0
\end{aligned}
\tag{5.1}
$$

with the boundary conditions

$$
\begin{aligned}
f(0) &= 0 \\
f'(0) &= 0 \\
f'(\infty) &= 1
\end{aligned}
$$

For adiabatic, compressible flow, assuming $Pr = 1$ and that the molecular viscosity varies linearly with the temperature, the velocity profile reduces to the solution of

M_∞	Re_{δ_o}	$Re_{\delta_{(end)}}$	# of Pts	$\Delta\left(\frac{y^*}{\delta_o}\right)$	$\Delta\left(\frac{x^*}{\delta_o}\right)_{max}$
0.05	250.	2500.	300	.004	.1
2.00	250.	2500.	300	.004	.1
4.00	250.	2500.	300	.004	.1

Table 5.1: Cases Run for Laminar Flow

equation 5.1 and the temperature profile is given by

$$\frac{T^*}{T_\infty} = 1 + \frac{1}{2}(\gamma - 1)M_\infty^2(f')^2 \tag{5.2}$$

The numerical algorithm has been tested for laminar flow by setting $\mu_T = 0$ and solving only the equations for conservation of mass, momentum and energy subject to adiabatic and no slip boundary conditions at the wall and matching the values in the free stream for T and u at the edge of the computational domain. Table 5.1 shows the cases which have been run.

Figures 5.1 - 5.5 compare the computed Blasius solution with the theoretical solution. The calculation is carried out by assuming an initial velocity and temperature profile and then marching downstream for $100\delta_o$. This represents a 10 fold increase in the height of the boundary layer, with any transients associated with the initial guesses for the profiles washing out. Excellent agreement is seen between the theoretical Blasius solution and the computed solution. It is concluded that the code is accurately solving those parts of the governing equations responsible for laminar flow.
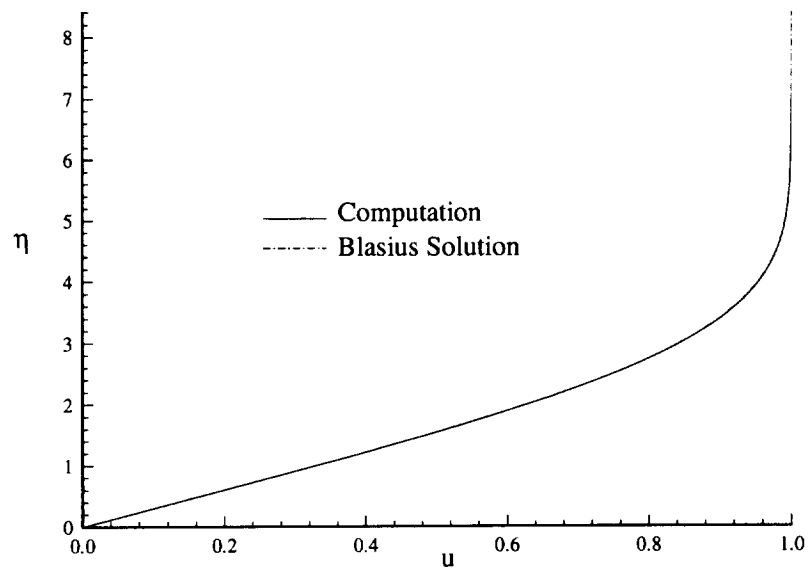
Figure 5.1: u vs. η at $x = 100\delta_o$ for $M_\infty = .05$
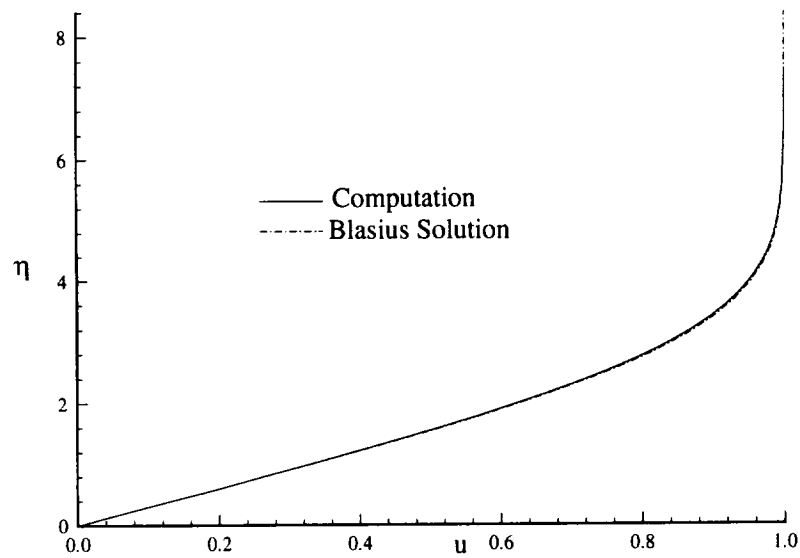
Figure 5.2: u vs. η at $x = 100\delta_o$ for $M_\infty = 2.0$
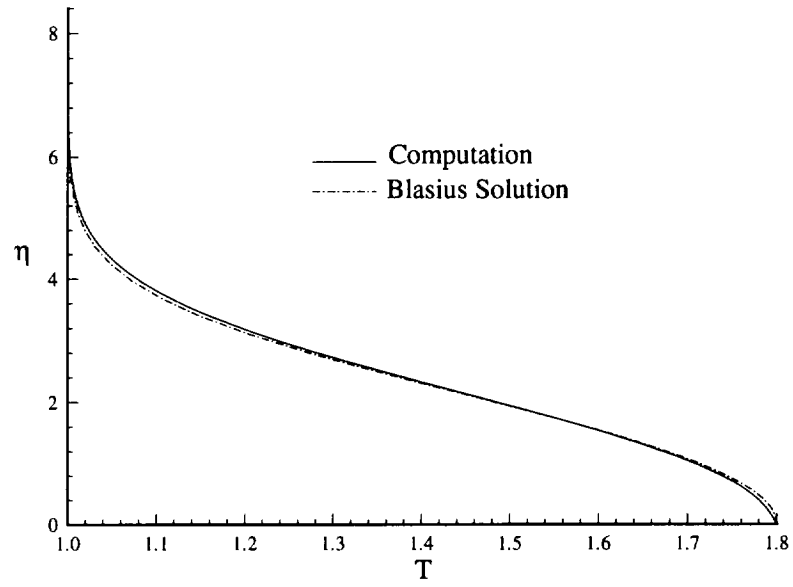
Figure 5.3: T vs. η at $x = 100\delta_o$ for $M_\infty = 2.0$
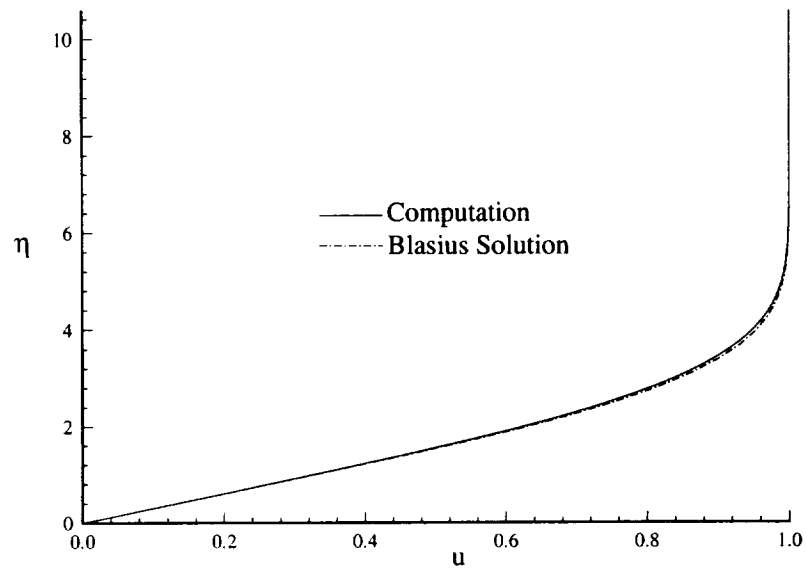
Figure 5.4: u vs. η at $x = 100\delta_o$ for $M_\infty = 4.0$
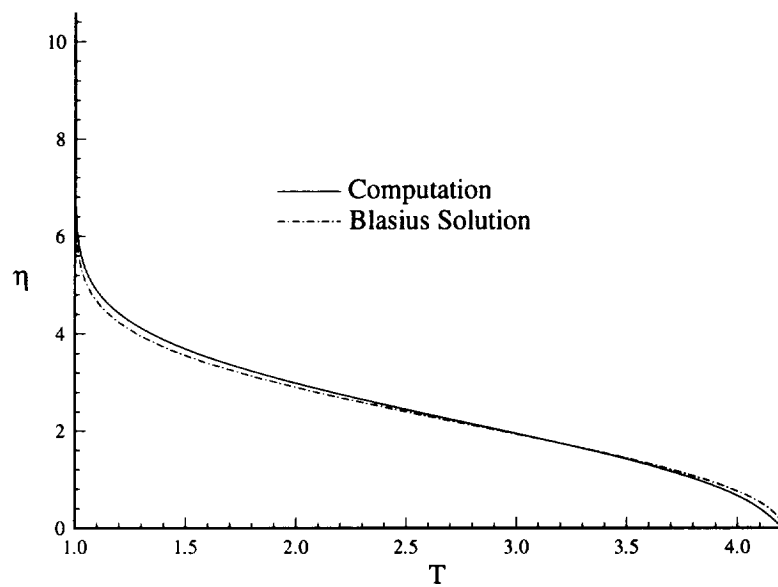
Figure 5.5: T vs. η at $x = 100\delta_o$ for $M_\infty = 4.0$

M_∞	Re_{δ_o}	# of Pts	$\Delta\left(\frac{y^*}{\delta_o}\right)_{min}$	$\Delta\left(\frac{x^*}{\delta_o}\right)_{max}$
.05	47,530	300	.004	.02
.05	47,530	600	.002	.01

Table 5.2: Cases Run for Validation of $x - y$ Code with Existing $\xi - \eta$ Code Using Wall Functions

5.2 Turbulent Validation

In order to validate that the code is correctly solving the equations of motion for turbulent flow problems, the code is compared to an existing standard $k - \epsilon$ model code which utilizes wall functions as the boundary conditions [31]. This second code uses the Levy-Lees transformation ($\xi - \eta$ coordinates) and regrids the TNT interface in the same manner as the first code. [1] For the purpose of validation, the code to be validated also uses wall functions for boundary conditions near the wall, and the low Reynolds number modification is turned off. The governing equations for the two codes are the same, except the $\xi - \eta$ code solves the turbulent kinetic energy equation for k and not $\sqrt{k}$; and a stream function is used in place of the normal velocity v. The incompressible boundary conditions for both codes are given in Tables 2.1 and 2.4.

An incompressible case has been run to verify that the code is accurately solving the solution for the independent variables. Results are seen for the independent variables u,k and ϵ and for the skin friction in Figures 5.6 - 5.12. For convenience the $\bar{}$ has been removed. The solutions for u, k, and ϵ are plotted at $x = 100\delta_o$ and $x = 200\delta_o$. Extremely close agreement is seen between the two codes with errors typically being less than 1%. There is also no appreciable difference in the solutions at the two x locations. The grid resolution study yielded no appreciable difference in the solution for each of the codes, either. As these two codes were developed independently, utilizing two different non-dimensional parameterizations and coordinate systems the possibility

---

[1]This second code was originally developed to test new terms in modeling hypersonic effects in the $k - \epsilon$ model [25]. However, the lack of an acceptable low Reynolds number correction to $k - \epsilon$ model prompted the current research. The second code has been validated against the Blasius solution and adapted to solve boundary layer flow problems using Wall Function boundary conditions by the current author.

of an identical error in coding is highly improbable. We therefore conclude that the present turbulent boundary layer code is validated.
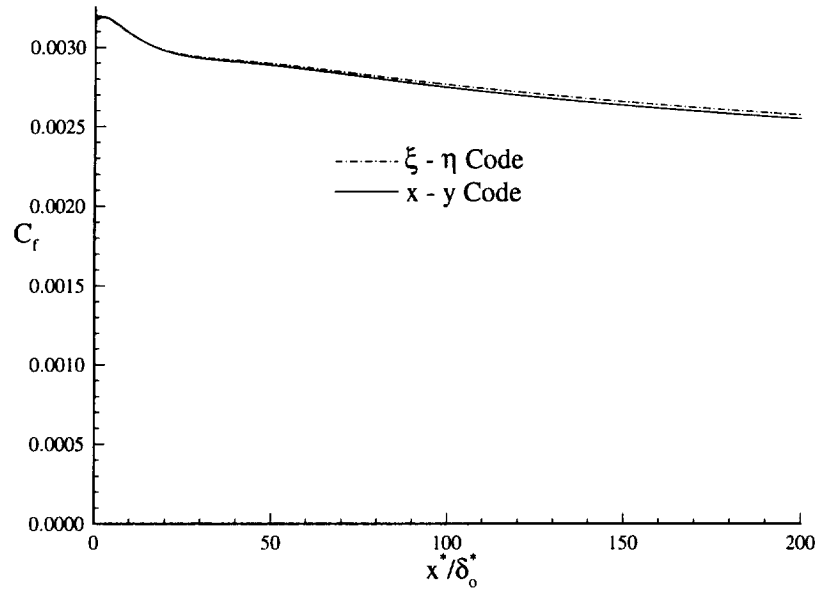
Figure 5.6: Skin Friction vs. $\frac{x}{\delta_o}$ for $\xi - \eta$ and $x - y$ Codes
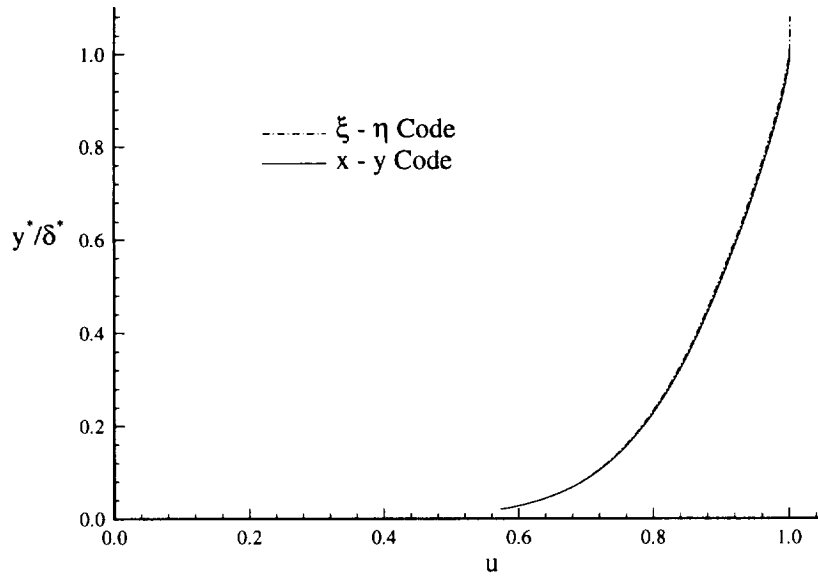
Figure 5.7: $\frac{u}{U_\infty}$ vs. $\frac{y}{\delta}$ at $x = 100\delta_o$
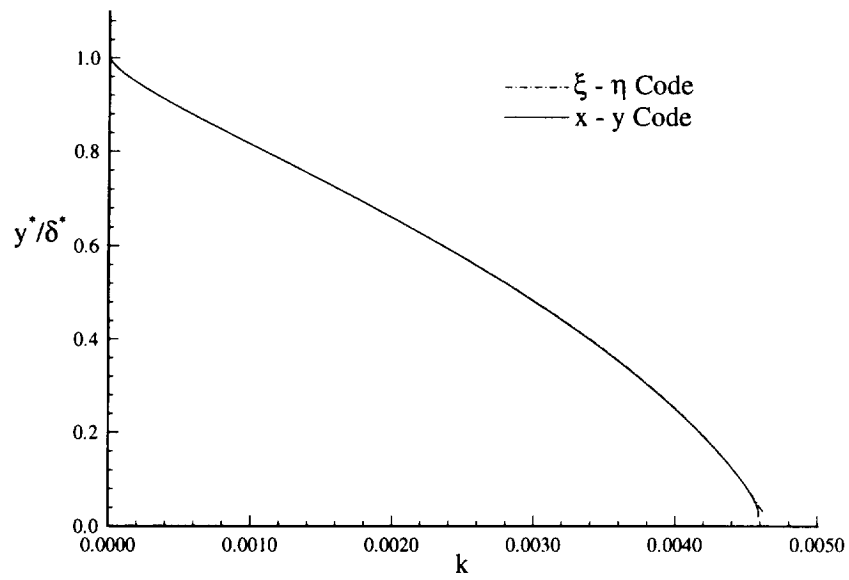
Figure 5.8: $\frac{k}{U_\infty^2}$ vs. $\frac{y}{\delta}$ at $x = 100\delta_o$
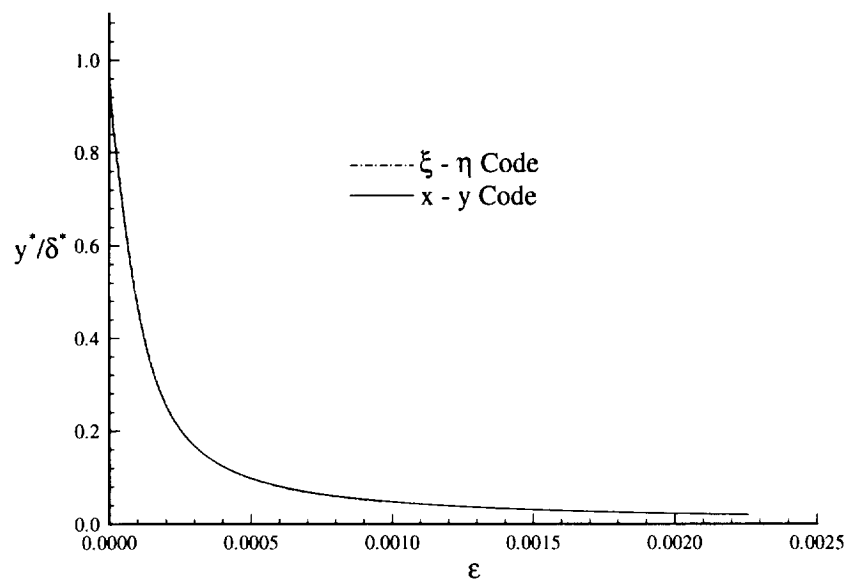
Figure 5.9: $\frac{\epsilon\delta_o}{U_\infty^3}$ vs. $\frac{y}{\delta}$ at $x = 100\delta_o$
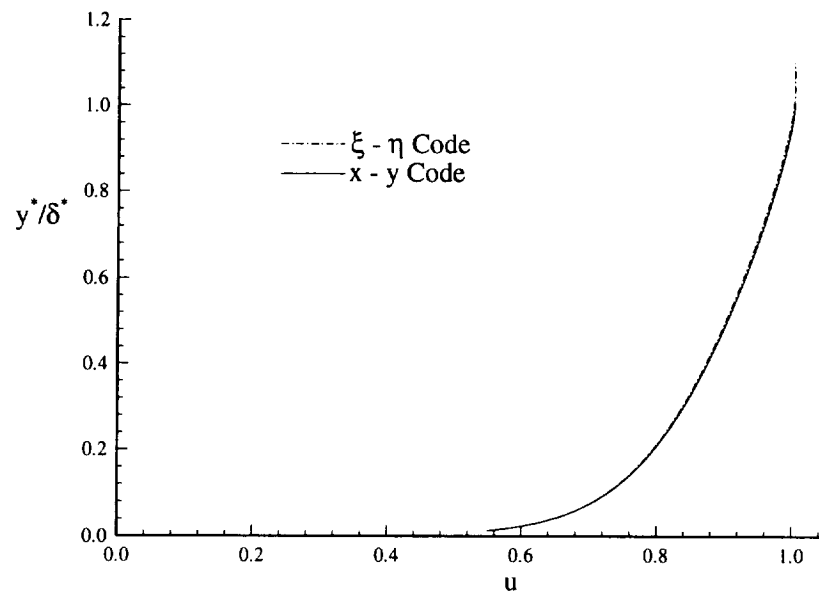
Figure 5.10: $\frac{u}{U_\infty}$ vs. $\frac{y}{\delta}$ at $x = 100\delta_o$
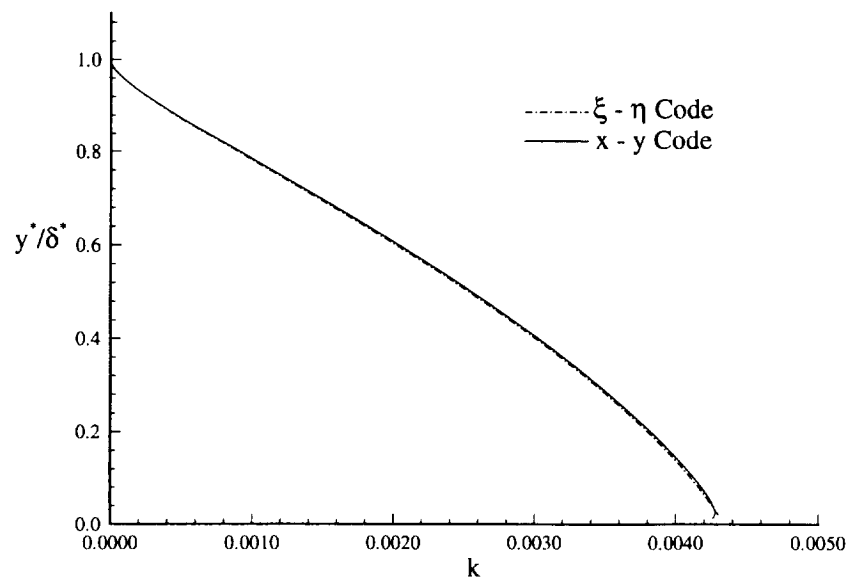
Figure 5.11: $\frac{k}{U_\infty^2}$ vs. $\frac{y}{\delta}$ at $x = 200\delta_o$
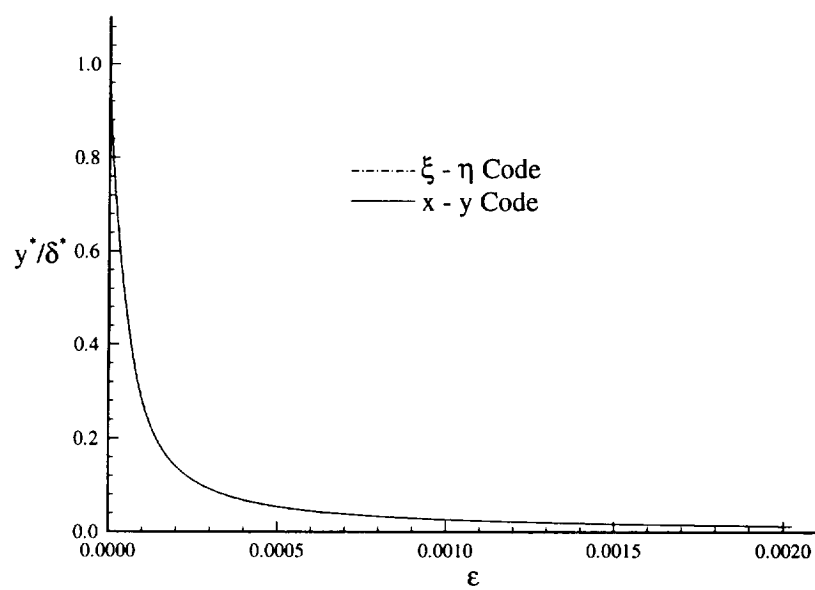
Figure 5.12: $\frac{\epsilon\delta_o}{U_\infty^3}$ vs. $\frac{y}{\delta}$ at $x = 200\delta_o$

Chapter 6

RESULTS

The proposed turbulence model has been tested by examining both high and low Mach number adiabatic flow, high Mach number isothermal flow, and high Mach number adverse pressure gradient flow over a flat plate. Comparisons are made with the experimental results of Weighardt for low Mach number flow; and Fernando and Smits for high Mach number, adverse pressure gradient flow. Solutions are also compared with experimental correlations.

6.1 Incompressible Adiabatic Boundary Layer

Table 6.1 shows the cases run for flows with low Mach number, $M_\infty = .05$, for which the flow is essentially incompressible. Comparisons of the computed profiles have been made with both the experimental data of Weighardt and theoretical correlations. The correlation used in comparing the velocity profile is the Law of the Wall and Wake [6]; while the computed skin friction coefficient is compared to the Karman-Schoenherr equation [16].

- The Incompressible Law of the Wall and Wake

$$u^+ = \frac{1}{\kappa}\ln y^+ + B + \frac{2\Pi}{\kappa}\sin^2\left(\frac{\pi}{2}\frac{y}{\delta}\right) \tag{6.1}$$

$$\kappa = .43$$

$$B = 5.0$$

$$\Pi = .55$$

$$u^+ = \frac{u}{u_\tau}$$

M_∞	Re_{δ_o}	# of Points	$\Delta\left(\frac{y}{\delta_o}\right)_{min}$	$\Delta\left(\frac{x}{\delta_o}\right)_{max}$	$kiso$	$kgrad$	x_{end}/δ_o
.05	14,260	500	4×10^{-6}	.1	0	1	653
.05	14,260	1000	4×10^{-7}	.05	0	1	653

Table 6.1: Cases Run for Low Mach Number, Adiabatic Wall, Integrating to the Wall

- Karman-Schoenherr Equation

$$\frac{1}{\bar{C}_f} = 27.08 \left(\log_{10} \overline{Re_\theta}\right)^2 + 25.11 \log_{10} \overline{Re_\theta} + 6.012 \tag{6.2}$$

For incompressible flows $\bar{C}_f$ and $\overline{Re_\theta}$ are the computed skin friction and momentum thickness Reynolds number respectively. For compressible flows these variables are the transformed values. Experimental data correlates with equation 6.2 to within $\pm 10\%$ of the skin friction [16].

Figures 6.1 and 6.2 compare the computed skin friction with the data of Weighardt and the theoretical value as given by equation 6.2. In these figures, the transient region associated with the initial guess for the independent variables is retained in the plot; however, only the region downstream of the transient should be compared with experiment. The region outside of this initial transient falls within $\pm 10\%$ for both the Weighardt data and the Karman-Schoenherr correlation.

Figure 6.3 compares the computed velocity profile with the experimental data of Weighardt at $Re_\theta = 12,222$. Excellent agreement is achieved between the computation and experimental data. Figure 6.4 compares the same velocity profile against the Law of the Wall. Again excellent agreement is seen, with an almost perfect match in the log region. In this region there is a less than 1% difference between the theoretical and computed velocity. Very good agreement is also achieved between the computed and theoretical velocity defects, $U_\infty^+ - u^+$, as seen in Figure 6.5.

Figure 6.6 compares the computed profile for ϵ^+ and the profile predicted by the DNS data of Spalart [46]. As described in Chapter 3 the choice of $C_{\epsilon 3}$ is made so that the calculated value of ϵ_{wall}^+ matches the value predicted by Spalart. As expected the model accurately predicts the wall value of ϵ^+.

Doubling the number of points perpendicular to the plate, decreasing the order of the first grid point by a factor of 10 and halving the time stepping is seen to have a minimal effect on the solution. The computed solution is found to be independent of the grid employed to less than 1%.
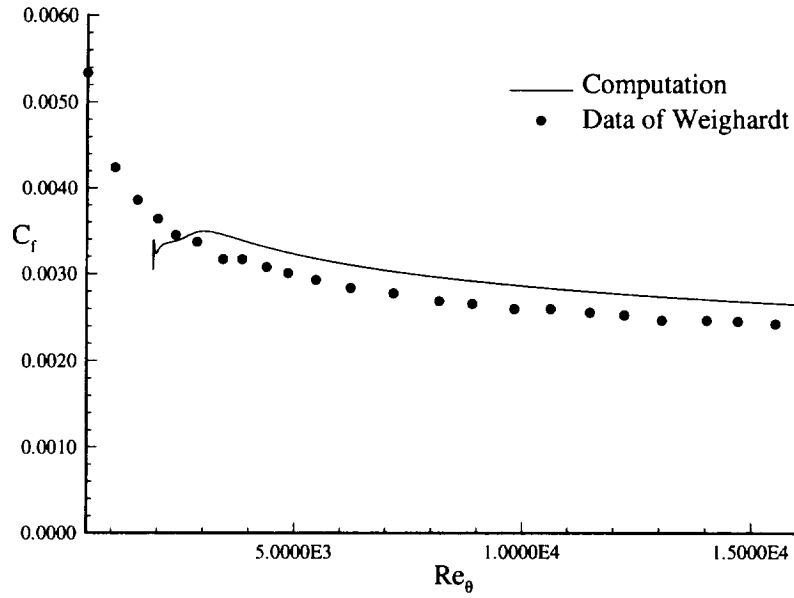
Figure 6.1: Computed Skin Friction and Experimental Data of Weighardt at $M_\infty = .05$ Flow
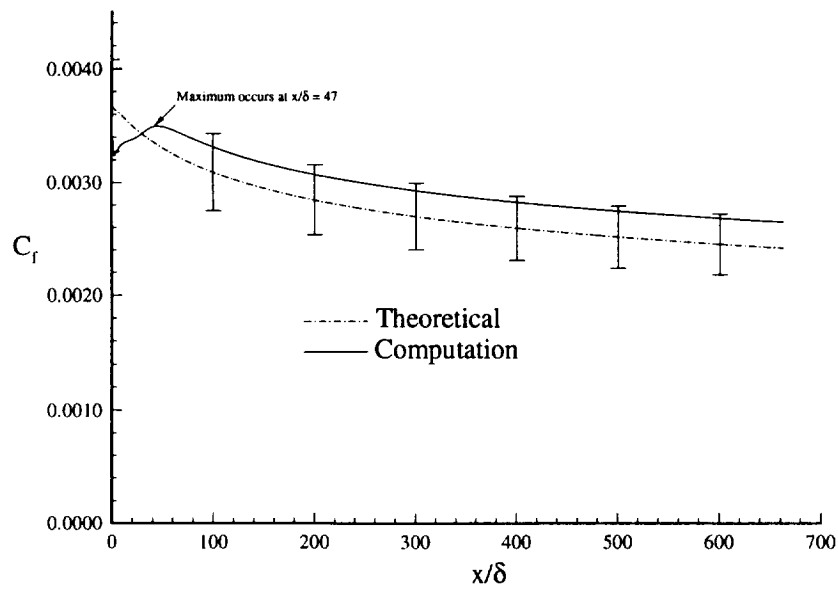
Figure 6.2: Computed and Karman-Schoenherr Theoretical Skin Friction Profiles for $M_\infty = .05$ Flow, Uncertainty in the correlation is $\pm 10\%$.
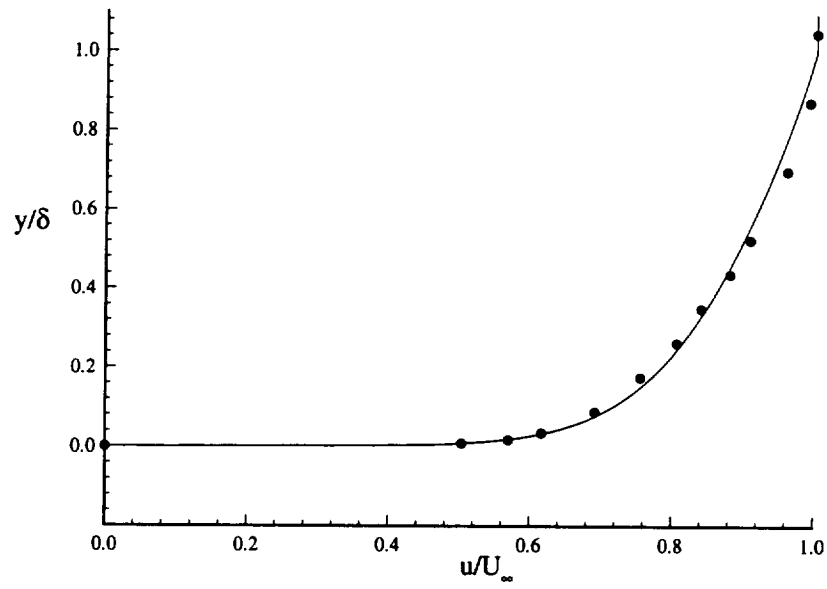
Figure 6.3: Computed Velocity Profile and Experimental Velocity Profile of Weighardt for $M_\infty = .05$
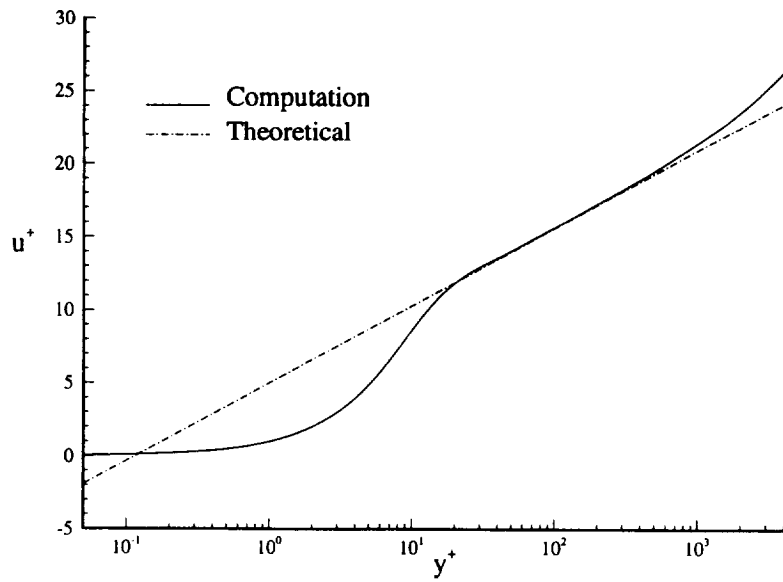
Figure 6.4: Computed and Theoretical Velocity Profiles for $M_\infty = .05$
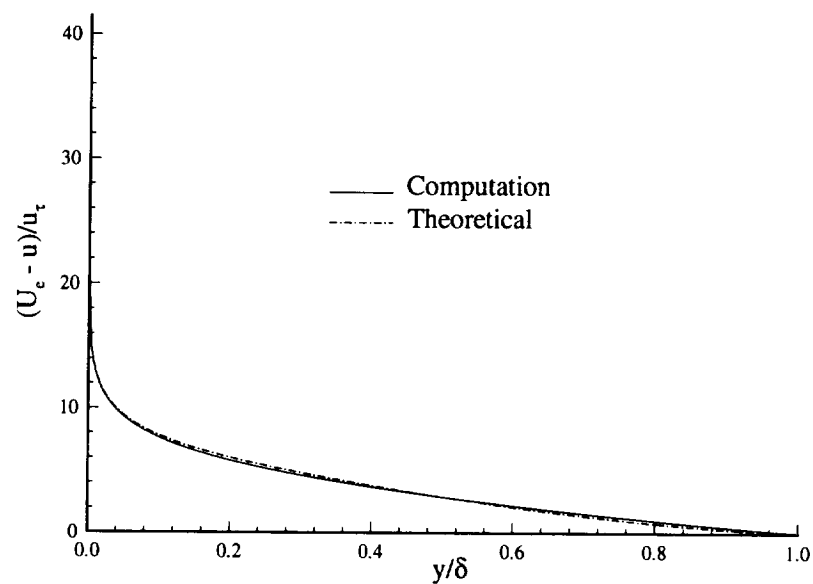
Figure 6.5: Computed and Theoretical Velocity Defect Profiles for $M_\infty = .05$
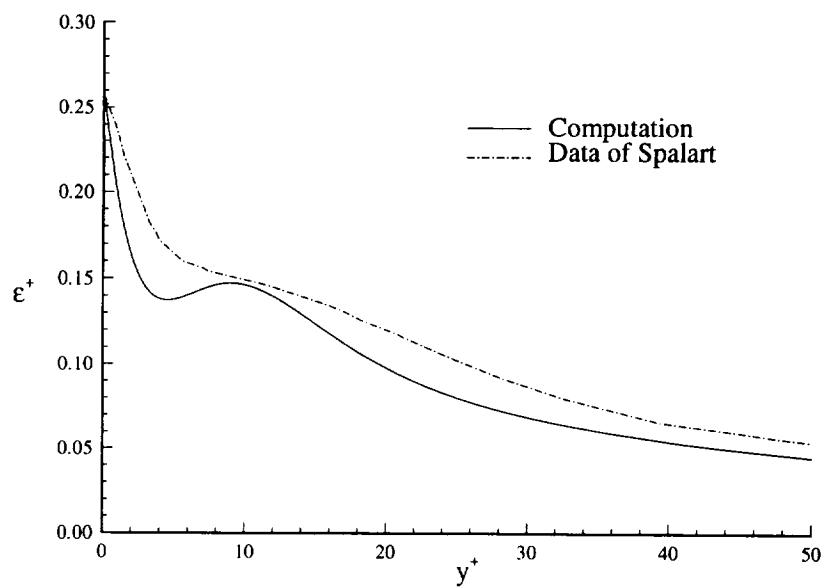
Figure 6.6: Computed and DNS Data of Spalart for ϵ^+

6.2 High Mach Number

Three different Mach numbers have been examined, each with two boundary conditions for the temperature. These conditions correspond to an adiabatic wall and an isothermal wall with $T_{wall}/T_{adia} = 0.4$. An examination has been made comparing the transformed velocity profile with the compressible Law of the Wall and the Law of the Wake [6], and comparing the computed skin friction with the Van Driest II theory [16].

The low Reynolds number correction employed has been developed based upon incompressible assumptions, but has been utilized for compressible flow cases in order to see the effect compressibility has on the solution. As many practical engineering applications requiring two equation turbulence models occur at high Mach numbers, it is important to test any model in the supersonic regime. In performing this analysis no new modifications have been made to the governing equations to account for compressibility effects. Morkovin's hypothesis has been assumed. Therefore only changes in the mean density are taken into account, with fluctuations to the mean density assumed small relative to changes in the mean density [54], [37]. The turbulent Reynolds number used in calculating the low Reynolds number modifications is defined by

$$R_t = \frac{\rho k^2}{\mu \epsilon} \tag{6.3}$$

For each of the cases run a grid analysis has been completed demonstrating that the solution of the independent variables is independent of the grid employed to within less than 1%.

Comparisons have been made between the computed skin friction coefficient, the computed velocity, and the computed wall temperature with theoretical values. The theoretical skin friction coefficient is based upon the Van Driest II theory [16]. The Van Driest II theory modifies the Karman-Schoenherr equation and the computed Reynolds number based on the momentum thickness by a compressibility correction

$$C_f = \bar{C}_f F_c \tag{6.4}$$

$$\overline{Re_\theta} = F_\theta Re_\theta \tag{6.5}$$

where

$$F_c = .18M_e^2 / \left(\sin^{-1}\alpha + \sin^{-1}\beta \right) \tag{6.6}$$

$$F_\theta = \frac{\mu_e}{\mu_{wall}} \tag{6.7}$$

$$\alpha = (2A^2 - B)/(4A^2 + B^2)^{\frac{1}{2}} \tag{6.8}$$

$$\beta = B/(4A^2 + B^2)^{\frac{1}{2}} \tag{6.9}$$

$$A = .9T_e/T_{wall} \tag{6.10}$$

$$B = \frac{T_e \left(1.9 - \frac{T_e}{T_{wall}} \right)}{T_{wall}} \tag{6.11}$$

As in the Karman-Schoenherr equation there is an estimated uncertainty of $\pm 10\%$ in the Van Driest II theory [16].

The computed velocity profile is compared to the compressible Law of the Wall and Wake by transforming the computed stream-wise velocity. The transformed non-dimensional velocity is defined by

$$u_c = \frac{1}{A}\sin^{-1}\left(\frac{2A^2 u - B}{\sqrt{B^2 + 4A^2}} \right) + \frac{1}{A}\sin^{-1}\left(\frac{B}{\sqrt{B^2 + 4A^2}} \right) \tag{6.12}$$

where

$$A = \sqrt{Pr_T \frac{\gamma - 1}{2} M_\infty^2 \frac{1}{T_{wall}}} \tag{6.13}$$

$$B = -\frac{Pr_T Q_{wall}(\gamma - 1)M_\infty^2}{\rho_e T_e u_\tau^2} \tag{6.14}$$

The theoretical compressible Law of the Wall and Wake is given by

$$u_c = \frac{u_\tau}{\kappa}\ln y^+ + Bu_\tau + \frac{2\Pi u_\tau}{\kappa}\sin^2\left(\frac{\pi}{2}\frac{y}{\delta} \right) \tag{6.15}$$

The constants are the same as used for the incompressible Law of the Wall and Wake. Both the inner log region and outer wake region are examined. The inner, log region directly compares the transformed velocity profile with the Law of the Wall, while the outer region is compared by examining the velocity Defect Law

$$U_{c\infty}^+ - u_c^+ = \frac{1}{\kappa}\left(2\Pi\left[1 - \sin^2\left(\frac{\pi}{2}\frac{y}{\delta} \right) \right] - \ln\frac{y}{\delta} \right) \tag{6.16}$$

which arises from equation 6.15. $U_{c\infty}^+$ is the transformed velocity at the edge of the boundary layer, δ, divided by the friction velocity.

M_∞	$Re_{\delta_o} \times 10^3$	# of Points	$\Delta \left(\frac{y}{\delta_o}\right)_{min}$	$\Delta \left(\frac{x}{\delta_o}\right)_{max}$	$kiso$	$kgrad$	x_{end}/δ_o
2.0	1,901	500	4×10^{-6}	.02	0	1	200
2.0	1,901	1000	4×10^{-7}	.01	0	1	100
4.0	3,802	500	4×10^{-6}	.02	0	1	200
4.0	3,802	1000	4×10^{-7}	.01	0	1	100
6.0	5,703	500	4×10^{-6}	.02	0	1	200
6.0	5,703	1000	4×10^{-7}	.01	0	1	100

Table 6.2: Cases Run for High Mach Number, Adiabatic Wall, Integrating to the Wall

6.2.1 Compressible Adiabatic Boundary Layer

Table 6.4 shows the cases run while integrating to an adiabatic wall employing the low Reynolds correction at three different high Mach numbers. It has been observed that there is less than a 1% difference between the solutions when the grid spacing is modified as shown. For each of these cases the computation is run until the transient associated with initial guess for dependent variables vanishes. At this point the computation is continued for another $1000\delta_o$, to acquire solutions with which to compare with theoretical profiles. Figures 6.7, 6.8 and 6.9 compare the computed and theoretical skin friction profiles. For each of the Mach numbers, the computed skin friction falls within the 10% uncertainty in the Van Driest II theory [16].

Figures 6.10, 6.11 and 6.12 compare the computed, transformed velocity profile to the Law of the Wall. It may be seen that in the log region there is excellent agreement between the computed and theoretical solutions. For the theoretical solutions κ is chosen to be equal to .43 as predicted by the standard $k - \epsilon$ model [54]. With increased Mach number it is seen that the height of the log region decreases.

Figures 6.13, 6.14 and 6.15 compare the computed and theoretical transformed velocity defect as described by equation 6.16. Excellent agreement is achieved at $M_\infty = 2.0$. There is increasing deviation from the anticipated result with higher Mach number.

Figures 6.16, 6.17 and 6.18 and Table 6.3 compare the evolution of the computed adiabatic wall temperature with the result, as seen in equation 6.17, obtained from the

asymptotic analysis of the turbulence model equations [28].

$$\frac{T_{adia}}{T_\infty} = 1 + \frac{\gamma - 1}{2}\sqrt{Pr_T}M_\infty^2 \tag{6.17}$$

Close agreement is achieved, but it is observed that the deviation from the theoretical increases with increasing Mach number. The more common expression for the theoretical adiabatic wall temperature is to replace $\sqrt{Pr_T}$ by Pr_T in equation 6.17. A comparison of the computed result with this new theoretical value shows a difference of less than 2% over the range of Mach numbers.

M_∞	$T_{adia|calc}/T_\infty$	$T_{adia|theory}/T_\infty$	$\%error$
2.0	1.71	1.76	2.8
4.0	3.85	4.04	4.7
6.0	7.34	7.83	6.3

LEGEND

$T_{adia|calc}/T_\infty$ is the calculated adiabatic wall temperature

$T_{adia|theory}/T_\infty$ is the theoretical adiabatic wall temperature from equation 6.17

Table 6.3: Theoretical and Calculated Adiabatic Wall Temperature
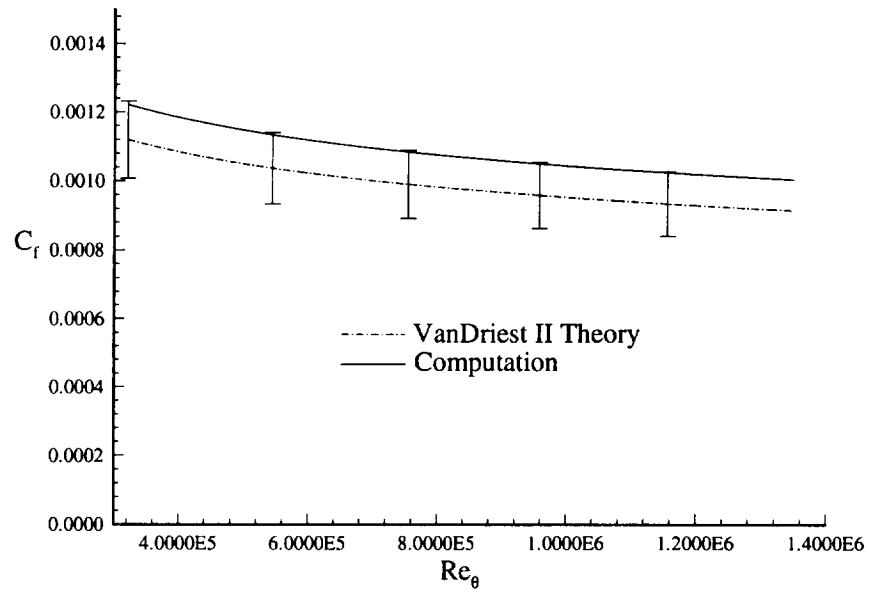
Figure 6.7: Computed and Theoretical Skin Friction Profiles for Adiabatic, $M_\infty = 2$ Flow
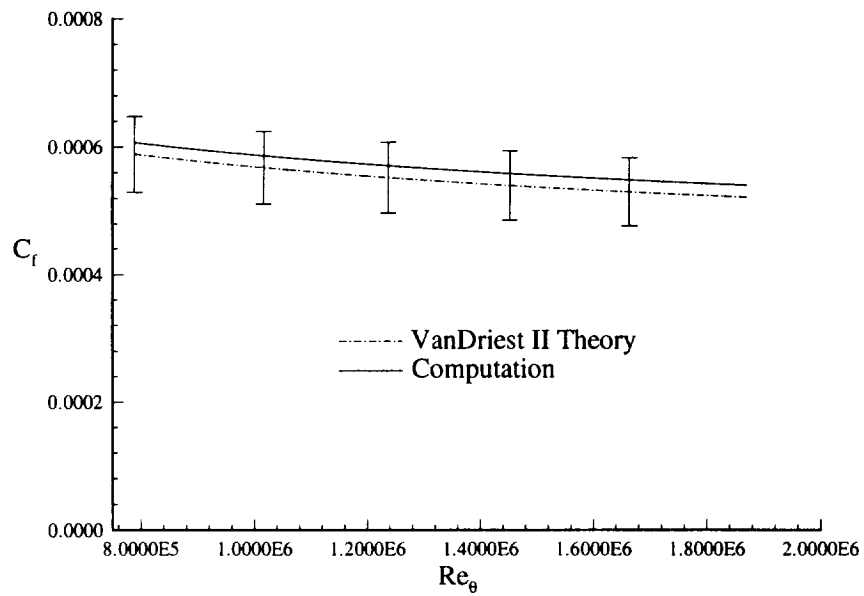
Figure 6.8: Computed and Theoretical Skin Friction Profiles for Adiabatic, $M_\infty = 4$ Flow
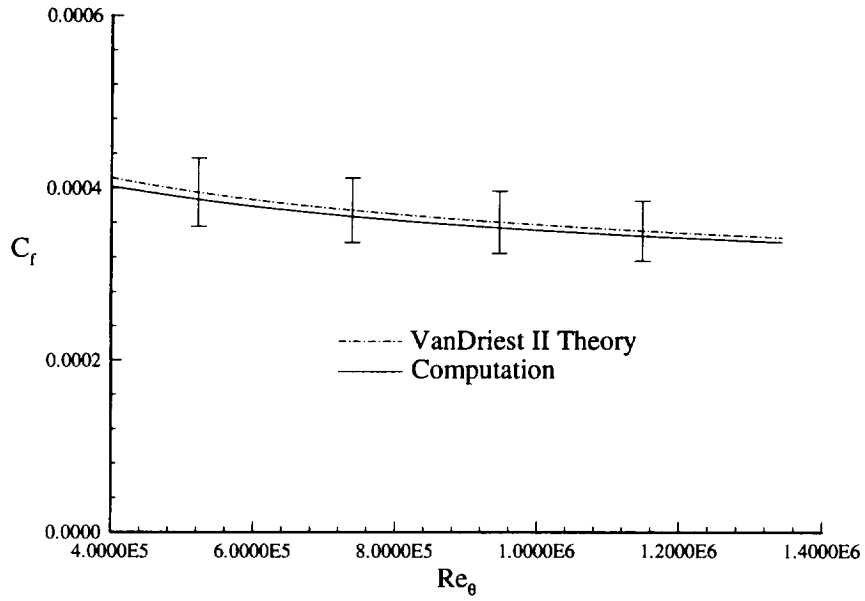
Figure 6.9: Computed and Theoretical Skin Friction Profiles for Adiabatic, $M_\infty = 6$ Flow
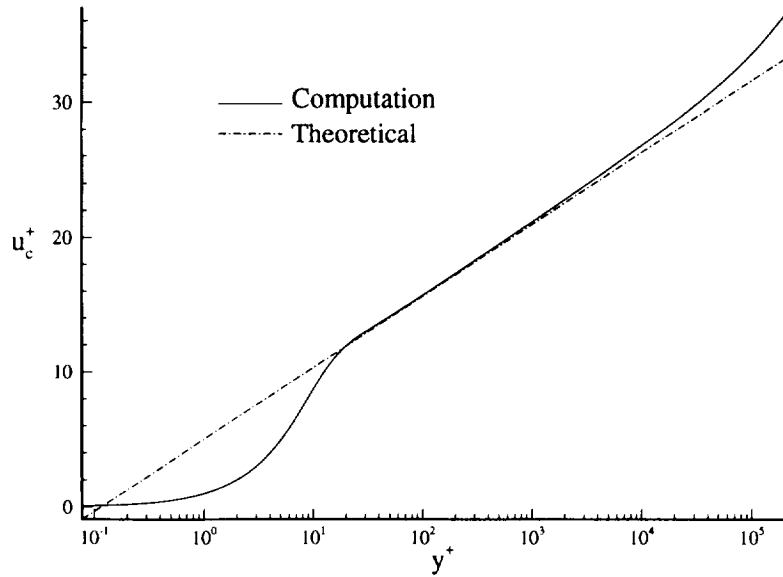
Figure 6.10: Computed and Theoretical Transformed Velocity Profiles for Adiabatic, $M_\infty = 2$ Flow
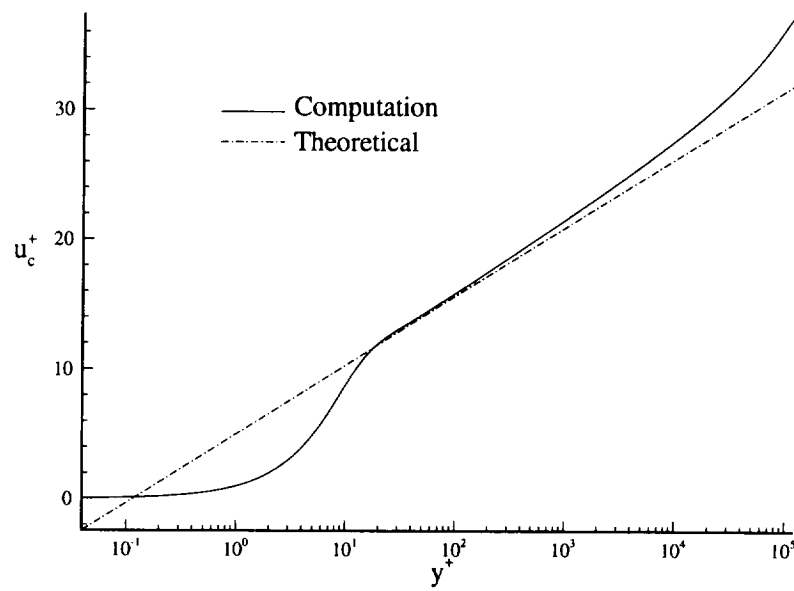
Figure 6.11: Computed and Theoretical Transformed Velocity Profiles for Adiabatic, $M_\infty = 4$ Flow
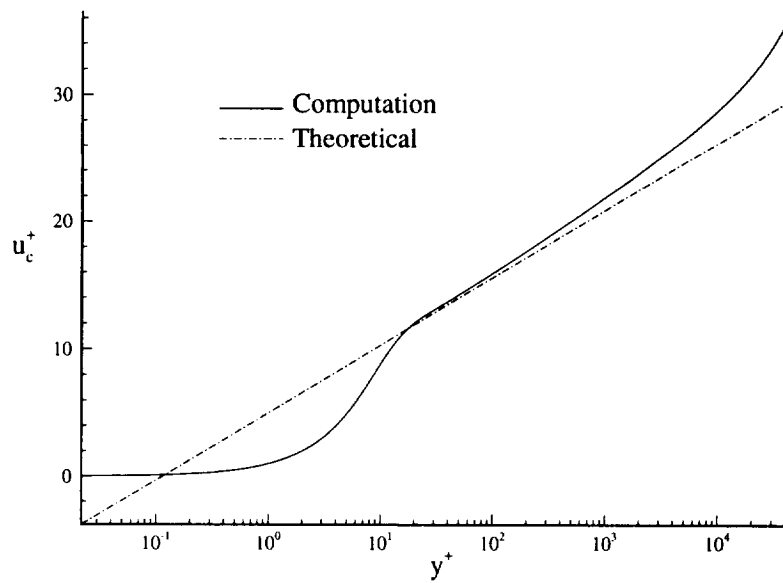
Figure 6.12: Computed and Theoretical Transformed Velocity Profiles for Adiabatic, $M_\infty = 6$ Flow
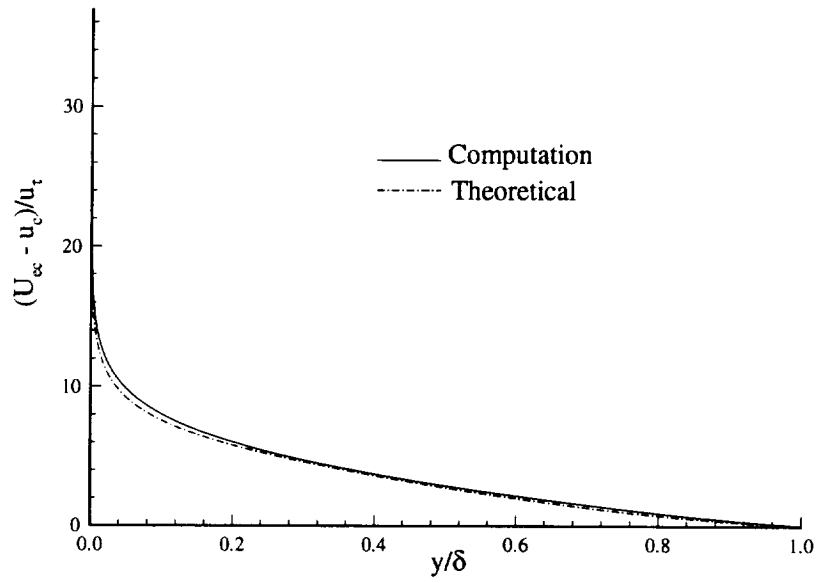
Figure 6.13: Computed and Theoretical Transformed Velocity Defect Profiles for Adiabatic, $M_\infty = 2$ Flow
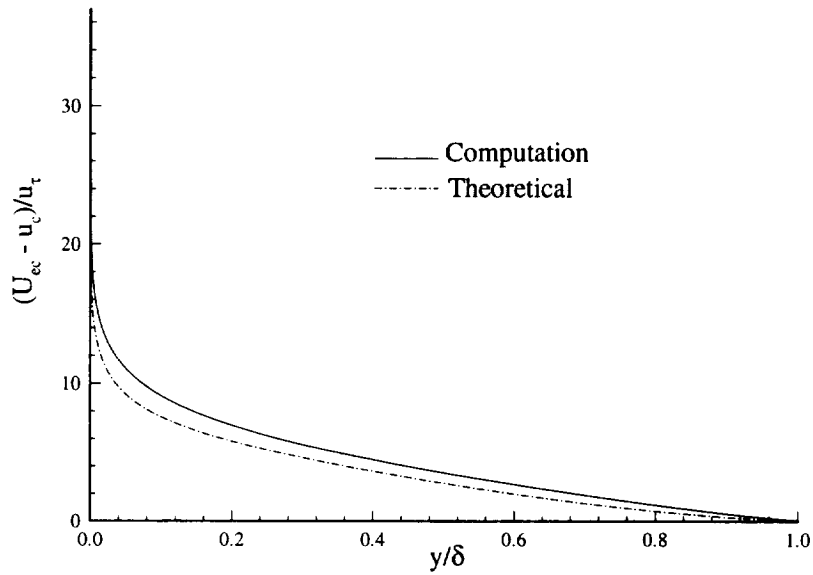
Figure 6.14: Computed and Theoretical Transformed Velocity Defect Profiles for Adiabatic, $M_\infty = 4$ Flow
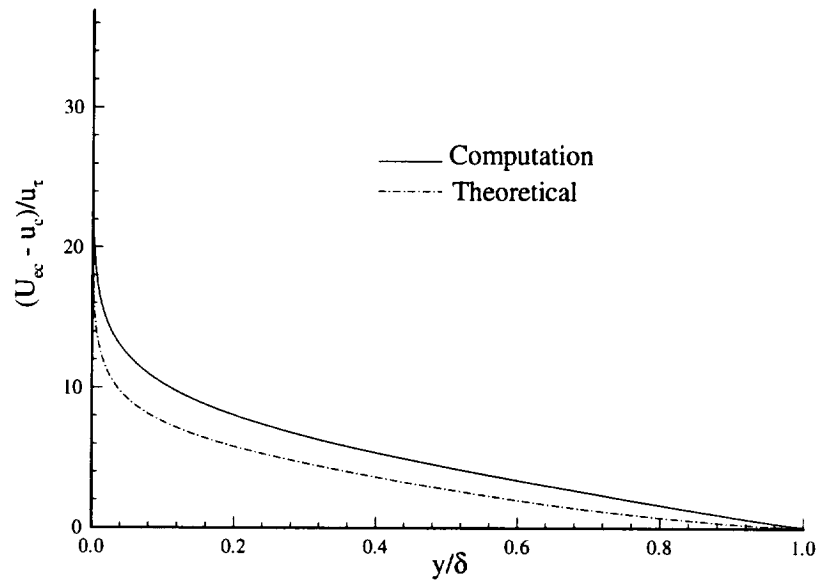
Figure 6.15: Computed and Theoretical Transformed Velocity Defect Profiles for Adiabatic, $M_\infty = 6$ Flow
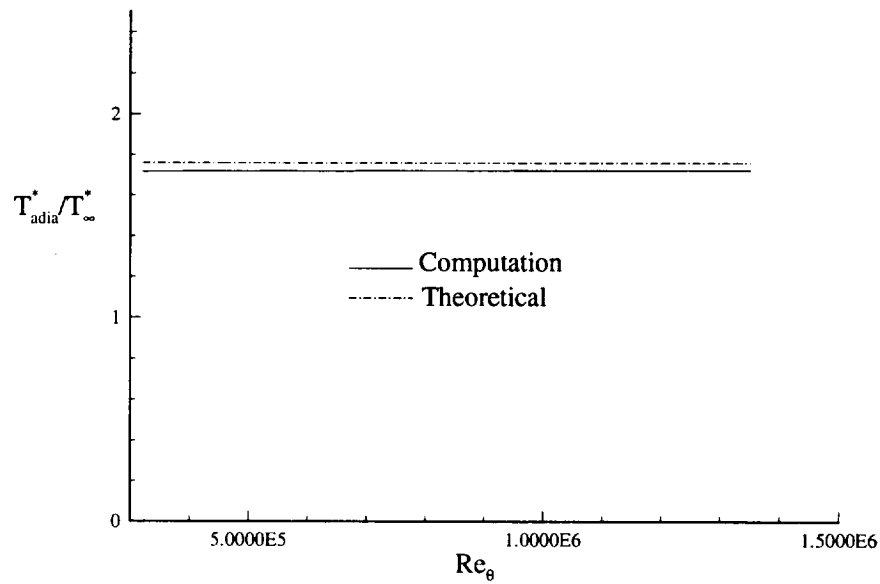
Figure 6.16: Computed and Theoretical Adiabatic Wall Temperature for $M_\infty = 2$ Flow
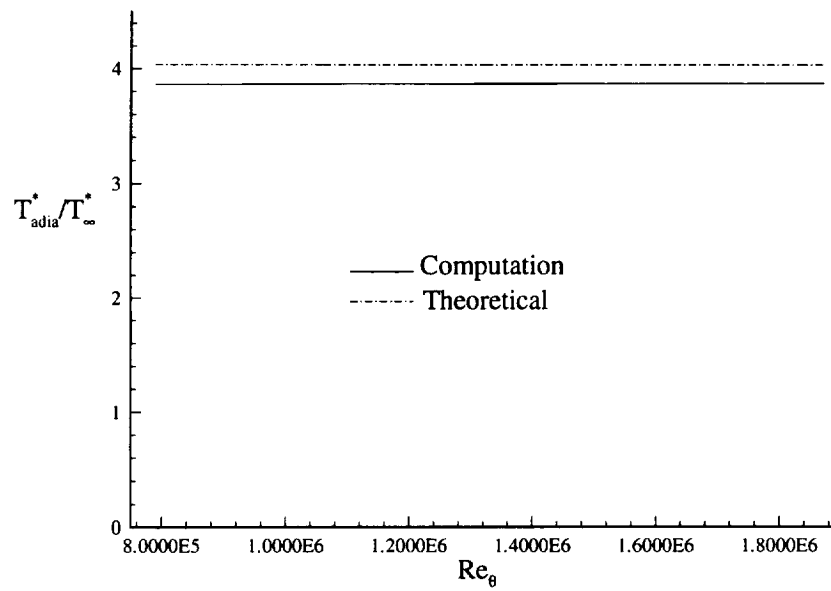
Figure 6.17: Computed and Theoretical Adiabatic Wall Temperature for $M_\infty = 4$ Flow
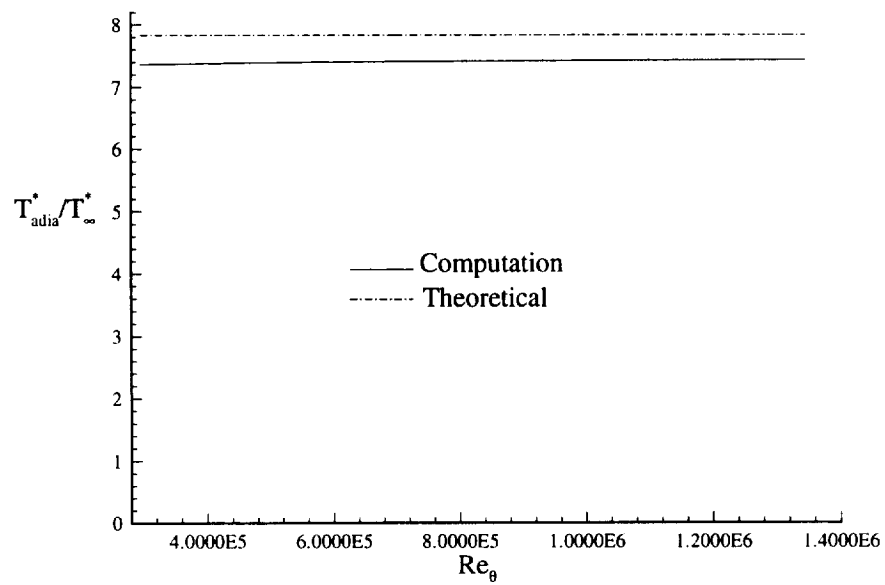
Figure 6.18: Computed and Theoretical Adiabatic Wall Temperature for $M_\infty = 6$ Flow

M_∞	$Re_{\delta_o} \times 10^3$	# of Pts	$\Delta\left(\frac{y}{\delta_o}\right)_{min}$	$\Delta\left(\frac{x}{\delta_o}\right)_{max}$	$kiso$	$kgrad$	x_{end}/δ_o
2.0	1,901	500	4×10^{-6}	.02	1	1	200
2.0	1,901	1000	4×10^{-7}	.01	1	1	100
4.0	3,802	500	4×10^{-6}	.02	1	1	200
4.0	3,802	1000	4×10^{-7}	.01	1	1	100
6.0	5,703	500	5×10^{-6}	.02	1	1	200
6.0	5,703	1000	5×10^{-7}	.01	1	1	100

Table 6.4: Cases Run for High Mach Number, Isothermal Wall ($T_{wall}/T_{adia} = 0.4$), Integrating to the Wall

6.2.2 Compressible Isothermal Boundary Layer

A series of cases have been examined for an isothermal, flat plate boundary layer with $T_{wall}/T_{adia} = 0.4$ where T_{adia} is given by equation 6.17. The Mach numbers and Reynolds numbers are the same as for the adiabatic, flat plate boundary layer. These cases are run by first computing the solution for the adiabatic, flat plate boundary layer and then modifying the boundary condition for the temperature such that the wall is slowly cooled. This precludes the necessity of finding a good first guess for the temperature profile in the viscous sublayer. The solution is found through a series of $5 - 6$ cooling steps. Once the desired wall temperature is obtained the solution is run until the transients associated with the initial profile at that wall temperature have become negligible. The solution is then marched downstream for another $2000\delta_o$, where δ_o is the initial guess for the boundary layer height associated with the initial adiabatic calculation. The value of the local boundary layer height at the beginning of the final cooling process is approximately $10 \times \delta_o$.

Figures 6.19, 6.20 and 6.21 compare the computed and theoretical skin friction profiles. It is seen that the computed skin friction falls within the 10% uncertainty of the Van Driest II theory for $M_\infty = 4$ and $M_\infty = 6$ and varies above this uncertainty at 15% for $M_\infty = 2$.

Figures 6.22, 6.23 and 6.24 compare the computed, transformed velocity profile to the compressible Law of the Wall. It may be seen that in the log region there is good agreement between the computed and theoretical solutions. There does appear

to be a deviation from the theoretical value of B in the compressible Law of the Wall. For an isothermal, compressible, flat plate boundary layer, with $T_{wall}/T_{adia} = 0.4$ the computation predicts B to be approximately equal to 4 instead of 5.

Figures 6.25, 6.26 and 6.27 compare the computed and theoretical transformed velocity defect. There is slightly better agreement achieved in the velocity defect for the isothermal flat plate boundary layer than that achieved at the same Mach number for an adiabatic wall.

Table 6.5 displays the computed Reynolds analogy factor and the deviation from the theoretical value. The Reynolds analogy factor is defined as

$$\frac{2C_h}{C_f} \equiv \frac{Q^*_{wall}}{\rho_\infty U_\infty C_p (T^*_{wall} - T^*_{adia})} \tag{6.18}$$

From asymptotic analysis of the model equations [28] the theoretical value is

$$\frac{2C_h}{C_f} = \frac{1}{Pr_T} = 1.1 \tag{6.19}$$

There is increased agreement between the theoretical value and the computation with increasing Mach number.

M_∞	$2C_h/C_f$	$\%error$
2.0	1.33	20.9
4.0	1.24	12.7
6.0	1.15	4.5

Table 6.5: Reynolds Analogy Factor, $T_{wall}/T_{adia} = 0.4$
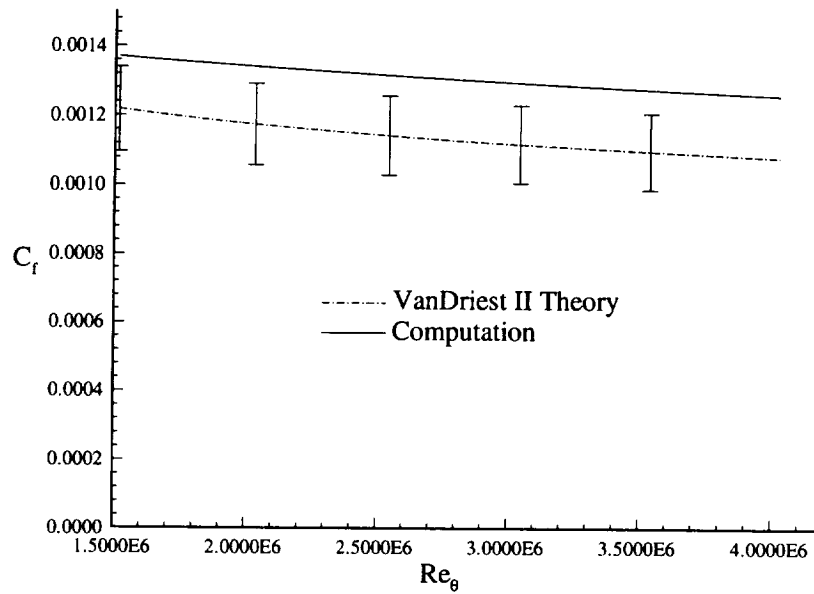
Figure 6.19: Computed and Theoretical Skin Friction Profiles for Isothermal $(T_{wall}/T_{adia} = 0.4)$, $M_\infty = 2$ Flow
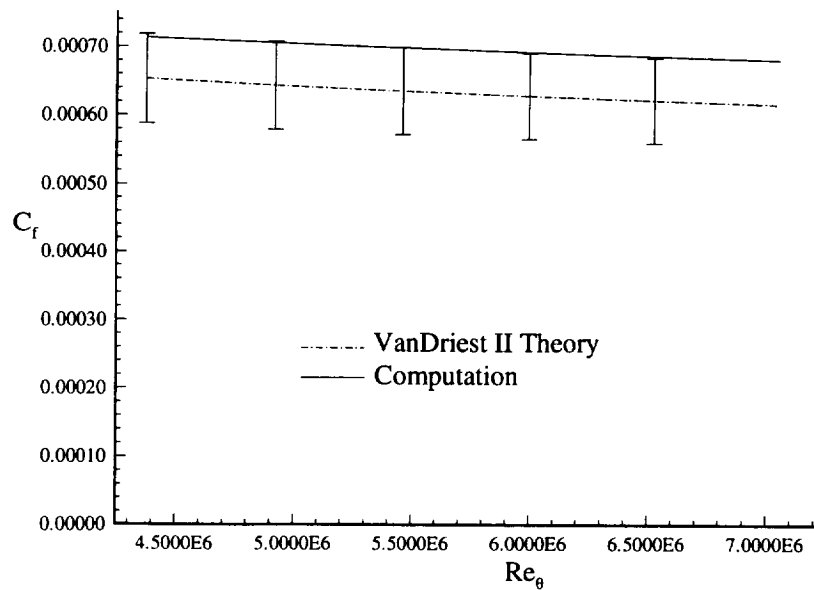
Figure 6.20: Computed and Theoretical Skin Friction Profiles for Isothermal $(T_{wall}/T_{adia} = 0.4)$, $M_\infty = 4$ Flow
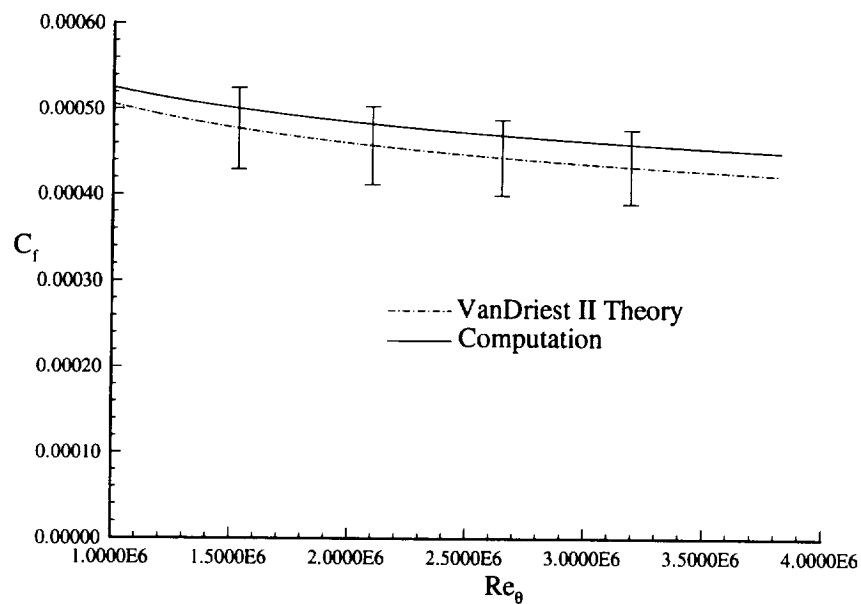
Figure 6.21: Computed and Theoretical Skin Friction Profiles for Isothermal $(T_{wall}/T_{adia} = 0.4)$, $M_\infty = 6$ Flow
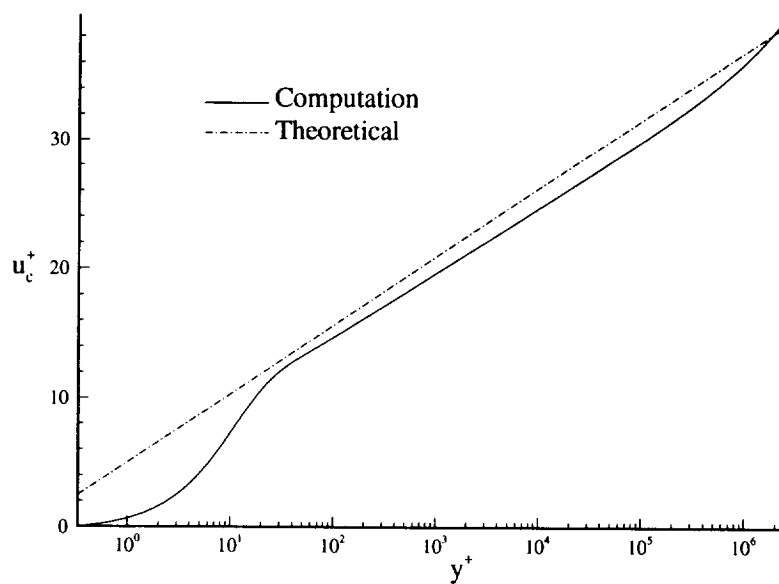
Figure 6.22: Computed and Theoretical Transformed Velocity Profiles for Isothermal $(T_{wall}/T_{adia} = 0.4)$, $M_\infty = 2$ Flow

Figure 6.23: Computed and Theoretical Transformed Velocity Profiles for Isothermal $(T_{wall}/T_{adia} = 0.4)$, $M_\infty = 4$ Flow
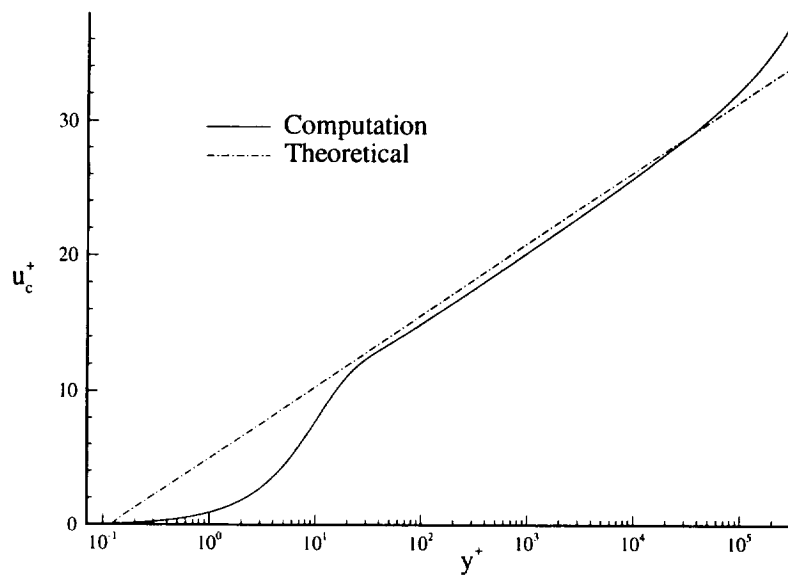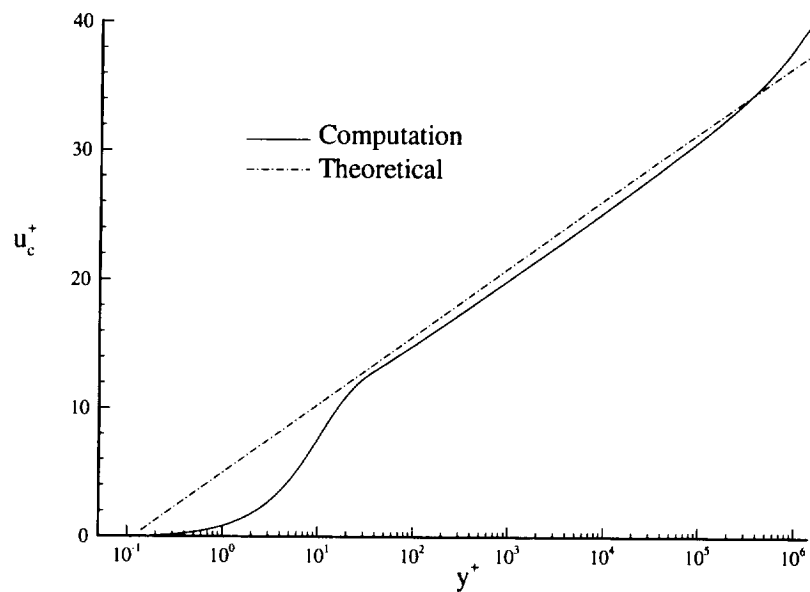
Figure 6.24: Computed and Theoretical Transformed Velocity Profiles for Isothermal $(T_{wall}/T_{adia} = 0.4)$, $M_\infty = 6$ Flow
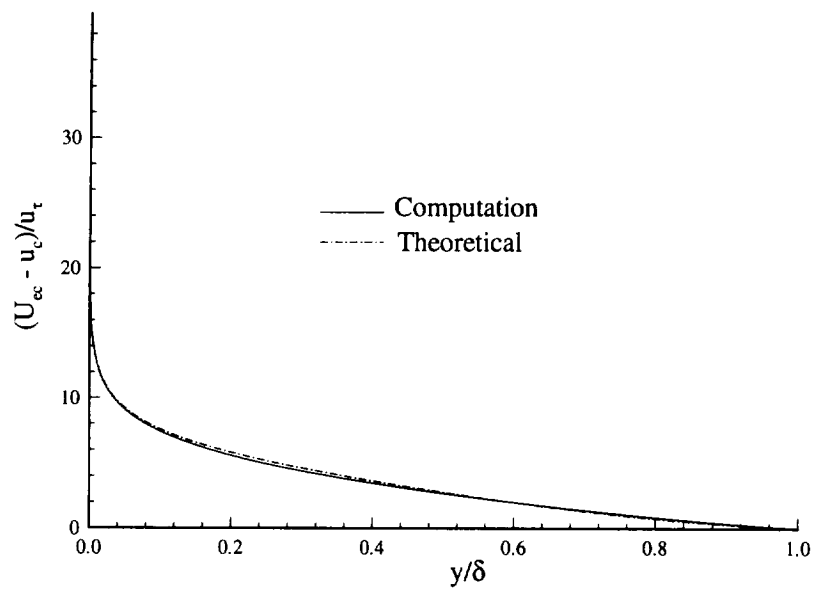
Figure 6.25: Computed and Theoretical Transformed Velocity Defect Profiles for Isothermal $(T_{wall}/T_{adia} = 0.4)$, $M_\infty = 2$ Flow
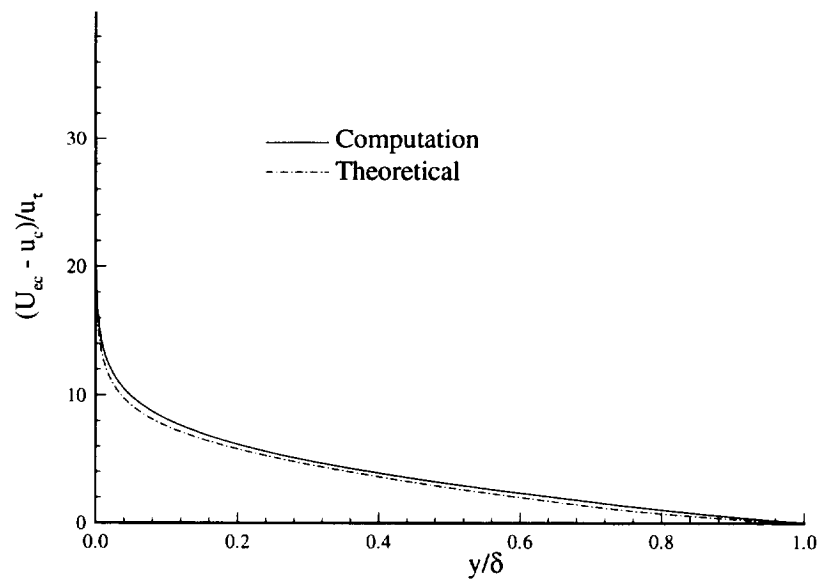
Figure 6.26: Computed and Theoretical Transformed Velocity Defect Profiles for Isothermal $(T_{wall}/T_{adia} = 0.4)$, $M_\infty = 4$ Flow
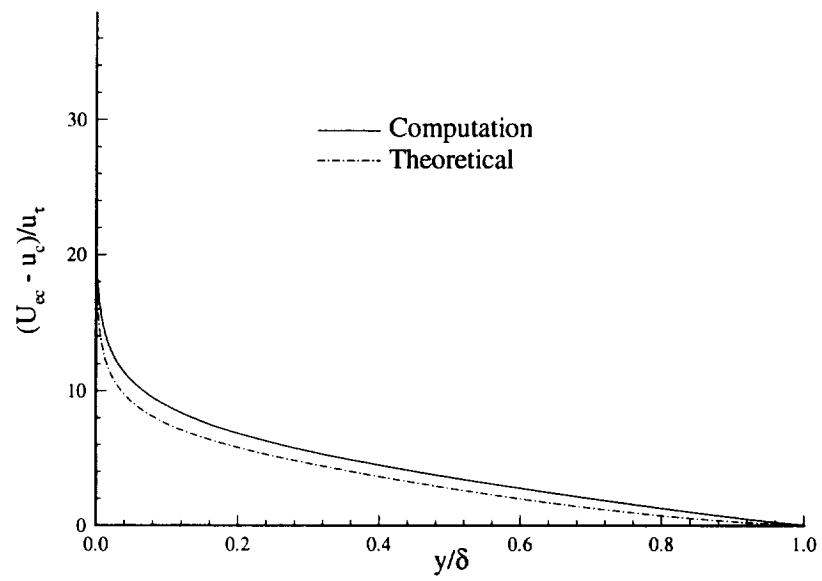
Figure 6.27: Computed and Theoretical Transformed Velocity Defect Profiles for Isothermal $(T_{wall}/T_{adia} = 0.4)$, $M_\infty = 6$ Flow

6.3 Adverse Pressure Gradient

A comparison of the computational result has been made for flow over a flat plate experiencing an adverse pressure gradient with the experimental results of Fernando and Smits [10], [11], [43]. Fernando and Smits calculated the properties of a $M_\infty = 2.92$ adverse pressure gradient flow. Complete details of this experiment are given in [11]. Single normal hot wire and crossed wires were utilized to acquire the data, including the velocity profile, surface shear stress, Mach profile and the Reynolds stress.

The same flow conditions at the flow inlet are employed as that given by Fernando. These conditions are denoted by ∞. For simplicity the point where the pressure gradient is begun is denoted $x = x^*/\delta_o = 0$ where $\delta_o = 24.69$mm is the initial boundary layer height at this point, as computed numerically. To ensure a converged solution at $x = 0$ the numerical solution is marched until the point where the Reynolds number based upon displacement thickness, Re_ψ, in the code matches the inlet value of the experimental data at $x = 0$. The properties of the inflow for the experiment and computation are given in Table 6.6. Using the definition of boundary layer height defined in Chapter 4 it is seen that the numerical solution underpredicts the value of the initial boundary layer height, δ_o, with the experimental result of Fernando by less than 5% at $x = 0$, however, the momentum thickness is overpredicted by approximately 10%. The definition of the boundary layer height employed by Fernando et al is that the "boundary layer height is the measurement point closest to that point where

$$P_{0e} - P_{0\delta} = .02[P_{0e} - P_w] \tag{6.20}$$

P_{0e} is the tunnel stagnation pressure in the freestream and it is equal to the tunnel stagnation pressure, within experimental error" [11]. This varies from the definition employed in the computation and may, along with experimental error, account for this small discrepancy.

Figure 6.28 shows the experimental surface pressure and the pressure employed in computationally calculating the flow behavior. The wall surface static pressure is used because, as seen in Chapter 2, it is assumed that the pressure is constant across the boundary layer. The data of Fernando shows this to be true within the ±4%

Property	Experiment	Code	Percent Error
M_∞	2.92	2.92	0.0
Re_ψ	453,600	453,600	0.0
Re_{δ_o}	1,663,200	1,582,000	4.8
Re_θ	75,600	83,400	9.4

Table 6.6: Adverse Pressure Gradient Incoming Flow Conditions at $x = 0$

experimental error. It is necessary to smooth the experimental pressure distribution of Fernando to avoid numerical oscillations. To evaluate the effect of this smoothing two pressure distributions are calculated to simulate the experimental data. The first (Case 1 Δp) is a very smooth case of the experimental pressure distribution, while the second case (Case 2 Δp) more accurately matches the given profile. It is seen below that there is little difference between the solution of these two cases. For this reason either may be chosen to represent the experimental pressure distribution.

In order to guarantee the solution is independent of the grid spacing, a grid resolution study has been performed. The parameters implemented in running each of the cases are given in Table 6.7. It is found that the solution is independent of the grid spacing chosen to less than 1% for both Case 1 Δp and Case 2 Δp.

M_∞	Re_ψ	# of Pts	$\Delta\left(\frac{y}{\delta_o}\right)_{min}$	$\Delta\left(\frac{x}{\delta_o}\right)_{max}$	$kiso$	$kgrad$	x_{end}/δ_o
2.92	453,600	500	2.63×10^{-6}	6.579×10^{-3}	0	1	16.0
2.92	453,600	1000	2.63×10^{-7}	3.290×10^{-3}	0	1	16.0

Table 6.7: Cases Run for High Mach Number, Adiabatic, Adverse Pressure Gradient Flow

Figure 6.29 compares the computed skin friction profile with that found by Fernando *et al*, where the assumed experimental uncertainty in the skin friction is $\pm 10\%$. In order to alleviate any problems that may arise with the definition of the boundary layer height, the skin friction is evaluated using the inlet conditions at ∞, such that

$$C_{f\infty} \equiv \frac{\tau_{wall}}{\frac{1}{2}\rho_\infty U_\infty^2} \tag{6.21}$$

Fernando calculates the wall shear stress in three ways. The first is to use Preston probe

measurements and reduce the data according to the calibration scheme of Bradshaw and Unsworth [2], [11]. The second method is to transform the measured velocity profile by the Van Driest transformation and find the value of u_τ that best fits the Law of the Wall. The third method is to transform the measured velocity profile by the Carvin *et al* compressibility transformation [3]

$$u_c = \frac{1}{a} \sin^{-1}\left(\frac{au}{u_\tau}\right) \tag{6.22}$$

$$a = M_\infty \frac{u_\tau}{\sqrt{T_{wall}}}\sqrt{Pr_T(\gamma - 1)/2} \tag{6.23}$$

and again find the value of u_τ that best fits the Law of the Wall. Each of these methods agree with each other within 6%. The computational results differ with the experimental results by a maximum of about 20% which occurs in the area of maximum pressure gradient. This is not an unexpected result as it is seen in Figure 6.7 that the error in the computed skin friction may be as high as 10% in a zero pressure gradient, adiabatic flow. The error between computation and experiment is seen to decrease in the area of favorable pressure gradient ($x/\delta_o > 11$).

Figures 6.30 and 6.31 compare the computational and experimental u-velocity and Mach profiles respectively at $x/\delta_o = 10.3$. Experimental data for the velocity and Mach profiles are found from pitot probe measurements. Very good agreement is seen between the numerical and experimental velocity profiles, with the maximum error being less than 4%. This error is well within the 5% experimental error [11]. There is an increased error in the Mach profile. This is expected as this profile is dependent upon the accurate numerical calculation of both the velocity and local temperature profiles. Errors at this location are less than 5% which is slightly higher than the 3% experimental error [11]. There are very negligible differences between the velocity and Mach profiles for the two different pressure gradient distributions examined. For both pressure distributions and profiles the differences are less than 2%. Figures 6.33 and 6.34 demonstrate similar results at $x/\delta_o = 15.5$. At this location the comparison between the computed and experimental results for the velocity and Mach number are about the same. The error is everywhere less than 2% for the velocity and again less than 5% for the Mach number. The difference between Case 1 Δp and Case 2 Δp is everywhere less than 1% for the

velocity and Mach profiles at this location.

Figure 6.32 and Figure 6.35 compare the computed Reynolds stress with the experimental Reynolds stress. The computed Reynolds stress is the Favre averaged Reynolds stress, $-\overline{\rho u'' v''}$, which is slightly different than the stress, $-\overline{\rho u' v'}$, found by experiment. According to the data of Fernando [43] and the analysis given in Appendix E it may be shown that $-\overline{\rho u'' v''}$ differs from $-\overline{\rho u' v'}$ everywhere by less than 10%. This is less than the -5% to $+30\%$ experimental error given for the kinematic Reynolds stress by Fernando [10].

There is a significant difference between the computed and theoretical Reynolds stresses at both locations. At $x/\delta_o = 10.2$ the peak value of the computed non-dimensional Reynolds stress is .00174 for Case 2 Δp and .00168 for Case 1 Δp, with this maximum occurring at $y/\delta = .28$ and $y/\delta = .29$ respectively. The experimental data predicts this maximum to be .0013 at $y/\delta = .49$. The difference in the Reynolds stress between the two pressure distributions may be attributed to the fact that the Reynolds stress is influenced to a greater extent than either the velocity or Mach profiles by the pressure distribution, and even a slight modification in the distribution will have a noticeable effect on the Reynolds stress. The largest difference between the computation and experiment occurs in the region $y/\delta < 0.5$. According to Fernando, due to Mach number effects the crossed-wire underpredicts the Reynolds stresses below $y/\delta = .46$ at $x/\delta_o = 10.2$ and $y/\delta = .42$ at $x/\delta_o = 15.4$. Fernando warns that "crossed-wire results below these limits must be treated with caution" [11]. In the outer half of the boundary layer there is better agreement between the computation and experiment. There is also very close agreement between the computations of the two pressure distributions employed.

The comparison of the computational results with the experimental data for the Reynolds stress at $x/\delta_o = 15.4$ is slightly better than at $x/\delta_o = 10.2$. At $x/\delta_o = 15.4$ the peak non-dimensional Reynolds stress is computed to be .00134 at at $y/\delta = .335$; while the experimental data predicts the peak non-dimensional Reynolds stress to be .00130 at $y/\delta = .468$. Although there is only a 3% difference in the peak Reynolds stress, the experimental prediction of this peak occurs farther into the boundary layer.

The experimental data also predicts a faster decay of the stress as $y \to 0$. In the outer half of the boundary layer there is better agreement at this location. There is also very close agreement between the computations of the two pressure distributions employed.
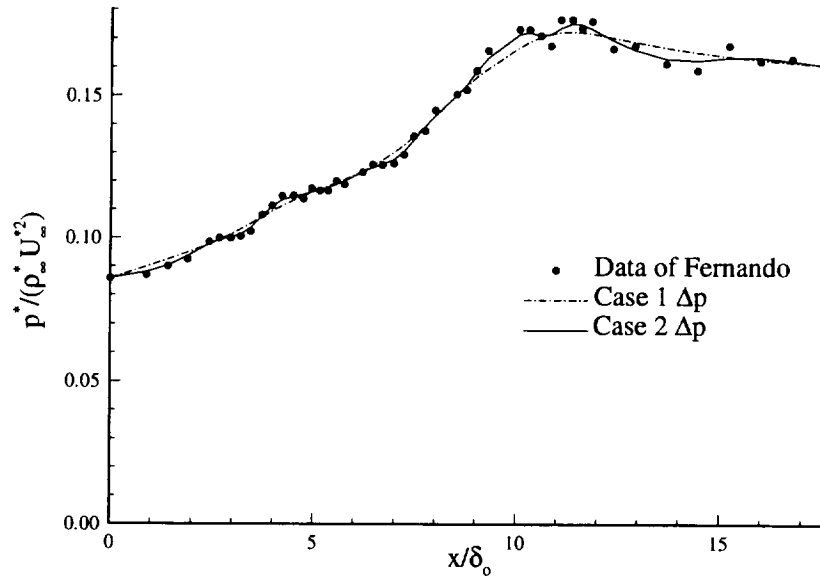
Figure 6.28: Experimental Surface Pressure of Fernando *et al* and the Computational Pressure Distributions Employed
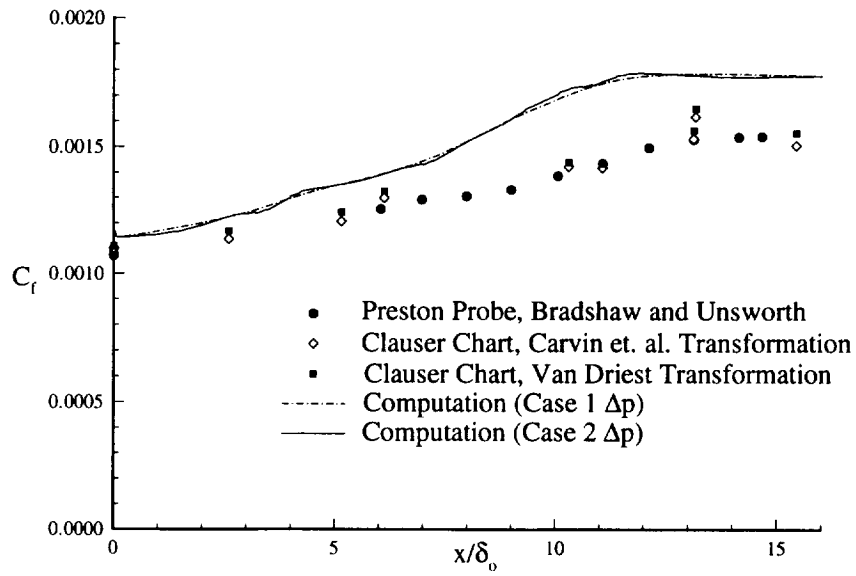
Figure 6.29: Skin Friction Data for an Adverse Pressure Gradient at $M_\infty = 2.92$ as Found by Experiment and Computed Numerically
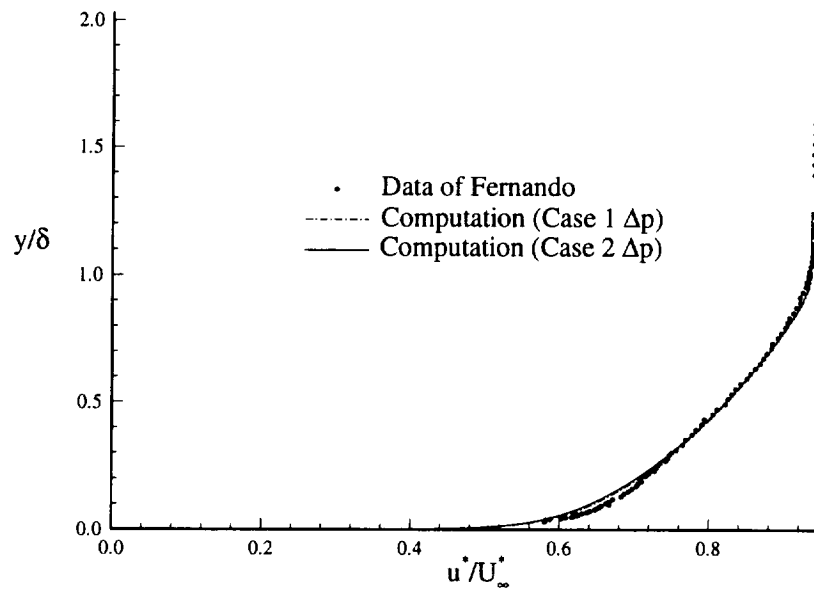
Figure 6.30: Experimental and Numerical Velocity Profiles at $x^*/\delta_o = 10.3$ for an Adverse Pressure Gradient
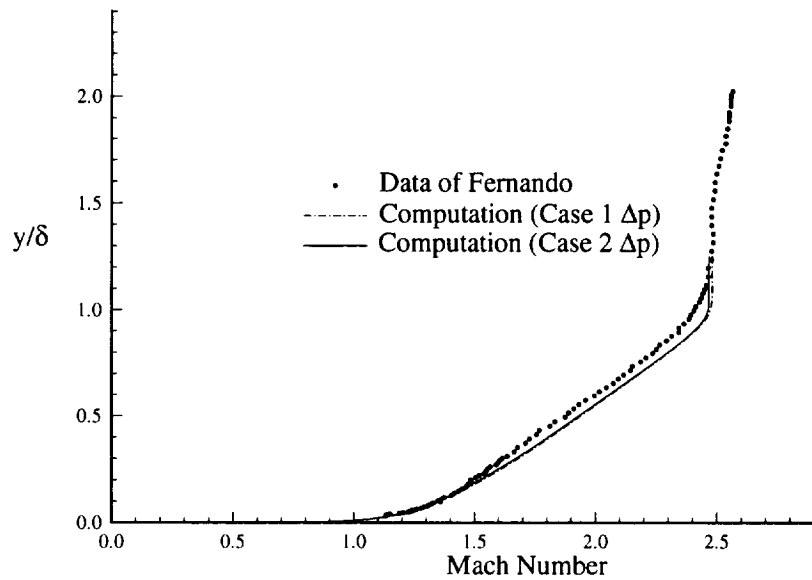
Figure 6.31: Experimental and Numerical Mach Profiles at $x^*/\delta_o = 10.3$ for an Adverse Pressure Gradient
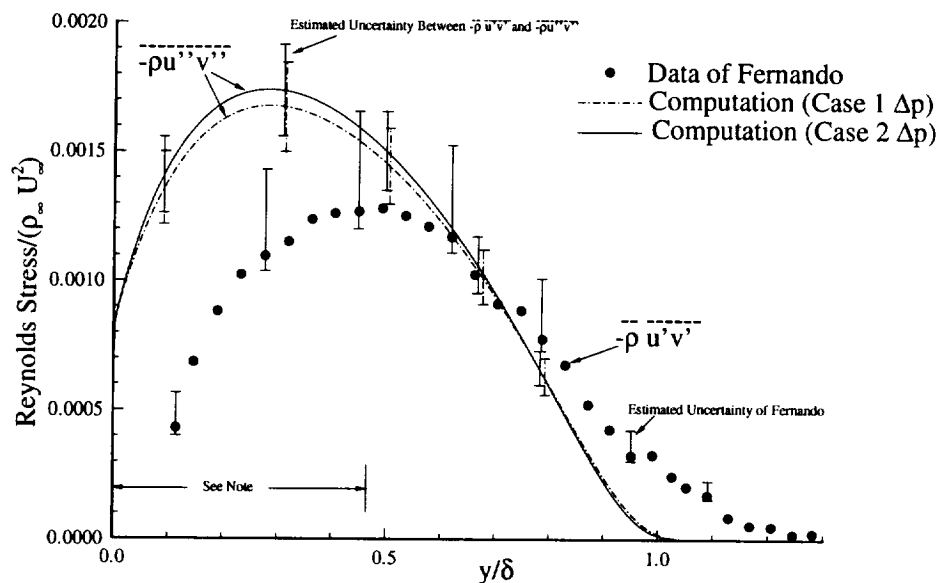
Figure 6.32: Experimental and Numerical Reynolds Stress Profiles at $x^*/\delta_o = 10.2$ for an Adverse Pressure Gradient

Note: According to Fernando "... due to Mach number effects...crossed-wire results below these limits must be treated with caution" ([11] page 53).
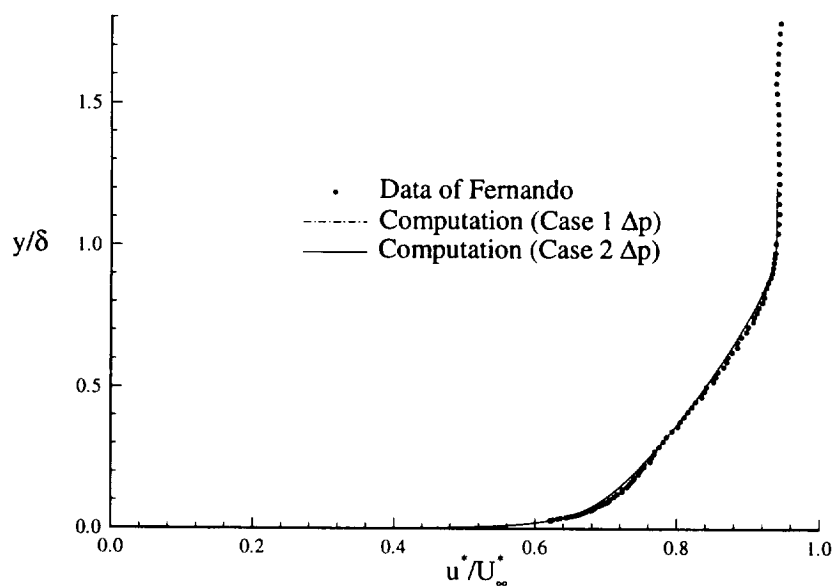
Figure 6.33: Experimental and Numerical Velocity Profiles at $x^*/\delta_o = 15.5$ for an Adverse Pressure Gradient
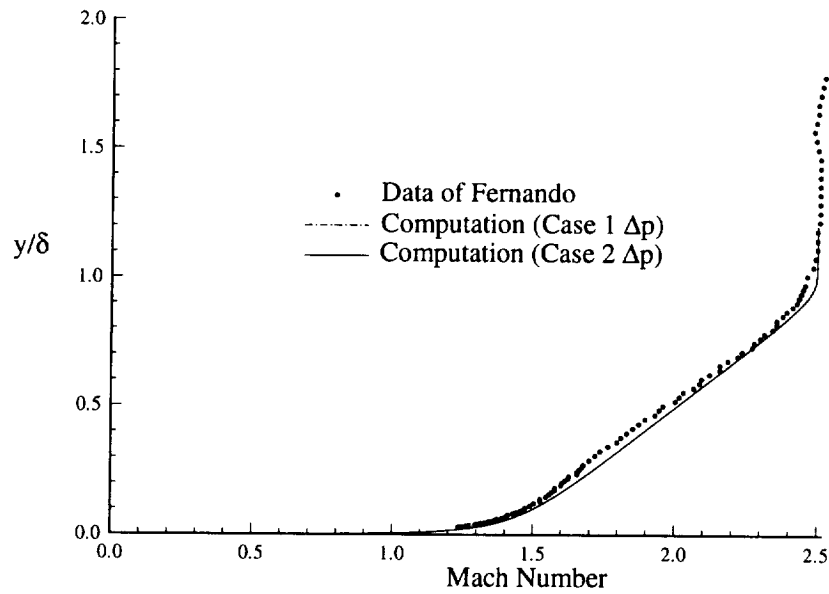
Figure 6.34: Experimental and Numerical Mach Profiles at $x^*/\delta_o = 15.5$ for an Adverse Pressure Gradient
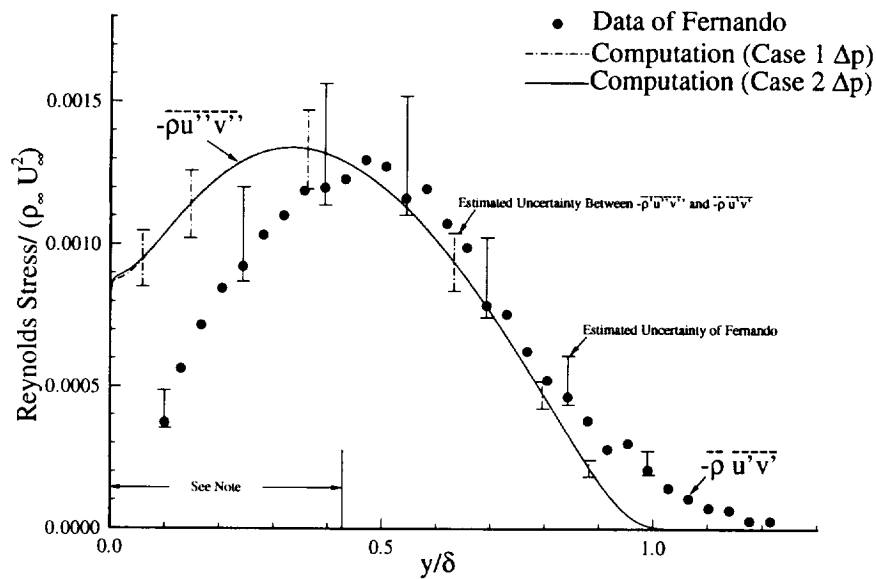
Note: According to Fernando "... due to Mach number effects...crossed-wire results below these limits must be treated with caution" ([11] page 53).

Figure 6.35: Experimental and Numerical Reynolds Stress Profiles at $x^*/\delta_o = 15.4$ for an Adverse Pressure Gradient

6.4 Conclusions

A low Reynolds number correction to the $k - \epsilon$ two equation compressible turbulence model has been proposed. This model avoids many of the limitations of other models. The proposed model is independent of the physical coordinate away from the wall, it uses the physically correct boundary condition for the dissipation and does not require a pseudo-dissipation rate, and it uses the minimum number of modifications required to integrate to the wall. The current model, unlike previous models, accurately predicts the DNS data of Spalart for the dissipation at the wall. For the above reasons the proposed model presents advantages over current "proven" models.

It has been shown that the proposed model accurately predicts the flow fields of both incompressible and compressible two dimensional flat plate boundary layers. For most cases the predicted skin friction falls within the $\pm 10\%$ experimental uncertainty, and the computed velocity profiles often lie on or are near the Law of the Wall. The model also reasonably predicts the velocity defect at low Mach numbers, but the error increases with increasing Mach number.

The proposed model moderately predicts the behavior of two dimensional, compressible flat plate, pressure gradient flows. The results of these computations do show promise. The model works very well in being able to predict both the velocity and Mach profiles of this type of flow as compared to the experimental work of Fernando. It also predicts a similar profile for the Reynolds stress. In the region close to the wall, $y/\delta < 0.5$, there are large discrepancies between the computation and experiment. These differences become smaller farther into the boundary layer. Although a large discrepancy does exist between the calculation and experiment; as stated by Fernando, the region of highest discrepancy is also the region where the experimental results are suspect.

6.5 Future Work

Although the results presented for both low and high Mach number flows over a flat plate are encouraging, future testing of this turbulence model is required. Future testing

should include comparisons against solutions of more complicated two dimensional configurations such as a curved ramp or an expansion corner. Comparisons could be made with the experimental work of Taylor [50] and Jayaram *et al* [19] and Zheltovodov *et al* [58]. A brief description of these and other experimental cases is described by Settles and Dodson [43].

The logical progression after these two dimensional cases have been examined is the application of the proposed model to more complicated three dimensional flow configurations. Such examinations should include both single fin [29] and double fin ("crossing shock") configurations [30], [12]. The examination and accurate prediction of the flow field structure for the crossing shock configuration is important in its application to hypersonic inlet design. Current computational models demonstrate general agreement with experimental data for surface pressure and shock structure. Boundary layer variables such as pitot pressure, and yaw angle also demonstrate general agreement; however, the computation of surface heat transfer is not yet accurately predicted [30]. It is the surface heat transfer which is especially important in the design of inlets to gauge the optimum amount of cooling required and the materials necessary for fabrication.

Appendix A

Tabular Form of the Low Reynolds Number Correction for f_μ

The following are the partial results found by Knight for the computation of f_μ versus R_t [27].

R_t	f_μ	R_t	f_μ	R_t	f_μ
0.0	0.031481	0.11572E-07	0.031481	0.65107E-07	0.031481
0.22891E-06	0.031481	0.62229E-06	0.031481	0.14382E-05	0.031481
0.29723E-05	0.031481	0.56618E-05	0.031481	0.10136E-04	0.031481
0.17282E-04	0.031481	0.28333E-04	0.031481	0.44974E-04	0.031481
0.69491E-04	0.031481	0.10495E-03	0.031481	0.15544E-03	0.031481
0.22637E-03	0.031481	0.32485E-03	0.031481	0.46016E-03	0.031481
0.64444E-03	0.031481	0.89336E-03	0.031481	0.12272E-02	0.031481
0.16722E-02	0.031481	0.22617E-02	0.031481	0.30388E-02	0.031481
0.40582E-02	0.031481	0.53898E-02	0.031481	0.71224E-02	0.031481
0.93687E-02	0.031481	0.12271E-01	0.031481	0.16010E-01	0.031481
0.20814E-01	0.031481	0.26968E-01	0.031481	0.34833E-01	0.031481
0.44863E-01	0.031481	0.57624E-01	0.031481	0.73828E-01	0.031481
0.94362E-01	0.031481	0.12034E+00	0.031481	0.15313E+00	0.031481
0.19446E+00	0.031481	0.24645E+00	0.031481	0.31175E+00	0.031481
0.39360E+00	0.031481	0.49603E+00	0.031481	0.62395E+00	0.031481
0.78339E+00	0.031481	0.98173E+00	0.031481	0.12279E+01	0.031481
1.5327	0.031481	1.9092	0.031481	2.3729	0.031481
2.9424	0.031481	3.6394	0.031481	4.4897	0.031481
5.5228	0.031481	6.7728	0.031481	8.2783	0.031481
10.083	0.031481	12.233	0.031481	14.781	0.031481
17.782	0.031481	21.293	0.031481	25.369	0.031481
30.068	0.031481	35.439	0.031481	41.529	0.031481
48.372	0.031633	55.991	0.031972	64.394	0.032508
73.570	0.033258	83.491	0.034240	94.107	0.035475
105.35	0.036988	117.13	0.038812	129.35	0.040981

Table A.1: Tabular Form of f_μ vs. Re_t

R_t	f_μ	R_t	f_μ	R_t	f_μ
141.89	0.043536	154.64	0.046524	167.49	0.049999
180.31	0.054020	193.02	0.058652	205.53	0.063969
217.78	0.070048	229.74	0.076975	241.37	0.084840
252.68	0.093735	263.67	0.103757	274.37	0.115004
284.80	0.127571	295.00	0.141547	305.00	0.157011
314.84	0.174022	324.53	0.192609	334.12	0.212758
343.62	0.234389	353.05	0.257334	362.44	0.281294
371.81	0.305798	381.20	0.330134	390.66	0.353272
399.79	0.372845	408.68	0.387696	417.44	0.397520
426.14	0.406392	434.79	0.414960	443.39	0.423240
451.95	0.431248	460.46	0.439000	468.93	0.446509
477.36	0.453786	485.76	0.460845	494.12	0.467695
502.46	0.474347	510.76	0.480810	519.04	0.487093
527.29	0.493203	535.51	0.499150	543.71	0.504939
551.88	0.510578	560.03	0.516072	568.17	0.521429
576.28	0.526653	584.37	0.531750	592.44	0.536724
600.50	0.541582	608.53	0.546326	616.55	0.550962
624.56	0.555493	632.55	0.559923	640.52	0.564256
648.48	0.568495	656.42	0.572644	664.35	0.576705
672.27	0.580682	680.18	0.584577	688.07	0.588393
695.95	0.592133	703.82	0.595800	711.68	0.599394
719.52	0.602920	727.36	0.606378	735.18	0.609772
743.00	0.613102	750.80	0.616371	758.60	0.619581
766.39	0.622733	774.16	0.625829	781.93	0.628871
789.69	0.631860	797.44	0.634798	805.18	0.637686
812.92	0.640525	820.64	0.643317	828.36	0.646063
836.07	0.648764	843.77	0.651422	851.47	0.654037
859.16	0.656610	866.84	0.659144	874.51	0.661638
882.18	0.664094	889.84	0.666513	897.50	0.668895
905.14	0.671241	912.79	0.673553	920.42	0.675831
928.05	0.678076	935.68	0.680288	943.29	0.682469
950.91	0.684619	958.51	0.686739	966.11	0.688830
973.71	0.690892	981.30	0.692925	988.89	0.694931
996.47	0.696910	1004.04	0.698863	1011.61	0.700790
1019.18	0.702692	1026.74	0.704569	1034.29	0.706422
1041.84	0.708251	1049.39	0.710057	1056.93	0.711840
1064.47	0.713601	1072.00	0.715340	1079.53	0.717058
1087.05	0.718755	1094.57	0.720431	1102.09	0.722087
1109.60	0.723723	1117.11	0.725340	1124.61	0.726938
1132.11	0.728517	1139.61	0.730078	1147.10	0.731621

Table A.2: Tabular Form of f_μ vs. Re_t (Continued)

R_t	f_μ	R_t	f_μ	R_t	f_μ
1154.59	0.733147	1162.07	0.734655	1169.56	0.736146
1177.03	0.737621	1184.51	0.739079	1191.98	0.740521
1199.44	0.741947	1206.91	0.743358	1214.37	0.744753
1221.82	0.746134	1229.27	0.747499	1236.72	0.748851
1244.17	0.750188	1251.61	0.751511	1259.05	0.752820
1266.49	0.754116	1273.92	0.755399	1281.36	0.756668
1288.78	0.757925	1296.21	0.759169	1303.63	0.760401
1311.05	0.761620	1318.46	0.762827	1325.88	0.764023
1333.29	0.765206	1340.69	0.766379	1348.10	0.767540
1355.50	0.768690	1362.90	0.769829	1370.30	0.770957
1377.69	0.772074	1385.08	0.773182	1392.47	0.774278
1399.85	0.775365	1407.24	0.776442	1414.62	0.777509
1422.00	0.778566	1429.37	0.779613	1436.74	0.780651
1444.12	0.781680	1451.48	0.782700	1458.85	0.783711
1466.21	0.784713	1473.57	0.785706	1480.93	0.786690
1488.29	0.787666	1495.64	0.788634	1503.00	0.789593
1510.35	0.790544	1517.69	0.791487	1525.04	0.792422
1532.38	0.793350	1539.72	0.794269	1547.06	0.795181
1554.40	0.796086	1561.73	0.796983	1569.06	0.797872
1576.39	0.798755	1583.72	0.799630	1591.05	0.800499
1598.37	0.801360	1605.70	0.802215	1613.02	0.803062
1620.33	0.803903	1627.65	0.804738	1634.96	0.805566
1642.28	0.806387	1649.59	0.807203	1656.90	0.808012
1664.20	0.808814	1671.51	0.809611	1678.81	0.810402
1686.11	0.811186	1693.41	0.811965	1700.71	0.812738
1708.00	0.813505	1715.30	0.814267	1722.59	0.815023
1729.88	0.815773	1737.17	0.816518	1744.46	0.817257
1751.74	0.817992	1759.02	0.818720	1766.31	0.819444
1773.59	0.820163	1780.86	0.820876	1788.14	0.821584
1795.42	0.822288	1802.69	0.822986	1809.96	0.823680
1817.23	0.824368	1824.50	0.825052	1831.77	0.825731
1839.03	0.826406	1846.29	0.827076	1853.56	0.827742
1860.82	0.828402	1868.08	0.829059	1875.33	0.829711
1882.59	0.830359	1889.84	0.831002	1897.10	0.831641
1904.35	0.832276	1911.60	0.832907	1918.85	0.833534
1926.10	0.834156	1933.34	0.834775	1940.58	0.835389
1947.83	0.836000	1955.07	0.836607	1962.31	0.837209
1969.55	0.837808	1976.78	0.838403	1984.02	0.838995
1991.25	0.839583	1998.49	0.840167	2005.72	0.840747
2012.95	0.841324	2020.18	0.841897	2027.41	0.842467

Table A.3: Tabular Form of f_μ vs. Re_t (Continued)

R_t	f_μ	R_t	f_μ	R_t	f_μ
2034.63	0.843033	2041.86	0.843596	2049.08	0.844155
2056.30	0.844711	2063.52	0.845263	2070.74	0.845813
2077.96	0.846359	2085.18	0.846901	2092.39	0.847441
2099.61	0.847977	2106.82	0.848510	2114.03	0.849040
2121.24	0.849567	2128.45	0.850091	2135.66	0.850612
2142.87	0.851129	2150.07	0.851644	2157.28	0.852156
2164.48	0.852665	2171.68	0.853171	2178.89	0.853674
2186.09	0.854174	2193.28	0.854672	2200.48	0.855166
2207.68	0.855658	2214.87	0.856147	2222.07	0.856633
2229.26	0.857117	2236.45	0.857598	2243.64	0.858077
2250.83	0.858552	2258.02	0.859025	2265.21	0.859496
2272.39	0.859964	2279.58	0.860429	2286.76	0.860892
2293.94	0.861353	2301.12	0.861811	2308.31	0.862267
2315.48	0.862720	2322.66	0.863170	2329.84	0.863619
2337.02	0.864065	2344.19	0.864509	2351.37	0.864950
2358.54	0.865389	2365.71	0.865826	2372.88	0.866260
2380.05	0.866693	2387.22	0.867123	2394.39	0.867550
2401.55	0.867976	2408.72	0.868400	2415.88	0.868821
2423.05	0.869240	2430.21	0.869657	2437.37	0.870072
2444.53	0.870485	2451.69	0.870896	2458.85	0.871305
2466.01	0.871712	2473.17	0.872117	2480.32	0.872520
2487.48	0.872921	2494.63	0.873319	2501.78	0.873716
2508.94	0.874111	2516.09	0.874505	2523.24	0.874896
2530.39	0.875285	2537.53	0.875673	2544.68	0.876058
2551.83	0.876442	2558.97	0.876824	2566.12	0.877204
2573.26	0.877582	2580.40	0.877959	2587.54	0.878334
2594.68	0.878707	2601.82	0.879078	2608.96	0.879448
2616.10	0.879815	2623.24	0.880181	2630.37	0.880546
2637.51	0.880909	2644.64	0.881270	2651.78	0.881629
2658.91	0.881987	2666.04	0.882343	2673.17	0.882698
2680.30	0.883051	2687.43	0.883402	2694.56	0.883752
2701.69	0.884100	2708.82	0.884447	2715.94	0.884792
2723.07	0.885136	2730.19	0.885478	2737.31	0.885819
2744.44	0.886158	2751.56	0.886495	2758.68	0.886832
2765.80	0.887166	2772.92	0.887499	2780.04	0.887831
2787.15	0.888162	2794.27	0.888491	2801.39	0.888818
2808.50	0.889144	2815.61	0.889469	2822.73	0.889792
2829.84	0.890114	2836.95	0.890435	2844.06	0.890754
2851.17	0.891072	2858.28	0.891388	2865.39	0.891704
2872.50	0.892018	2879.61	0.892330	2886.71	0.892642

Table A.4: Tabular Form of f_μ vs. Re_t (Continued)

R_t	f_μ	R_t	f_μ	R_t	f_μ
2893.82	0.892952	2900.92	0.893260	2908.03	0.893568
2915.13	0.893874	2922.23	0.894179	2929.33	0.894483
2936.43	0.894785	2943.53	0.895086	2950.63	0.895386
2957.73	0.895685	2964.83	0.895983	2971.93	0.896279
2979.02	0.896574	2986.12	0.896868	2993.21	0.897161
3000.31	0.897453	3007.40	0.897744	3014.49	0.898033
3021.59	0.898321	3028.68	0.898608	3035.77	0.898894
3042.86	0.899179	3049.95	0.899463	3057.04	0.899746
3064.12	0.900027	3071.21	0.900308	3078.30	0.900587
3085.38	0.900865	3092.47	0.901143	3099.55	0.901419
3106.63	0.901694	3113.72	0.901968	3120.80	0.902241
3127.88	0.902513	3134.96	0.902784	3142.04	0.903054
3149.12	0.903323	3156.20	0.903591	3163.28	0.903858
3170.35	0.904124	3177.43	0.904388	3184.51	0.904652
3191.58	0.904915	3198.66	0.905177	3205.73	0.905438
3212.80	0.905698	3219.88	0.905957	3226.95	0.906216
3234.02	0.906473	3241.09	0.906729	3248.16	0.906984
3255.23	0.907239	3262.30	0.907492	3269.36	0.907745
3276.43	0.907997	3283.50	0.908247	3290.56	0.908497
3297.63	0.908746	3304.69	0.908994	3311.76	0.909241
3318.82	0.909488	3325.88	0.909733	3332.95	0.909978
3340.01	0.910222	3347.07	0.910464	3354.13	0.910706
3361.19	0.910948	3368.25	0.911188	3375.31	0.911427
3382.36	0.911666	3389.42	0.911904	3396.48	0.912141
3403.53	0.912377	3410.59	0.912612	3417.64	0.912847
3424.70	0.913081	3431.75	0.913314	3438.80	0.913546
3445.86	0.913777	3452.91	0.914008	3459.96	0.914238
3467.01	0.914467	3474.06	0.914695	3481.11	0.914923
3488.16	0.915149	3495.20	0.915375	3502.25	0.915600
3509.30	0.915825	3516.34	0.916049	3523.39	0.916272
3530.44	0.916494	3537.48	0.916715	3544.52	0.916936
3551.57	0.917156	3558.61	0.917376	3565.65	0.917594
3572.69	0.917812	3579.73	0.918029	3586.77	0.918246
3593.81	0.918462	3600.85	0.918677	3607.89	0.918891
3614.93	0.919105	3621.97	0.919318	3629.01	0.919530
3636.04	0.919742	3643.08	0.919953	3650.11	0.920163
3657.15	0.920373	3664.18	0.920582	3671.22	0.920790
3678.25	0.920998	3685.28	0.921205	3692.31	0.921411
3699.34	0.921617	3706.38	0.921822	3713.41	0.922026
3720.44	0.922230	3727.46	0.922433	3734.49	0.922636

Table A.5: Tabular Form of f_μ vs. Re_t (Continued)

R_t	f_μ	R_t	f_μ	R_t	f_μ
3741.52	0.922838	3748.55	0.923039	3755.58	0.923239
3762.60	0.923440	3769.63	0.923639	3776.65	0.923838
3783.68	0.924036	3790.70	0.924234	3797.73	0.924430
3804.75	0.924627	3811.77	0.924823	3818.80	0.925018
3825.82	0.925212	3832.84	0.925406	3839.86	0.925600
3846.88	0.925793	3853.90	0.925985	3860.92	0.926177
3867.94	0.926368	3874.96	0.926558	3881.97	0.926748
3888.99	0.926938	3896.01	0.927127	3903.02	0.927315
3910.04	0.927503	3917.05	0.927690	3924.07	0.927877
3931.08	0.928063	3938.10	0.928248	3945.11	0.928433
3952.12	0.928618	3959.13	0.928802	3966.15	0.928985
3973.16	0.929168	3980.17	0.929351	3987.18	0.929532
3994.19	0.929714	4001.20	0.929894	4008.20	0.930075
4015.21	0.930254	4022.22	0.930434	4029.23	0.930612
4036.23	0.930791	4043.24	0.930968	4050.25	0.931146
4057.25	0.931322	4064.26	0.931499	4071.26	0.931674
4078.26	0.931849	4085.27	0.932024	4092.27	0.932198
4099.27	0.932372	4106.27	0.932545	4113.28	0.932718
4120.28	0.932891	4127.28	0.933062	4134.28	0.933234
4141.28	0.933405	4148.27	0.933575	4155.27	0.933745
4162.27	0.933914	4169.27	0.934084	4176.27	0.934252
4183.26	0.934420	4190.26	0.934588	4197.25	0.934755
4204.25	0.934922	4211.24	0.935088	4218.24	0.935254
4225.23	0.935419	4232.23	0.935584	4239.22	0.935749
4246.21	0.935913	4253.20	0.936076	4260.20	0.936239
4267.19	0.936402	4274.18	0.936564	4281.17	0.936726
4288.16	0.936888	4295.15	0.937049	4302.14	0.937209
4309.12	0.937369	4316.11	0.937529	4323.10	0.937688
4330.09	0.937847	4337.07	0.938006	4344.06	0.938164
4351.05	0.938322	4358.03	0.938479	4365.02	0.938636
4372.00	0.938792	4378.99	0.938948	4385.97	0.939104
4392.95	0.939259	4399.94	0.939414	4406.92	0.939568
4413.90	0.939722	4420.88	0.939876	4427.86	0.940029
4434.84	0.940182	4441.82	0.940334	4448.80	0.940486
4455.78	0.940638	4462.76	0.940789	4469.74	0.940940
4476.72	0.941091	4483.70	0.941241	4490.67	0.941391
4497.65	0.941540	4504.63	0.941689	4511.60	0.941838
4518.58	0.941986	4525.55	0.942134	4532.53	0.942281
4539.50	0.942428	4546.48	0.942575	4553.45	0.942722
4560.42	0.942868	4567.40	0.943013	4574.37	0.943159

Table A.6: Tabular Form of f_μ vs. Re_t (Continued)

R_t	f_μ	R_t	f_μ	R_t	f_μ
4581.34	0.943304	4588.31	0.943448	4595.28	0.943593
4602.25	0.943736	4609.22	0.943880	4616.19	0.944023
4623.16	0.944166	4630.13	0.944309	4637.10	0.944451
4644.07	0.944593	4651.04	0.944734	4658.00	0.944875
4664.97	0.945016	4671.94	0.945156	4678.90	0.945296
4685.87	0.945436	4692.84	0.945576	4699.80	0.945715
4706.77	0.945854	4713.73	0.945992	4720.69	0.946130
4727.66	0.946268	4734.62	0.946405	4741.58	0.946542
4748.55	0.946679	4755.51	0.946816	4762.47	0.946952
4769.43	0.947088	4776.39	0.947223	4783.35	0.947358
4790.31	0.947493	4797.27	0.947628	4804.23	0.947762
4811.19	0.947896	4818.15	0.948030	4825.11	0.948163
4832.06	0.948296	4839.02	0.948429	4845.98	0.948561
4852.94	0.948693	4859.89	0.948825	4866.85	0.948956
4873.80	0.949087	4880.76	0.949218	4887.71	0.949349
4894.67	0.949479	4901.62	0.949609	4908.58	0.949739
4915.53	0.949868	4922.48	0.949997	4929.44	0.950126
4936.39	0.950254	4943.34	0.950383	4950.29	0.950511
4957.24	0.950638	4964.19	0.950766	4971.14	0.950893
4978.09	0.951019	4985.04	0.951146	4991.99	0.951272
4998.94	0.951398	5005.89	0.951524	5012.84	0.951649
5019.79	0.951774	5026.73	0.951899	5033.68	0.952023
5040.63	0.952147	5047.58	0.952271	5054.52	0.952395
5061.47	0.952518	5068.41	0.952642	5075.36	0.952764
5082.30	0.952887	5089.25	0.953009	5096.19	0.953131
5103.14	0.953253	5110.08	0.953375	5117.02	0.953496
5123.96	0.953617	5130.91	0.953738	5137.85	0.953858
5144.79	0.953978	5151.73	0.954098	5158.67	0.954218
5165.61	0.954337	5172.55	0.954456	5179.49	0.954575
5186.43	0.954694	5193.37	0.954812	5200.31	0.954931
5207.25	0.955048	5214.19	0.955166	5221.13	0.955283
5228.07	0.955401	5235.00	0.955517	5241.94	0.955634
5248.88	0.955750	5255.81	0.955867	5262.75	0.955982
5269.68	0.956098	5276.62	0.956214	5283.56	0.956329
5290.49	0.956444	5297.42	0.956558	5304.36	0.956673
5311.29	0.956787	5318.23	0.956901	5325.16	0.957015
5332.09	0.957128	5339.02	0.957241	5345.96	0.957354
5352.89	0.957467	5359.82	0.957580	5366.75	0.957692
5373.68	0.957804	5380.61	0.957916	5387.54	0.958027
5394.47	0.958139	5401.40	0.958250	5408.33	0.958361

Table A.7: Tabular Form of f_μ vs. Re_t (Continued)

R_t	f_μ	R_t	f_μ	R_t	f_μ
5415.26	0.958471	5422.19	0.958582	5429.12	0.958692
5436.05	0.958802	5442.97	0.958912	5449.90	0.959021
5456.83	0.959131	5463.75	0.959240	5470.68	0.959349
5477.61	0.959457	5484.53	0.959566	5491.46	0.959674
5498.38	0.959782	5505.31	0.959890	5512.23	0.959997
5519.16	0.960105	5526.08	0.960212	5533.01	0.960319
5539.93	0.960425	5546.85	0.960532	5553.78	0.960638
5560.70	0.960744	5567.62	0.960850	5574.54	0.960956
5581.46	0.961061	5588.39	0.961166	5595.31	0.961271
5602.23	0.961376	5609.15	0.961481	5616.07	0.961585
5622.99	0.961689	5629.91	0.961793	5636.83	0.961897
5643.75	0.962000	5650.66	0.962104	5657.58	0.962207
5664.50	0.962310	5671.42	0.962412	5678.34	0.962515
5685.25	0.962617	5692.17	0.962719	5699.09	0.962821
5706.00	0.962923	5712.92	0.963025	5719.84	0.963126
5726.75	0.963227	5733.67	0.963328	5740.58	0.963429
5747.50	0.963529	5754.41	0.963630	5761.33	0.963730
5768.24	0.963830	5775.15	0.963930	5782.07	0.964029
5788.98	0.964129	5795.89	0.964228	5802.81	0.964327
5809.72	0.964426	5816.63	0.964524	5823.54	0.964623
5830.45	0.964721	5837.36	0.964819	5844.28	0.964917
5851.19	0.965015	5858.10	0.965112	5865.01	0.965209
5871.92	0.965307	5878.83	0.965404	5885.74	0.965500
5892.64	0.965597	5899.55	0.965693	5906.46	0.965790
5913.37	0.965886	5920.28	0.965981	5927.19	0.966077
5934.09	0.966173	5941.00	0.966268	5947.91	0.966363
5954.81	0.966458	5961.72	0.966553	5968.63	0.966647
5975.53	0.966742	5982.44	0.966836	5989.34	0.966930
5996.25	0.967024	6003.15	0.967118	6010.06	0.967211
6016.96	0.967305	6023.87	0.967398	6030.77	0.967491
6037.67	0.967584	6044.58	0.967677	6051.48	0.967769
6058.38	0.967861	6065.28	0.967954	6072.19	0.968046
6079.09	0.968137	6085.99	0.968229	6092.89	0.968321
6099.79	0.968412	6106.69	0.968503	6113.60	0.968594
6120.50	0.968685	6127.40	0.968776	6134.30	0.968866
6141.20	0.968957	6148.10	0.969047	6155.00	0.969137
6161.89	0.969227	6168.79	0.969316	6175.69	0.969406
6182.59	0.969495	6189.49	0.969584	6196.39	0.969673
6203.28	0.969762	6210.18	0.969851	6217.08	0.969940
6223.98	0.970028	6230.87	0.970116	6237.77	0.970204

Table A.8: Tabular Form of f_μ vs. Re_t (Continued)

R_t	f_μ	R_t	f_μ	R_t	f_μ
6244.67	0.970292	6251.56	0.970380	6258.46	0.970468
6265.35	0.970555	6272.25	0.970642	6279.14	0.970729
6286.04	0.970816	6292.93	0.970903	6299.83	0.970990
6306.72	0.971076	6313.61	0.971163	6320.51	0.971249
6327.40	0.971335	6334.29	0.971421	6341.19	0.971507
6348.08	0.971592	6354.97	0.971678	6361.87	0.971763
6368.76	0.971848	6375.65	0.971933	6382.54	0.972018
6389.43	0.972103	6396.32	0.972187	6403.21	0.972272
6410.11	0.972356	6417.00	0.972440	6423.89	0.972524
6430.78	0.972608	6437.67	0.972692	6444.56	0.972775
6451.45	0.972859	6458.33	0.972942	6465.22	0.973025
6472.11	0.973108	6479.00	0.973191	6485.89	0.973273
6492.78	0.973356	6499.67	0.973438	6506.55	0.973520
6513.44	0.973602	6520.33	0.973684	6527.22	0.973766
6534.10	0.973848	6540.99	0.973929	6547.88	0.974011
6554.76	0.974092	6561.65	0.974173	6568.53	0.974254
6575.42	0.974335	6582.30	0.974416	6589.19	0.974496
6596.07	0.974577	6602.96	0.974657	6609.84	0.974737
6616.73	0.974817	6623.61	0.974897	6630.50	0.974977
6637.38	0.975056	6644.26	0.975136	6651.15	0.975215
6658.03	0.975294	6664.91	0.975373	6671.80	0.975452
6678.68	0.975531	6685.56	0.975610	6692.44	0.975688
6699.33	0.975766	6706.21	0.975845	6713.09	0.975923
6719.97	0.976001	6726.85	0.976079	6733.73	0.976156
6740.61	0.976234	6747.49	0.976311	6754.37	0.976389
6761.26	0.976466	6768.14	0.976543	6775.02	0.976620
6781.89	0.976697	6788.77	0.976773	6795.65	0.976850
6802.53	0.976926	6809.41	0.977003	6816.29	0.977079
6823.17	0.977155	6830.05	0.977231	6836.93	0.977307
6843.80	0.977382	6850.68	0.977458	6857.56	0.977533
6864.44	0.977609	6871.31	0.977684	6878.19	0.977759
6885.07	0.977834	6891.94	0.977909	6898.82	0.977983
6905.70	0.978058	6912.57	0.978132	6919.45	0.978207
6926.33	0.978281	6933.20	0.978355	6940.08	0.978429
6946.95	0.978502	6953.83	0.978576	6960.70	0.978650
6967.58	0.978723	6974.45	0.978797	6981.33	0.978870
6988.20	0.978943	6995.08	0.979016	7001.95	0.979089
7008.82	0.979161	7015.70	0.979234	7022.57	0.979306
7029.44	0.979379	7036.32	0.979451	7043.19	0.979523
7050.06	0.979595	7056.93	0.979667	7063.81	0.979739
7070.68	0.979811	7077.55	0.979882	7084.42	0.979954

Table A.9: Tabular Form of f_μ vs. Re_t (Continued)

R_t	f_μ	R_t	f_μ	R_t	f_μ
7091.30	0.980025	7098.17	0.980096	7105.04	0.980167
7111.91	0.980238	7118.78	0.980309	7125.65	0.980380
7132.52	0.980450	7139.39	0.980521	7146.26	0.980591
7153.13	0.980662	7160.00	0.980732	7166.87	0.980802
7173.74	0.980872	7180.61	0.980942	7187.48	0.981011
7194.35	0.981081	7201.22	0.981151	7208.09	0.981220
7214.96	0.981289	7221.83	0.981358	7228.70	0.981427
7235.57	0.981496	7242.43	0.981565	7249.30	0.981634
7256.17	0.981703	7263.04	0.981771	7269.91	0.981840
7276.77	0.981908	7283.64	0.981976	7290.51	0.982044
7297.38	0.982112	7304.24	0.982180	7311.11	0.982248
7317.98	0.982315	7324.84	0.982383	7331.71	0.982450
7338.58	0.982518	7345.44	0.982585	7352.31	0.982652
7359.17	0.982719	7366.04	0.982786	7372.91	0.982853
7379.77	0.982919	7386.64	0.982986	7393.50	0.983052
7400.37	0.983119	7407.23	0.983185	7414.10	0.983251
7420.96	0.983317	7427.83	0.983383	7434.69	0.983449
7441.55	0.983515	7448.42	0.983580	7455.28	0.983646
7462.15	0.983711	7469.01	0.983776	7475.87	0.983842
7482.74	0.983907	7489.60	0.983972	7496.46	0.984037
7503.33	0.984102	7510.19	0.984166	7517.05	0.984231
7523.91	0.984295	7530.78	0.984360	7537.64	0.984424
7544.50	0.984488	7551.36	0.984552	7558.23	0.984616
7565.09	0.984680	7571.95	0.984744	7578.81	0.984808
7585.67	0.984871	7592.53	0.984935	7599.40	0.984998
7606.26	0.985062	7613.12	0.985125	7619.98	0.985188
7626.84	0.985251	7633.70	0.985314	7640.56	0.985377
7647.42	0.985439	7654.28	0.985502	7661.14	0.985565
7668.00	0.985627	7674.86	0.985689	7681.72	0.985752
7688.58	0.985814	7695.44	0.985876	7702.30	0.985938
7709.16	0.986000	7716.02	0.986061	7722.88	0.986123
7729.74	0.986185	7736.60	0.986246	7743.46	0.986307
7750.32	0.986369	7757.17	0.986430	7764.03	0.986491
7770.89	0.986552	7777.75	0.986613	7784.61	0.986674
7791.47	0.986734	7798.32	0.986795	7805.18	0.986855
7812.04	0.986916	7818.90	0.986976	7825.76	0.987036
7832.61	0.987097	7839.47	0.987157	7846.33	0.987217
7853.19	0.987277	7860.04	0.987336	7866.90	0.987396
7873.76	0.987456	7880.61	0.987515	7887.47	0.987575
7894.33	0.987634	7901.18	0.987693	7908.04	0.987752
7914.90	0.987811	7921.75	0.987870	7928.61	0.987929

Table A.10: Tabular Form of f_μ vs. Re_t (Continued)

R_t	f_μ	R_t	f_μ	R_t	f_μ
7935.47	0.987988	7942.32	0.988047	7949.18	0.988105
7956.03	0.988164	7962.89	0.988222	7969.74	0.988280
7976.60	0.988339	7983.46	0.988397	7990.31	0.988455
7997.17	0.988513	8004.02	0.988571	8010.88	0.988629
8017.73	0.988686	8024.59	0.988744	8031.44	0.988801
8038.30	0.988859	8045.15	0.988916	8052.01	0.988974
8058.86	0.989031	8065.71	0.989088	8072.57	0.989145
8079.42	0.989202	8086.28	0.989259	8093.13	0.989315
8099.99	0.989372	8106.84	0.989429	8113.69	0.989485
8120.55	0.989541	8127.40	0.989598	8134.26	0.989654
8141.11	0.989710	8147.96	0.989766	8154.82	0.989822
8161.67	0.989878	8168.52	0.989934	8175.38	0.989990
8182.23	0.990045	8189.08	0.990101	8195.94	0.990156
8202.79	0.990212	8209.64	0.990267	8216.49	0.990322
8223.35	0.990377	8230.20	0.990432	8237.05	0.990487
8243.90	0.990542	8250.76	0.990597	8257.61	0.990652
8264.46	0.990706	8271.31	0.990761	8278.17	0.990815
8285.02	0.990870	8291.87	0.990924	8298.72	0.990978
8305.58	0.991032	8312.43	0.991086	8319.28	0.991140
8326.13	0.991194	8332.98	0.991248	8339.83	0.991302
8346.69	0.991355	8353.54	0.991409	8360.39	0.991462
8367.24	0.991516	8374.09	0.991569	8380.94	0.991622
8387.79	0.991676	8394.65	0.991729	8401.50	0.991782
8408.35	0.991835	8415.20	0.991887	8422.05	0.991940
8428.90	0.991993	8435.75	0.992045	8442.60	0.992098
8449.45	0.992150	8456.30	0.992203	8463.16	0.992255
8470.01	0.992307	8476.86	0.992359	8483.71	0.992411
8490.56	0.992463	8497.41	0.992515	8504.26	0.992567
8511.11	0.992619	8517.96	0.992670	8524.81	0.992722
8531.66	0.992774	8538.51	0.992825	8545.36	0.992876
8552.21	0.992928	8559.06	0.992979	8565.91	0.993030
8572.76	0.993081	8579.61	0.993132	8586.46	0.993183
8593.31	0.993234	8600.16	0.993284	8607.01	0.993335
8613.86	0.993385	8620.71	0.993436	8627.56	0.993486
8634.41	0.993537	8641.26	0.993587	8648.11	0.993637
8654.96	0.993687	8661.81	0.993737	8668.66	0.993787
8675.51	0.993837	8682.36	0.993887	8689.21	0.993937
8696.06	0.993986	8702.91	0.994036	8709.76	0.994085
8716.61	0.994135	8723.46	0.994184	8730.31	0.994234
8737.15	0.994283	8744.00	0.994332	8750.85	0.994381
8757.70	0.994430	8764.55	0.994479	8771.40	0.994528

Table A.11: Tabular Form of f_μ vs. Re_t (Continued)

R_t	f_μ	R_t	f_μ	R_t	f_μ
8778.25	0.994576	8785.10	0.994625	8791.95	0.994674
8798.80	0.994722	8805.65	0.994771	8812.50	0.994819
8819.35	0.994867	8826.19	0.994916	8833.04	0.994964
8839.89	0.995012	8846.74	0.995060	8853.59	0.995108
8860.44	0.995156	8867.29	0.995204	8874.14	0.995251
8880.99	0.995299	8887.84	0.995347	8894.68	0.995394
8901.53	0.995442	8908.38	0.995489	8915.23	0.995536
8922.08	0.995584	8928.93	0.995631	8935.78	0.995678
8942.63	0.995725	8949.48	0.995772	8956.33	0.995819
8963.17	0.995865	8970.02	0.995912	8976.87	0.995959
8983.72	0.996005	8990.57	0.996052	8997.42	0.996098
9004.27	0.996145	9011.12	0.996191	9017.97	0.996237
9024.81	0.996283	9031.66	0.996330	9038.51	0.996376
9045.36	0.996422	9052.21	0.996467	9059.06	0.996513
9065.91	0.996559	9072.76	0.996605	9079.61	0.996650
9086.46	0.996696	9093.30	0.996741	9100.15	0.996787
9107.00	0.996832	9113.85	0.996877	9120.70	0.996922
9127.55	0.996968	9134.40	0.997013	9141.25	0.997058
9148.10	0.997103	9154.95	0.997147	9161.79	0.997192
9168.64	0.997237	9175.49	0.997282	9182.34	0.997326
9189.19	0.997371	9196.04	0.997415	9202.89	0.997459
9209.74	0.997504	9216.59	0.997548	9223.44	0.997592
9230.29	0.997636	9237.14	0.997680	9243.99	0.997724
9250.83	0.997768	9257.68	0.997812	9264.53	0.997856
9271.38	0.997899	9278.23	0.997943	9285.08	0.997987
9291.93	0.998030	9298.78	0.998073	9305.63	0.998117
9312.48	0.998160	9319.33	0.998203	9326.18	0.998247
9333.03	0.998290	9339.88	0.998333	9346.73	0.998376
9353.58	0.998418	9360.43	0.998461	9367.28	0.998504
9374.13	0.998547	9380.98	0.998589	9387.83	0.998632
9394.68	0.998674	9401.53	0.998717	9408.38	0.998759
9415.23	0.998802	9422.08	0.998844	9428.93	0.998886
9435.78	0.998928	9442.63	0.998970	9449.48	0.999012
9456.33	0.999054	9463.18	0.999096	9470.03	0.999138
9476.88	0.999179	9483.73	0.999221	9490.58	0.999263
9497.43	0.999304	9504.28	0.999345	9511.13	0.999387
9517.98	0.999428	9524.83	0.999469	9531.68	0.999511
9538.54	0.999552	9545.39	0.999593	9552.24	0.999634
9559.09	0.999675	9565.94	0.999716	9572.79	0.999756
9579.64	0.999797	9586.49	0.999838	9593.34	0.999879
9600.20	0.999919	9613.90	1.000000	∞	1.000000

Table A.12: Tabular Form of f_μ vs. Re_t (Continued)

Appendix B

Discretized Equations

The following are the discretized equations of motion for equations 4.1 - 4.9; the boundary conditions given in Table 2.1, Table 2.3, and Table 2.4; and the additional equations for friction velocity, T_{wall}, and Q_{wall} required when integrating only to the wall layer. These equations are discretized by Keller's Box Scheme as described in Chapter Four and are given in nondimensional form, neglecting the ¯ and ˜ for simplicity. The subscript j refers to grid locations perpendicular to the plate, and the superscript n refers to spacing in the direction of the flow.

B.1 Discretized Boundary Conditions at the Wall and in the Wall Layer

The wall function boundary conditions employed in the code include modifcations for adiabatic, compressible flow.

$kwall = 0$ corresponds to wall function boundary conditions. These boundary conditions are only used for adiabatic boundary layers.

$kwall = 1$ corresponds to wall surface boundary conditions

$kiso = 0$ corresponds to adiabatic surface boundary conditions

$kiso = 1$ corresponds to isothermal surface boundary conditions

$kvvel = 0$ corresponds to $v_1^n = 0$ in the wall layer

$kvvel = 1$ corresponds to v_1^n satisfying the continuity equation in the wall layer, for incompressible boundary layers only.

For all independent variables, $\bar{w}$, w_j^n is defined as the value of the variable w at the jth node perpendicular to the plate and the nth node parallel the plate.

Boundary Condition on u at $j = 1$

$$BCuwall = u_1^n$$
$$- (1 - kwall)\left(\frac{1}{A_1}\sin(A_1 u_c)\right)$$
$$- (kwall)(0) = 0 \qquad\qquad \text{(B.1)}$$

where

$$u_c = \left(\frac{u_\tau^n}{\kappa}\ln\left(Re_{\delta o}\frac{u_\tau^n y_1 \rho_e^n T_e^n}{\mu_{wall}^n T_{wall}^n}\right) + Bu_\tau^n\right)$$
$$A_1 = \sqrt{Pr_T\frac{\gamma - 1}{2}M_\infty^2\frac{1}{T_{wall}^n}}$$

Boundary Condition on v at $j = 1$

$$BCvwall = v_1^n$$
$$- (1 - kvvel)(0)$$
$$- (kvvel)\frac{y_1 u_1^n}{u_\tau^n}\frac{u_\tau^n - u_\tau^{n-1}}{\Delta x^n} = 0 \qquad\qquad \text{(B.2)}$$

$kvvel = 1$ is valid only for incompressible boundary layers

Boundary Condition on ϵ_v at $j = 1$

$$BC\epsilon wall = \epsilon_{v1}^n$$
$$- (1 - kwall)\left(\frac{(u_\tau^n)^3}{\kappa y_1}\right)\left(\frac{T_1^n}{T_{wall}^n}\right)^{\frac{1}{4}}$$
$$- (kwall)\left(2\frac{\mu_1^n T_1^n (b_1^n)^2}{\rho_e^n T_e^n Re_{\delta o}}\right) = 0 \qquad\qquad \text{(B.3)}$$

Boundary Condition on q at $j = 1$

$$BCqwall = q_1^n$$
$$- (1 - kwall)\left(\frac{u_\tau^n}{(C_\mu)^{\frac{1}{4}}}\right)\left(\frac{T_1^n}{T_{wall}^n}\right)^{\frac{1}{2}}$$
$$- (kwall)(0) = 0 \qquad\qquad \text{(B.4)}$$

Boundary Condition on T at $j = 1$

$$BCTwall = (kiso)\left(T_{wall}^n - T_1^n - \frac{1}{2}Pr_T u_1^{n2}(\gamma - 1)M_\infty^2\right)$$
$$+ (1 - kiso)(Q_{wall}^n + \frac{\mu_{wall}}{Re_{\delta o}M_\infty^2(\gamma - 1)Pr}$$
$$\times \left(c_1^n + Pr_T u_1^n h_1^n(\gamma - 1)M_\infty^2\right)) = 0 \qquad\qquad \text{(B.5)}$$

B.2 Discretized Boundary Conditions at the Edge of the Computational Domain

$kgrad = 0$ corresponds to Dirichlet Boundary Condition

$kgrad = 1$ corresponds to Neuman Boundary Condition

Boundary Condition on u at Edge of Computational Domain

$$BCuedge = u_{jl}^n - U_e^n = 0 \tag{B.6}$$

Boundary Condition on ϵ_v at Edge of Computational Domain

$$BC\epsilon edge = (1 - kgrad)(\epsilon_{vjl}^n - \epsilon_{ve})^n + (kgrad)(a_{jl}^n - 0) = 0 \tag{B.7}$$

Boundary Condition on q at Edge of Computational Domain

$$BCqedge = (1 - kgrad)(q_{jl}^n - q_e)^n + (kgrad)(b_{jl}^n - 0) = 0 \tag{B.8}$$

Boundary Condition on T at Edge of Computational Domain

$$BCTedge = (1 - kgrad)(T_{jl}^n - T_e)^n + (kgrad)(c_{jl}^n - 0) = 0 \tag{B.9}$$

B.3 Discretized Additional Equations Required for u_τ, T_{wall} and Q_{wall}

Additional Equation for u_τ

$$
\begin{aligned}
EQNu_\tau &= (1 - kwall)\left(u_\tau^n - \sqrt{\frac{T_{wall}^n \mu_{T1}^n h_1^n}{\rho_e^n T_e^n Re_{\delta o}}}\right) \\
&+ (kwall)\left(u_\tau^n - \sqrt{\frac{T_{wall}^n \mu_{wall}^n h_1^n}{\rho_e^n T_e^n Re_{\delta o}}}\right) = 0
\end{aligned} \tag{B.10}
$$

Additional Equation for T_{wall}

$$
\begin{aligned}
EQNT_{wall} &= (kiso)\left(T_{wall}^n - \frac{T_{wall}^*}{T_\infty^*}\right) \\
&+ (1 - kiso)\left(T_{wall}^n - T_1^n - \frac{1}{2}Pr_T u_1^{n2}(\gamma - 1)M_\infty^2\right) = 0
\end{aligned} \tag{B.11}
$$

Additional Equation for Q_{wall}

$$
\begin{aligned}
EQNQ_{wall} &= (kiso)\left(Q_{wall}^n + \frac{\mu_{wall}^n}{Re_{\delta o}M_\infty^2(\gamma - 1)Pr}(c_1^n)\right) \\
&+ (1 - kiso)\left(Q_{wall}^n + \frac{Q_{wall}^*}{U_\infty^{*3}\rho_\infty^*}\right) = 0
\end{aligned} \tag{B.12}
$$

T_{wall}^* is the specified wall temperature for an isothermal wall

Q_{wall}^* is the specified wall heat flux for an adiabatic wall

B.4 Discretized Equations of Motion

Definitions

$$\alpha_j^n = \frac{\Delta y_j}{\Delta x^n} \tag{B.13}$$

$$Re_{\delta o} = \frac{\rho_\infty^* M_\infty \sqrt{\gamma R T_\infty^*} \delta_o^*}{\mu_\infty^*} \tag{B.14}$$

$$\mu_j^n = (T_j^n)^{\frac{3}{2}} \left(\frac{1.0 + T_{ref}}{T_j^n + T_{ref}} \right) \tag{B.15}$$

where

$$T_{ref} = \frac{T_{ref}^*}{T_\infty^*} \tag{B.16}$$

$$(M_t^2)|_j^n = \frac{2.0 M_\infty^2 (q_j^n)^2}{T_j^n} \tag{B.17}$$

$$R_{tj}^n = Re_{\delta o} \rho_e^n T_e^n \frac{(q_j^n)^4}{T_j^n \mu_j^n \epsilon_{vj}^n (1 + C_k (M_t^2)|_j^n)} \tag{B.18}$$

$$\mu_{Tj}^n = Re_{\delta o} \frac{\rho_e^n T_e^n C_\mu f_{mu}|_j^n (q_j^n)^4}{T_j^n \epsilon_{vj}^n (1 + C_k (M_t^2)|_j^n)} \tag{B.19}$$

Where

$f_\mu|_j^n = 1.0$ if $kwall = 0$

$f_\mu|_j^n = f_\mu(R_{tj}^n)$ given by Appendix A if $kwall = 1$

$C_k = 0$

$$B_j^n = 2.0 \left(\frac{\mu_{Tj}^n}{\sigma_k} + \mu_j^n \right) q_j^n b_j^n - \frac{\mu_{Tj}^n (q_j^n)^2 c_j^n}{T_j^n \sigma_k} \tag{B.20}$$

In the limit as $y \to 0$ both the production and dissipation of dissipation terms in the dissipation equation become computationally ill defined, as their denominators will go to 0. This necessitates the employment of two new variables, $f_2 byqsq|_j^n$ and $\mu_T byqsq|_j^n$, whose limit may be separately defined at $y_1 = 0$. Therefore

$$f_2 byqsq|_j^n = \frac{f_2|_j^n}{(q_n^j)^2} \quad \text{(if } j > 1 \text{ or } kwall = 0) \tag{B.21}$$

$$f_2 byqsq|_j^n = C_{\epsilon 3} \sqrt{\frac{\rho_e^n T_e^n Re_{\delta o}}{T_1^n \mu_1^n \epsilon_{v1}^n}} \quad \text{(if } j = 1 \text{ and } kwall = 1) \tag{B.22}$$

$$\mu_T byqsq|_j^n = \frac{\mu_{Tj}^n}{(q_j^n)^2} \quad \text{(if } j > 1 \text{ or } kwall = 0) \tag{B.23}$$

$$\mu_T byqsq|_1^n = 0 \quad \text{(if } j = 1 \text{ and } kwall = 1) \tag{B.24}$$

Discretized Continuity Equation (Equation 4.13)

$$Cont|_j^n = \alpha_j^n \rho_e^n T_e^n \left(\frac{u_j^n}{T_j^n} + \frac{u_{j-1}^n}{T_{j-1}^n} \right) \quad -$$

$$\alpha_j^n \rho_e^{n-1} T_e^{n-1} \left(\frac{u_j^{n-1}}{T_j^{n-1}} + \frac{u_{j-1}^{n-1}}{T_{j-1}^{n-1}} \right) \quad +$$

$$\rho_e^n T_e^n \left(\frac{v_j^n}{T_j^n} - \frac{v_{j-1}^n}{T_{j-1}^n} \right) \quad +$$

$$\rho_e^{n-1} T_e^{n-1} \left(\frac{v_j^{n-1}}{T_j^{n-1}} - \frac{v_{j-1}^{n-1}}{T_{j-1}^{n-1}} \right) \quad = \quad 0 \tag{B.25}$$

Discretized Momentum Equation (Equation 4.14)

$$
\begin{aligned}
Momt|_j^n = {} & \frac{1}{32}(\rho_e^n T_e^n + \rho_e^{n-1} T_e^{n-1})\alpha_j^n(u_j^n + u_{j-1}^n + u_j^{n-1} + u_{j-1}^{n-1}) \\
& \times \left(\frac{1}{T_j^n} + \frac{1}{T_{j-1}^n} + \frac{1}{T_j^{n-1}} + \frac{1}{T_{j-1}^{n-1}} \right)(u_j^n + u_{j-1}^n - u_j^{n-1} - u_{j-1}^{n-1}) \\
& + \frac{1}{64}(\rho_e^n T_e^n + \rho_e^{n-1} T_e^{n-1})\Delta y^j \left(\frac{1}{T_j^n} + \frac{1}{T_{j-1}^n} + \frac{1}{T_j^{n-1}} + \frac{1}{T_{j-1}^{n-1}} \right) \\
& \times (v_j^n + v_{j-1}^n + v_j^{n-1} + v_{j-1}^{n-1})(h_j^n + h_{j-1}^n + h_j^{n-1} + h_{j-1}^{n-1}) \\
& - \Delta y^j(\beta^n + \beta^{n-1}) \\
& - \frac{1}{Re_{\delta o}}\left[(\mu + \mu_T)h|_j^n + (\mu + \mu_T)h|_j^{n-1} - (\mu + \mu_T)h|_{j-1}^n - (\mu + \mu_T)h|_{j-1}^{n-1} \right] \\
= {} & 0 \tag{B.26}
\end{aligned}
$$

where

$$\beta^n = -\frac{p_e^n - p_e^{n-1}}{\Delta x^n} \tag{B.27}$$

Discretized Energy Equation (Equation 4.20)

$$
\begin{aligned}
Energy|_j^n = {} & \frac{1}{32M_\infty^2(\gamma - 1)}(\rho_e^n T_e^n + \rho_e^{n-1} T_e^{n-1})[\alpha_j^n(u_j^n + u_{j-1}^n + u_j^{n-1} + u_{j-1}^{n-1}) \\
& \times \left(\frac{1}{T_j^n} + \frac{1}{T_{j-1}^n} + \frac{1}{T_j^{n-1}} + \frac{1}{T_{j-1}^{n-1}} \right)(T_j^n + T_{j-1}^n - T_j^{n-1} - T_{j-1}^{n-1}) \\
& + \frac{\Delta y^j}{2}(v_j^n + v_{j-1}^n + v_j^{n-1} + v_{j-1}^{n-1})\left(\frac{1}{T_j^n} + \frac{1}{T_{j-1}^n} + \frac{1}{T_j^{n-1}} + \frac{1}{T_{j-1}^{n-1}} \right) \\
& \times (c_j^n + c_{j-1}^n + c_j^{n-1} + c_{j-1}^{n-1})] \\
& + \frac{1}{64}(\rho_e^n T_e^n + \rho_e^{n-1} T_e^{n-1})(q_j^n + q_{j-1}^n + q_j^{n-1} + q_{j-1}^{n-1}) \\
& \times \left(\frac{1}{T_j^n} + \frac{1}{T_{j-1}^n} + \frac{1}{T_j^{n-1}} + \frac{1}{T_{j-1}^{n-1}} \right)
\end{aligned}
$$

$$\times \ [\alpha_j^n(u_j^n + u_{j-1}^n + u_j^{n-1} + u_{j-1}^{n-1})(q_j^n + q_{j-1}^n - q_j^{n-1} - q_{j-1}^{n-1})$$

$$+ \ \frac{\Delta y^j}{2}(v_j^n + v_{j-1}^n + v_j^{n-1} + v_{j-1}^{n-1})(b_j^n + b_{j-1}^n + b_j^{n-1} + b_{j-1}^{n-1})]$$

$$- \ \frac{1}{M_\infty^2(\gamma - 1)Re_{\delta o}}[\left(\frac{\mu_T}{Pr_T} + \frac{\mu}{Pr}\right)c|_j^n + \left(\frac{\mu_T}{Pr_T} + \frac{\mu}{Pr}\right)c|_j^{n-1}$$

$$- \ \left(\frac{\mu_T}{Pr_T} + \frac{\mu}{Pr}\right)c|_{j-1}^n - \left(\frac{\mu_T}{Pr_T} + \frac{\mu}{Pr}\right)c|_{j-1}^{n-1}]$$

$$+ \ \frac{\Delta y^j}{4}(u_j^n + u_{j-1}^n + u_j^{n-1} + u_{j-1}^{n-1})(\beta^n + \beta^{n-1})$$

$$- \ \frac{\Delta y^j}{32Re_{\delta o}}[(\mu_T + \mu)|_j^n + (\mu_T + \mu)|_{j-1}^n + (\mu_T + \mu)|_j^{n-1} + (\mu_T + \mu)|_{j-1}^{n-1}]$$

$$\times \ (h_j^n + h_{j-1}^n + h_j^{n-1} + h_{j-1}^{n-1})^2$$

$$= \ 0 \qquad\qquad\qquad\qquad\qquad\qquad\qquad (B.28)$$

Discretized Dissipation Equation (Equation 4.16)

$$Dissip|_j^n \ = \ \frac{1}{32}(\rho_e^n T_e^n + \rho_e^{n-1}T_e^{n-1})\alpha_j^n(u_j^n + u_{j-1}^n + u_j^{n-1} + u_{j-1}^{n-1})$$

$$\times \ \left(\frac{1}{T_j^n} + \frac{1}{T_{j-1}^n} + \frac{1}{T_j^{n-1}} + \frac{1}{T_{j-1}^{n-1}}\right)(\epsilon_{vj}^n + \epsilon_{vj-1}^n - \epsilon_{vj}^{n-1} - \epsilon_{vj-1}^{n-1})$$

$$+ \ \frac{1}{64}(\rho_e^n T_e^n + \rho_e^{n-1}T_e^{n-1})\Delta y^j(v_j^n + v_{j-1}^n + v_j^{n-1} + v_{j-1}^{n-1})$$

$$\times \ \left(\frac{1}{T_j^n} + \frac{1}{T_{j-1}^n} + \frac{1}{T_j^{n-1}} + \frac{1}{T_{j-1}^{n-1}}\right)(a_j^n + a_{j-1}^n + a_j^{n-1} + a_{j-1}^{n-1})$$

$$- \ \frac{C_{e1}\Delta y^j}{128Re_{\delta o}}(\mu_T byqsq|_j^n + \mu_T byqsq|_{j-1}^n + \mu_T byqsq|_j^{n-1} + \mu_T byqsq|_{j-1}^{n-1})$$

$$\times \ (\epsilon_{vj}^n + \epsilon_{vj-1}^n + \epsilon_{vj}^{n-1} + \epsilon_{vj-1}^{n-1})(h_j^n + h_{j-1}^n + h_j^{n-1} + h_{j-1}^{n-1})^2$$

$$+ \ \frac{C_{e2}\Delta y^j}{256}(f_2 byqsq|_j^n + f_2 byqsq|_{j-1}^n + f_2 byqsq|_j^{n-1} + f_2 byqsq|_{j-1}^{n-1})$$

$$\times \ (\epsilon_{vj}^n + \epsilon_{vj-1}^n + \epsilon_{vj}^{n-1} + \epsilon_{vj-1}^{n-1})^2 \left(\frac{1}{T_j^n} + \frac{1}{T_{j-1}^n} + \frac{1}{T_j^{n-1}} + \frac{1}{T_{j-1}^{n-1}}\right)$$

$$= \ 0 \qquad\qquad\qquad\qquad\qquad\qquad\qquad (B.29)$$

Discretized Turbulence Kinetic Energy Equation (Equation 4.18)

$$Tke|_j^n \ = \ \frac{1}{64}(\rho_e^n T_e^n + \rho_e^{n-1}T_e^{n-1})\alpha_j^n(u_j^n + u_{j-1}^n + u_j^{n-1} + u_{j-1}^{n-1})$$

$$\times \ \left(\frac{1}{T_j^n} + \frac{1}{T_{j-1}^n} + \frac{1}{T_j^{n-1}} + \frac{1}{T_{j-1}^{n-1}}\right)(q_j^n + q_{j-1}^n + q_j^{n-1} + q_{j-1}^{n-1})$$

$$\times \ (q_j^n + q_{j-1}^n - q_j^{n-1} - q_{j-1}^{n-1})$$

$$+ \ \frac{1}{128}(\rho_e^n T_e^n + \rho_e^{n-1}T_e^{n-1})\Delta y^j(v_j^n + v_{j-1}^n + v_j^{n-1} + v_{j-1}^{n-1})$$

$$\times \quad \left(\frac{1}{T_j^n} + \frac{1}{T_{j-1}^n} + \frac{1}{T_j^{n-1}} + \frac{1}{T_{j-1}^{n-1}}\right)$$

$$\times \quad (q_j^n + q_{j-1}^n + q_j^{n-1} + q_{j-1}^{n-1})(b_j^n + b_{j-1}^n + b_j^{n-1} + b_{j-1}^{n-1})$$

$$- \quad \frac{1}{32Re_{\delta o}}\Delta y^j(\mu_{Tj}^n + \mu_{Tj-1}^n + \mu_{Tj}^{n-1} + \mu_{Tj-1}^{n-1})(h_j^n + h_{j-1}^n + h_j^{n-1} + h_{j-1}^{n-1})^2$$

$$- \quad \frac{1}{Re_{\delta o}}(B_j^n + B_j^{n-1} - B_{j-1}^n - B_{j-1}^{n-1})$$

$$+ \quad \frac{1}{16}(\rho_e^n T_e^n + \rho_e^{n-1}T_e^{n-1})\Delta y^j(\epsilon_{vj}^n + \epsilon_{vj-1}^n + \epsilon_{vj}^{n-1} + \epsilon_{vj-1}^{n-1})$$

$$\times \quad \left(\frac{1}{T_j^n} + \frac{1}{T_{j-1}^n} + \frac{1}{T_j^{n-1}} + \frac{1}{T_{j-1}^{n-1}}\right)$$

$$\times \quad (1 + \frac{C_k}{4}[(M_t^2)|_{j-1}^n + (M_t^2)|_j^{n-1} + (M_t^2)|_j^n + (M_t^2)|_{j-1}^{n-1}]$$

$$= \quad 0 \tag{B.30}$$

Discretized Equation for $\partial u/\partial y$

$$Derivu|_j^n = -\frac{\Delta y^j}{2}(h_j^n + h_{j-1}^n) + u_j^n - u_{j-1}^n = 0 \tag{B.31}$$

Discretized Equation for $\partial \epsilon_v/\partial y$

$$Derive|_j^n = -\frac{\Delta y^j}{2}(a_j^n + a_{j-1}^n) + \epsilon_{vj}^n - \epsilon_{vj-1}^n = 0 \tag{B.32}$$

Discretized Equation for $\partial q/\partial y$

$$Derivq|_j^n = -\frac{\Delta y^j}{2}(b_j^n + b_{j-1}^n) + q_j^n - q_{j-1}^n = 0 \tag{B.33}$$

Discretized Equation for $\partial T/\partial y$

$$DerivT|_j^n = -\frac{\Delta y^j}{2}(c_j^n + c_{j-1}^n) + T_j^n - T_{j-1}^n = 0 \tag{B.34}$$

B.5 System of of Discretized Equations

$$
\vec{F} =
\begin{pmatrix}
EQNu_\tau \\
EQNT_{wall} \\
EQNQ_{wall} \\
BCuwall \\
BCvwall \\
BC\epsilon wall \\
BCqwall \\
BCTwall \\
\cdot \\
\cdot \\
\cdot \\
Cont|_j^n \\
Momt|_j^n \\
Derivu|_j^n \\
Dissip|_j^n \\
Derive|_j^n \\
Tke|_j^n \\
Derivq|_j^n \\
Energy|_j^n \\
DerivT|_j^n \\
\cdot \\
\cdot \\
\cdot \\
BCuedge \\
BC\epsilon edge \\
BCqedge \\
BCTedge
\end{pmatrix}
$$

B.6 System of Independent Variables

$$\vec{w} = \begin{pmatrix} u_{tau}^n \\ T_{wall}^n \\ Q_{wall}^n \\ u_1^n \\ v_1^n \\ h_1^n \\ \epsilon_{v1}^n \\ a_1^n \\ q_1^n \\ \cdot \\ \cdot \\ \cdot \\ u_j^n \\ v_j^n \\ h_j^n \\ \epsilon_{vj}^n \\ a_j^n \\ q_j^n \\ b_j^n \\ T_j^n \\ c_j^n \\ \cdot \\ \cdot \\ \cdot \\ q_{jl}^n \\ b_{jl}^n \\ T_{jl}^n \\ c_{jl}^n \end{pmatrix}$$

Appendix C

The Jacobian

Enclosed in this Appendix is the form of the Jacobian matrix employed to solve by Newton's method. The Jacobian is obtained by differenciating the system of equations, $\vec{F}$, by the independent variables defined by $\vec{w}$ of Appendix C. The Jacobian matrix is defined by the equation

$$\vec{J} = \frac{\partial \vec{F}}{\partial \vec{w}} \tag{C.1}$$

There are $9 \times (jl - 1)$ algebraic, governing equations being solved in the boundary layer, plus nine boundary conditions, and three additional equations required when integrating to only the wall layer. This yields $9 \times jl + 3$ equations with the same number of unknowns. However, each of the equations in the boundary layer is only a function of the independent variables directly adjacent to the grid location in which it is being approximated. Therefore by formulating $\vec{F}$ and $\vec{w}$ in the manner employed the resulting Jacobian is a 9×9 block tridiagonal matrix of the form seen in Figure C.1.

C.1 Relevant Definitions

In calculating the Jacobian it is convenient to define the derivatives of certain functions that are employed multiple times.

$$\frac{d\mu_j^n}{dT_j^n} = \sqrt{T_j^n}(1. + T_{ref}) \left(\frac{\frac{3}{2}(T_j^n + T_{ref}) - T_j^n}{(T_j^n + T_{ref})^2} \right) \tag{C.2}$$

$$\frac{d\mu_{wall}^n}{dT_j^n} = \sqrt{T_{wall}^n}(1. + T_{ref}) \left(\frac{\frac{3}{2}(T_{wall}^n + T_{ref}) - T_j^n}{(T_{wall}^n + T_{ref})^2} \right) \tag{C.3}$$

$$\frac{\partial(M_t^2)}{\partial T_j^n} = -\frac{2M_\infty^2 q_j^{n2}}{T_j^{n2}} \tag{C.4}$$

$$\frac{\partial(M_t^2)}{\partial q_j^n} = \frac{4M_\infty^2 q_j^n}{T_j^n} \tag{C.5}$$

$$(C.6)$$

$$\frac{\partial R_{tj}^n}{\partial T_j^n} = -Re_{\delta o}\rho_e^n T_e^n \frac{q_j^{n4}\left(T_j^n\frac{d\mu_j^n}{dT_j^n} + \mu_j^n + \frac{T_j^n\mu_j^n C_k \frac{\partial(M_t^2)|_j^n}{\partial T_j^n}}{1+C_k(M_t^2)|_j^n}\right)}{\epsilon_{vj}^n(\mu_j^n T_j^n)^2(1 + C_k(M_t^2)|_j^n)} \qquad (C.7)$$

$$\frac{\partial R_{tj}^n}{\partial q_j^n} = \frac{Re_{\delta o}\rho_e^n T_e^n q_j^{n3}}{T_j^n \mu_j^n \epsilon_{vj}^n}\left(\frac{4(1 + C_k(M_t^2)|_j^n) - q_j^n C_k \frac{\partial(M_t^2)|_j^n}{\partial T_j^n}}{1 + C_k(M_t^2)|_j^n}\right) \qquad (C.8)$$

$$\frac{\partial R_{tj}^n}{\partial \epsilon_{vj}^n} = -\frac{Re_{\delta o}\rho_e^n T_e^n q_j^{n4}}{\mu_j^n T_j^n \epsilon_{vj}^{n2}(1 + C_k(M_t^2))} \qquad (C.9)$$

$$\frac{df_{\mu j}^n}{dR_{tj}^n} = \left\{\begin{array}{l} 0 \text{ if } kwall = 0 \\ \\ \text{is caculated from Table in Appendix A if kwall} = 1 \end{array}\right\} \qquad (C.10)$$

$$\frac{\partial \mu_{Tj}^n}{\partial T_j^n} = \frac{Re_{\delta o}\rho_e^n T_e^n C_\mu q_j^{n4}}{\epsilon_{vj}^n}$$

$$\times \left(\frac{T_j^n(1 + C_k(M_t^2)|_j^n)\frac{df_{\mu j}^n}{dR_{tj}^n}\frac{\partial R_{tj}^n}{\partial T_j^n} - f_{\mu j}^n\left(1 + C_k(M_t^2)|_j^n + C_k T_j^n\frac{\partial(M_t^2)}{\partial T_j^n}\right)}{\left(T_j^n(1 + C_k(M_t^2)|_j^n)\right)^2}\right) \qquad (C.11)$$

$$\frac{\partial \mu_{Tj}^n}{\partial \epsilon_{vj}^n} = \frac{Re_{\delta o}\rho_e^n T_e^n C_\mu q_j^{n4}}{T_j^n(1 + C_k(M_t^2)|_j^n)}\left(\frac{\epsilon_{vj}^n\frac{df_{\mu j}^n}{dR_{tj}^n}\frac{\partial R_{tj}^n}{\partial \epsilon_{vj}^n} - f_{\mu j}^n}{\epsilon_{vj}^{n2}}\right) \qquad (C.12)$$

$$\frac{\partial \mu_{Tj}^n}{\partial q_j^n} = \frac{Re_{\delta o}\rho_e^n T_e^n C_\mu}{\epsilon_{vj}^n T_j^n}$$

$$\times \left(\frac{(1 + C_k(M_t^2)|_j^n)\left(4q_j^{n3}f_{\mu j}^n + q_j^{n4}\frac{df_{\mu j}^n}{dR_{tj}^n}\frac{\partial R_{tj}^n}{\partial q_j^n}\right) - f_{\mu j}^n q_j^{n4}C_k\frac{\partial(M_t^2)}{\partial q_j^n}}{1 + C_k(M_t^2)|_j^n}\right) \qquad (C.13)$$

$$\frac{\partial mtbyqsq_j^n}{\partial q_j^n} = \frac{Re_{\delta o}\rho_e^n T_e^n C_\mu}{\epsilon_{vj}^n T_j^n} \qquad (C.14)$$

$$\times \left(\frac{(1 + C_k(M_t^2)|_j^n)\left(2q_j^n f_{\mu j}^n + q_j^{n2}\frac{df_{\mu j}^n}{dR_{tj}^n}\frac{\partial R_{tj}^n}{\partial q_j^n}\right) - f_{\mu j}^n q_j^{n2}C_k\frac{\partial(M_t^2)}{\partial q_j^n}}{1 + C_k(M_t^2)|_j^n}\right) \qquad (C.15)$$

Diffusion Term in Turblence Kinetic Energy Equation

$$B_j^n = 2q_j^n b_j^n\left(\frac{\mu_{Tj}^n}{\sigma_k} + \mu_j^n\right) - \frac{\mu_{Tj}^n}{\sigma_k}\frac{q_j^{n2}c_j^n}{T_j^n} \qquad (C.16)$$

$$\frac{\partial B_j^n}{\partial \epsilon_{vj}^n} = \frac{2q_j^n b_j^n}{\sigma_k}\frac{\partial \mu_{Tj}^n}{\partial \epsilon_{vj}^n} - \frac{q_j^{n2} c_j^n}{\sigma_k T_j^n}\frac{\partial \mu_{Tj}^n}{\partial \epsilon_{vj}^n} \tag{C.17}$$

$$\frac{\partial B_j^n}{\partial q_j^n} = 2b_j^n\left(\frac{\mu_{Tj}^n}{\sigma_k} + \mu_j^n\right) + 2\frac{q_j^n b_j^n}{\sigma_k}\frac{\partial \mu_{Tj}^n}{\partial q_j^n} - 2\frac{q_j^n \mu_{Tj}^n c_j^n}{\sigma_k T_j^n} - \frac{q_j^{n2} c_j^n}{\sigma_k T_j^n}\frac{\partial \mu_{Tj}^n}{\partial q_j^n} \tag{C.18}$$

$$\frac{\partial B_j^n}{\partial b_j^n} = 2q_j^n\left(\frac{\mu_{Tj}^n}{\sigma_k} + \mu_j^n\right) \tag{C.19}$$

$$\frac{\partial B_j^n}{\partial T_j^n} = 2q_j^n b_j^n\left(\frac{\partial \mu_{Tj}^n}{\partial T_j^n}\frac{1}{\sigma_k} + \frac{d\mu_j^n}{dT_j^n}\right) + \frac{\mu_{Tj}^n}{\sigma_k}\frac{q_j^{n2} c_j^n}{T_j^{n2}} - \frac{q_j^{n2} c_j^n}{\sigma_k T_j^n}\frac{\partial \mu_{Tj}^n}{\partial T_j^n} \tag{C.20}$$

$$\frac{\partial B_j^n}{\partial c_j^n} = -\frac{\mu_{Tj}^n q_j^{n2}}{\sigma_k T_j^n} \tag{C.21}$$

Low Reynolds Number Correction to Dissipation of Solenoidal Dissipation

if kwall = 0 then

$$f_2 byqsq_j^n = \frac{1}{q_j^{n2}} \tag{C.22}$$

$$\frac{\partial f_2 byqsq_j^n}{\partial q_j^n} = -\frac{2}{q_j^{n3}} \tag{C.23}$$

$$\frac{\partial f_2 byqsq_j^n}{\partial \epsilon_{vj}^n} = 0 \tag{C.24}$$

$$\frac{\partial f_2 byqsq_j^n}{\partial T_j^n} = 0 \tag{C.25}$$

if kwall = 1 then

$$f_2 byqsq_j^n = \frac{1 - e^{-C_{\epsilon 3}\sqrt{R_{tj}^n}}}{q_j^{n2}} \tag{C.26}$$

$$\frac{\partial f_2 byqsq_1^n}{\partial q_1^n} = 0 \tag{C.27}$$

$$\frac{\partial f_2 byqsq_1^n}{\partial \epsilon_{v1}^n} = -\frac{C_{\epsilon 3}}{2}\sqrt{Re_{\delta o}\frac{\rho_e^n T_e^n}{\mu_j^n T_j^n}}(\epsilon_{vj}^n)^{\frac{3}{2}} \tag{C.28}$$

$$\frac{\partial f_2 byqsq_1^n}{\partial T_1^n} = -\frac{C_{\epsilon 3}}{2}\sqrt{Re_{\delta o}\frac{\rho_e^n T_e^n}{\epsilon_{vj}^n}}\left(\frac{1}{\sqrt{T_j^n \mu_j^{n3}}}\frac{d\mu_j^n}{dT_j^n} + \frac{1}{\sqrt{T_j^{n3}\mu_j^n}}\right) \tag{C.29}$$

$$\frac{\partial f_2 byqsq_j^n}{\partial q_j^n} = \frac{\frac{1}{2}C_{\epsilon 3}\frac{q_j^n}{\sqrt{R_{tj}^n}}\frac{\partial R_{tj}^n}{\partial q_j^n}e^{-C_{\epsilon 3}\sqrt{R_{tj}^n}} - 2\left(1 - e^{-C_{\epsilon 3}\sqrt{R_{tj}^n}}\right)}{q_j^{n3}} \tag{C.30}$$

$$\frac{\partial f_2 byqsq_j^n}{\partial \epsilon_{vj}^n} = \frac{\frac{1}{2}\frac{C_{\epsilon 3}}{\sqrt{R_{tj}^n}}\frac{\partial R_{tj}^n}{\partial \epsilon_{vj}^n}e^{-C_{\epsilon 3}\sqrt{R_{tj}^n}}}{q_j^{n2}} \tag{C.31}$$

$$\frac{\partial f_2 byqsq_j^n}{\partial T_j^n} = \frac{\frac{1}{2}\frac{C_{\epsilon 3}}{\sqrt{R_{tj}^n}}\frac{\partial R_{tj}^n}{\partial T_j^n}e^{-C_{\epsilon 3}\sqrt{R_{tj}^n}}}{q_j^{n2}} \tag{C.32}$$

Notation Employed

$$\sum w = w_j^n + w_j^{n-1} + w_{j-1}^n + w_{j-1}^{n-1} \qquad (C.33)$$

C.2 The Jacobian

The first three rows of the jacobian are associated with the equations for friction velocity, wall temperature and wall heat transfer that are required when itegrating to only the wall layer. The next five rows are associated with the boundary conditions at the wall or in the wall layer. The next $9 \times (jl - 1)$ rows are associated with the governing equations, while the last four rows are associated with the boundary conditions at the edge of the boundary layer.

Each term of the Jacobian has an associated row and column denoting its location. The notation J_j^k represents the term of the Jacobian in j^{th} row and k^{th} column.

C.2.1 Portion of the Jacobian Associated with the Equations for u_τ, T_{wall} and Q_{wall}

- Jacobian for Equation for u_τ

$$\begin{aligned} J_1^2 &= (1 - kwall)\left(-\frac{1}{2}\sqrt{\frac{\mu_{T1}^n h_1^n}{\rho_e^n T_e^n Re_{\delta o} T_{wall}^n}}\right) \\ &+ (kwall)\left(-\frac{1}{2}\sqrt{\frac{\mu_1^n h_1^n}{\rho_e^n T_e^n Re_{\delta o} T_{wall}^n}}\right) \end{aligned} \qquad (C.34)$$

$$\begin{aligned} J_1^6 &= (1 - kwall)\left(-\frac{1}{2}\sqrt{\frac{\mu_{T1}^n T_{wall}^n}{\rho_e^n T_e^n Re_{\delta o} h_1^n}}\right) \\ &+ (kwall)\left(-\frac{1}{2}\sqrt{\frac{\mu_1^n T_{wall}^n}{\rho_e^n T_e^n Re_{\delta o} h_1^n}}\right) \end{aligned} \qquad (C.35)$$

$$J_1^7 = (1 - kwall)\left(-\frac{1}{2}\sqrt{\frac{h_1^n T_{wall}^n}{\rho_e^n T_e^n Re_{\delta o}\mu_{T1}^n}}\frac{\partial\mu_{T1}^n}{\partial\epsilon_{v1}^n}\right) \qquad (C.36)$$

$$J_1^9 = (1 - kwall)\left(-\frac{1}{2}\sqrt{\frac{h_1^n T_{wall}^n}{\rho_e^n T_e^n Re_{\delta o}\mu_{T1}^n}}\frac{\partial\mu_{T1}^n}{\partial q_1^n}\right) \qquad (C.37)$$

$$\begin{aligned} J_1^{11} &= (1 - kwall)\left(-\frac{1}{2}\sqrt{\frac{h_1^n T_{wall}^n}{\rho_e^n T_e^n Re_{\delta o}\mu_{T1}^n}}\frac{\partial\mu_{T1}^n}{\partial T_1^n}\right) \\ &+ (kwall)\left(-\frac{1}{2}\sqrt{\frac{h_1^n T_{wall}^n}{\rho_e^n T_e^n Re_{\delta o}\mu_1^n}}\frac{d\mu_1^n}{dT_1^n}\right) \end{aligned} \qquad (C.38)$$

- Jacobian for Equation for T_{wall}

$$J_2^2 = 1.0 \tag{C.39}$$

$$J_2^4 = (1 - kiso)\left(-Pr_T u_1^2(\gamma - 1)M_\infty^2\right) \tag{C.40}$$

$$J_2^{11} = (1 - kiso)(-1) \tag{C.41}$$

- Jacobian for Equation for Q_{wall}

$$J_3^3 = 1.0 \tag{C.42}$$

$$J_3^{12} = \frac{\mu_{wall}^n}{Re_{\delta_o} M_\infty^2 (\gamma - 1)Pr} \tag{C.43}$$

C.2.2 Portion of the Jacobian Associated with the Boundary Conditions at the Wall or in the Wall Layer

The form of the wall function boundary conditions employed includes modifications for compressibility.

- Jacobian for Boundary Condition on u

Definitions

$$\frac{\partial u_c}{\partial u_\tau^n} = \frac{1}{\kappa}\ln\left(Re_{\delta_0}\frac{u_\tau^n y_1 \rho_e^n T_e^n}{\mu_{wall}^n T_{wall}^n}\right) + \frac{1}{\kappa} + B \tag{C.44}$$

$$\frac{\partial u_c}{\partial T_{wall}^n} = \frac{u_\tau^n}{\kappa}\left(-\frac{1}{T_{wall}} - \frac{1}{\mu_{wall}}\frac{d\mu_{wall}}{dT_{wall}}\right) \tag{C.45}$$

$$\frac{\partial A_1}{\partial T_{wall}^n} = -\frac{1}{2}\sqrt{\frac{(\gamma - 1)Pr_T M_\infty^2}{T_{wall}^{n3}}} \tag{C.46}$$

$$J_4^1 = -(1 - kwall)\cos(A_1 u_c)\frac{\partial u_c}{\partial u_\tau^n} \tag{C.47}$$

$$J_4^3 = -\left(-\frac{1}{A_1^2}\frac{\partial A_1}{\partial T_{wall}^n}\sin(A_1 u_c) + \frac{1}{A_1}\cos(u_c A_1)u_c\frac{\partial A_1}{\partial T_{wall}^n}\right) \tag{C.48}$$

$$J_4^4 = 1.0 \tag{C.49}$$

- Jacobian for Boundary Condition on v

$$J_5^1 = kvvel\left(\frac{y_1 u_1^n}{\Delta x^n}\left(\frac{1}{u_\tau^n} - \left(\frac{u_\tau^n - u_\tau^{n-1}}{u_\tau^{n2}}\right)\right)\right) \tag{C.50}$$

$$J_5^4 = kvvel\left(\frac{y_1}{\Delta x^n}\left(\frac{u_\tau^n - u_\tau^{n-1}}{u_\tau^n}\right)\right) \tag{C.51}$$

$$J_5^5 = 1.0 \tag{C.52}$$

- Jacobian for Boundary Condition on ϵ_v

$$J_6^1 = (1 - kwall)\left(-3\frac{u_\tau^{n2}}{\kappa y_1}\left(\frac{T_1^n}{T_{wall}^n}\right)^{\frac{1}{4}}\right) \tag{C.53}$$

$$J_6^2 = (1 - kwall)\left(\frac{1}{4}\frac{u_\tau^{n3}}{\kappa y_1}\left(\frac{T_1^n}{(T_{wall}^n)^5}\right)^{\frac{1}{4}}\right) \tag{C.54}$$

$$J_6^7 = 1.0 \tag{C.55}$$

$$J_6^{10} = (kwall)\left(-4\frac{\mu_1^n T_1^n b_1^n}{\rho_e^n T_e^n Re_{\delta o}}\right) \tag{C.56}$$

$$J_6^{11} = (1 - kwall)\left(-\frac{3}{2}\frac{u_\tau^{n3}}{\kappa y_1}\left(\left(\frac{1}{T_1^n}\right)^3\left(\frac{1}{T_{wall}^n}\right)\right)^{\frac{1}{4}}\right)$$
$$+ (kwall)\left(-2\frac{b_1^{n2}}{\rho_e^n T_e^n Re_{\delta o}}\left(\mu_1^n + T_1^n\frac{d\mu_1^n}{dT_1^n}\right)\right) \tag{C.57}$$

- Jacobian for Boundary Condition on q

$$J_7^1 = (1 - kwall)\left(\frac{\sqrt{\frac{T_1^n}{T_{wall}^n}}}{(C_\mu)^{\frac{1}{4}}}\right) \tag{C.58}$$

$$J_7^2 = (1 - kwall)\left(\frac{1}{2}\frac{u_\tau^n}{(C_\mu)^{\frac{1}{4}}}\left(\sqrt{\frac{T_1^n}{T_{wall}^{n3}}}\right)\right) \tag{C.59}$$

$$J_7^9 = 1.0 \tag{C.60}$$

$$J_7^{11} = (1 - kwall)\left(-\frac{1}{2}\frac{u_\tau^n}{(C_\mu)^{\frac{1}{4}}}\sqrt{\frac{1}{T_1^n T_{wall}^n}}\right) \tag{C.61}$$

- Jacobian for Boundary Condition on T

$$J_8^2 = kiso + (1 - kiso)\left(c_1^n + Pr_T u_1^n h_1^n(\gamma - 1)M_\infty^2\right)\frac{M_\infty^2}{Pr(\gamma - 1)}\frac{d\mu_{wall}}{dT_{wall}^n} \tag{C.62}$$

$$J_8^3 = (1 - kiso) \tag{C.63}$$

$$J_8^4 = kiso\left(-u_1^n Pr_T(\gamma - 1)M_\infty^2\right) + (1 - kiso)\left(\frac{M_\infty^4 \mu_{wall} Pr_T h_1^n}{Pr}\right) \tag{C.64}$$

$$J_8^6 = (1 - kiso)\left(\frac{M_\infty^4 \mu_{wall} Pr_T u_1^n}{Pr}\right) \tag{C.65}$$

$$J_8^{11} = -kiso \tag{C.66}$$

$$J_8^{12} = (1 - kiso)\frac{M_\infty^2 \mu_{wall}}{Pr(\gamma - 1)} \tag{C.67}$$

C.2.3 Portion of the Jacobian Associated with the Governing Equations

The following are the terms of the Jacobian that arise from the governing equations. For these terms $2 \le j \le jl$.

- Jacobian for Continuity Equation

$$J_{9(j-1)}^{9(j-1)+4} = \frac{\alpha_j^n \rho_e^n T_e^n}{T_j^n} \tag{C.68}$$

$$J_{9(j-1)}^{9(j-1)+5} = \frac{\rho_e^n T_e^n}{T_j^n} \tag{C.69}$$

$$J_{9(j-1)}^{9(j-1)+11} = -\alpha_j^n \rho_e^n T_e^n \frac{u_j^n}{T_j^{n2}} - \rho_e^n T_e^n \frac{v_j^n}{T_j^{n2}} \tag{C.70}$$

$$J_{9(j-1)}^{9(j-2)+4} = \frac{\alpha_j^n \rho_e^n T_e^n}{T_{j-1}^{n2}} \tag{C.71}$$

$$J_{9(j-1)}^{9(j-2)+5} = -\frac{\rho_e^n T_e^n}{T_{j-1}^{n2}} \tag{C.72}$$

$$J_{9(j-1)}^{9(j-2)+11} = -\alpha_j^n \rho_e^n T_e^n \frac{u_{j-1}^n}{T_{j-1}^{n2}} + \rho_e^n T_e^n \frac{v_{j-1}^n}{T_{j-1}^{n2}} \tag{C.73}$$

- Jacobian for Momentum Equation

$$
\begin{aligned}
J_{9(j-1)+1}^{9(j-1)+4} &= \frac{1}{32}(\rho_e^n T_e^n + \rho_e^{n-1} T_e^{n-1})\alpha_j^n \sum \frac{1}{T} \\
&\times \left[u_j^n + u_{j-1}^n - u_j^{n-1} - u_{j-1}^{n-1} + \sum u \right]
\end{aligned} \tag{C.74}
$$

$$J_{9(j-1)+1}^{9(j-1)+5} = \frac{1}{64}(\rho_e^n T_e^n + \rho_e^{n-1} T_e^{n-1})\Delta y^j \sum \frac{1}{T} \sum h \tag{C.75}$$

$$J_{9(j-1)+1}^{9(j-1)+6} = \frac{1}{64}(\rho_e^n T_e^n + \rho_e^{n-1} T_e^{n-1})\Delta y^j \sum \frac{1}{T} \sum v - \frac{1}{Re_{\delta o}}(\mu_j^n + \mu_{Tj}^n) \tag{C.76}$$

$$J_{9(j-1)+1}^{9(j-1)+7} = -\frac{1}{Re_{\delta o}} \frac{\partial \mu_{Tj}^n}{\partial \epsilon_{vj}^n} h_j^n \tag{C.77}$$

$$J_{9(j-1)+1}^{9(j-1)+9} = -\frac{1}{Re_{\delta o}} \frac{\partial \mu_{Tj}^n}{\partial q_j^n} h_j^n \tag{C.78}$$

$$
\begin{aligned}
J_{9(j-1)+1}^{9(j-1)+11} &= -\frac{1}{32}(\rho_e^n T_e^n + \rho_e^{n-1} T_e^{n-1})\alpha_j^n \sum u \frac{1}{T_j^{n2}}(u_j^n + u_{j-1}^n - u_j^{n-1} - u_{j-1}^{n-1}) \\
&- \frac{1}{64}(\rho_e^n T_e^n + \rho_e^{n-1})\Delta y^j \frac{1}{T_j^{n2}} \sum v \sum h \\
&- \frac{1}{Re_{\delta o}} \left(\frac{d\mu_j^n}{dT_j^n} + \frac{\partial \mu_{Tj}^n}{\partial T_j^n} \right) h_j^n
\end{aligned} \tag{C.79}
$$

$$J^{9(j-2)+4}_{9(j-1)+1} = \frac{1}{32}(\rho_e^n T_e^n + \rho_e^{n-1} T_e^{n-1})\alpha_j^n \sum \frac{1}{T}$$
$$\times \left[u_j^n + u_{j-1}^n - u_j^{n-1} - u_{j-1}^{n-1} + \sum u \right] \qquad (C.80)$$

$$J^{9(j-2)+5}_{9(j-1)+1} = \frac{1}{64}(\rho_e^n T_e^n + \rho_e^{n-1} T_e^{n-1})\Delta y^j \sum \frac{1}{T} \sum h \qquad (C.81)$$

$$J^{9(j-2)+6}_{9(j-1)+1} = \frac{1}{64}(\rho_e^n T_e^n + \rho_e^{n-1} T_e^{n-1})\Delta y^j \sum \frac{1}{T} \sum v + \frac{1}{Re_{\delta o}}(\mu_{j-1}^n + \mu_{Tj-1}^n) \quad (C.82)$$

$$J^{9(j-2)+7}_{9(j-1)+1} = \frac{1}{Re_{\delta o}} \frac{\partial \mu_{Tj-1}^n}{\partial \epsilon_{vj-1}^n} h_{j-1}^n \qquad (C.83)$$

$$J^{9(j-2)+9}_{9(j-1)+1} = \frac{1}{Re_{\delta o}} \frac{\partial \mu_{Tj-1}^n}{\partial q_{j-1}^n} h_{j-1}^n \qquad (C.84)$$

$$J^{9(j-2)+11}_{9(j-1)+1} = -\frac{1}{32}(\rho_e^n T_e^n + \rho_e^{n-1} T_e^{n-1})\alpha_j^n \sum u \frac{1}{T_{j-1}^{n2}}(u_j^n + u_{j-1}^n - u_j^{n-1} - u_{j-1}^{n-1})$$
$$- \frac{1}{64}(\rho_e^n T_e^n + \rho_e^{n-1})\Delta y^j \frac{1}{T_{j-1}^{n2}} \sum v \sum h$$
$$+ \frac{1}{Re_{\delta o}} \left(\frac{d\mu_{j-1}^n}{dT_{j-1}^n} + \frac{\partial \mu_{Tj-1}^n}{\partial T_{j-1}^n} \right) h_{j-1}^n \qquad (C.85)$$

- Jacobian for Definition of $\partial u/\partial y$

$$J^{9(j-1)+4}_{9(j-1)+2} = 1.0 \qquad (C.86)$$

$$J^{9(j-1)+6}_{9(j-1)+2} = -\frac{\Delta y^j}{2} \qquad (C.87)$$

$$J^{9(j-2)+4}_{9(j-1)+2} = -1.0 \qquad (C.88)$$

$$J^{9(j-2)+6}_{9(j-1)+2} = -\frac{\Delta y^j}{2} \qquad (C.89)$$

- Jacobian for Dissipation Equation

$$J^{9(j-1)+4}_{9(j-1)+3} = \frac{1}{32}(\rho_e^n T_e^n + \rho_e^{n-1} T_e^{n-1}) \sum \frac{1}{T}\alpha_j^n(\epsilon_{vj}^n + \epsilon_{vj-1}^n - \epsilon_{vj}^{n-1} - \epsilon_{vj-1}^{n-1}) \quad (C.90)$$

$$J^{9(j-1)+5}_{9(j-1)+3} = \frac{1}{64}(\rho_e^n T_e^n + \rho_e^{n-1} T_e^{n-1})\Delta y^j \sum a \sum \frac{1}{T} \qquad (C.91)$$

$$J^{9(j-1)+6}_{9(j-1)+3} = -2\frac{C_{\epsilon 1}}{128 Re_{\delta o}} \sum \frac{\mu_T}{q^2} \sum \epsilon_v \Delta y^j \sum h \qquad (C.92)$$

$$J_{9(j-1)+3}^{9(j-1)+7} = \frac{1}{32}(\rho_e^n T_e^n + \rho_e^{n-1} T_e^{n-1}) \sum u \sum \frac{1}{T} \alpha_j^n$$

$$- \frac{C_{\epsilon 1}}{128 Re_{\delta o}} \left(\sum h\right)^2 \Delta y^j \left[\sum \frac{\mu_T}{q^2} + \sum \epsilon_v \left(\frac{\partial \mu_T byqsq_j^n}{\partial \epsilon_{vj}^n}\right)\right]$$

$$+ \frac{C_{\epsilon 2}}{256} \sum \frac{1}{T} \Delta y^j (\rho_e^n T_e^n + \rho_e^{n-1} T_e^{n-1})$$

$$\times \left[\left(\sum \epsilon_v\right)^2 \frac{\partial f_2 byqsq_j^n}{\partial \epsilon_{vj}^n} + 2 \sum f_2 byqsq \sum \epsilon_v\right]$$

$$- \frac{1}{Re_{\delta o}} \left[\frac{1}{\sigma_\epsilon} \frac{\partial \mu_{Tj}^n}{\partial \epsilon_{vj}^n} a_j^n\right] \qquad \text{(C.93)}$$

$$J_{9(j-1)+3}^{9(j-1)+8} = \frac{\Delta y^j}{64}(\rho_e^n T_e^n + \rho_e^{n-1} T_e^{n-1}) \sum v \sum \frac{1}{T} - \frac{1}{Re_{\delta o}}\left[\frac{\mu_{Tj}^n}{\sigma_\epsilon} + \mu_j^n\right] \quad \text{(C.94)}$$

$$J_{9(j-1)+3}^{9(j-1)+9} = -\frac{C_{\epsilon 1}}{128 Re_{\delta o}} \frac{\partial \mu_T byqsq_j^n}{\partial q_j^n} \sum \epsilon_v \left(\sum h\right)^2 \Delta y^j$$

$$+ \frac{C_{\epsilon 2}}{256}(\rho_e^n T_e^n + \rho_e^{n-1} T_e^{n-1}) \frac{\partial f_2 byqsq_j^n}{\partial q_j^n} \left(\sum \epsilon_v\right)^2 \sum \frac{1}{T} \Delta y^j$$

$$- \frac{1}{Re_{\delta o}} \frac{\partial \mu_{Tj}^n}{\partial q_j^n} \frac{a_j^n}{\sigma_\epsilon} \qquad \text{(C.95)}$$

$$J_{9(j-1)+3}^{9(j-1)+11} = -\frac{\alpha_j^n}{32}(\rho_e^n T_e^n + \rho_e^{n-1} T_e^{n-1}) \sum u(\epsilon_{vj}^n + \epsilon_{vj-1}^n - \epsilon_{vj}^{n-1} - \epsilon_{vj-1}^{n-1})\frac{1}{T_j^{n2}}$$

$$- \frac{\Delta y^j}{64}(\rho_e^n T_e^n + \rho_e^{n-1} T_e^{n-1}) \sum v \sum a \frac{1}{T_j^{n2}}$$

$$- \frac{C_{\epsilon 1}}{128 Re_{\delta o}} \sum \epsilon_v \left(\sum h\right)^2 \Delta y^j \frac{\partial \mu_T byqsq_j^n}{\partial T_j^n}$$

$$+ \frac{C_{\epsilon 2}}{256}(\rho_e^n T_e^n + \rho_e^{n-1} T_e^{n-1}) \left(\sum \epsilon_v\right)^2$$

$$\times \left(-\sum f_2 byqsq \frac{1}{T_j^{n2}} + \frac{\partial f_2 byqsq_j^n}{\partial T_j^n} \sum \frac{1}{T_j^n}\right) \Delta y^j$$

$$- \frac{1}{Re_{\delta o}} \left[\left(\frac{\partial \mu_{Tj}^n}{\partial T_j^n} \frac{1}{\sigma_\epsilon} + \frac{d\mu_j^n}{dT_j^n}\right) a_j^n\right] \qquad \text{(C.96)}$$

$$J_{9(j-1)+3}^{9(j-2)+4} = \frac{1}{32}(\rho_e^n T_e^n + \rho_e^{n-1} T_e^{n-1}) \sum \frac{1}{T} \alpha_j^n(\epsilon_{vj}^n + \epsilon_{vj-1}^n - \epsilon_{vj}^{n-1} - \epsilon_{vj-1}^{n-1}) \quad \text{(C.97)}$$

$$J_{9(j-1)+3}^{9(j-2)+5} = \frac{1}{64}(\rho_e^n T_e^n + \rho_e^{n-1} T_e^{n-1})\Delta y^j \sum a \sum \frac{1}{T} \qquad \text{(C.98)}$$

$$J_{9(j-1)+3}^{9(j-2)+6} = -2\frac{C_{\epsilon 1}}{128 Re_{\delta o}} \sum \frac{\mu_T}{q^2} \sum \epsilon_v \Delta y^j \sum h \qquad \text{(C.99)}$$

$$J_{9(j-1)+3}^{9(j-2)+7} = \frac{1}{32}(\rho_e^n T_e^n + \rho_e^{n-1} T_e^{n-1}) \sum u \sum \frac{1}{T} \alpha_j^n$$

$$- \frac{C_{\epsilon 1}}{128 Re_{\delta o}} \left(\sum h \right)^2 \Delta y^j \left[\sum \frac{\mu_T}{q^2} + \sum \epsilon_v \left(\frac{\partial \mu_T byqsq_{j-1}^n}{\partial \epsilon_{vj-1}^n} \right) \right]$$

$$+ \frac{C_{\epsilon 2}}{256} \sum \frac{1}{T} \Delta y^j (\rho_e^n T_e^n + \rho_e^{n-1} T_e^{n-1})$$

$$\times \left[\left(\sum \epsilon_v \right)^2 \frac{\partial f_2 byqsq_{j-1}^n}{\partial \epsilon_{vj-1}^n} + 2 \sum f_2 byqsq \sum \epsilon_v \right]$$

$$- \frac{1}{Re_{\delta o}} \left[\frac{1}{\sigma_\epsilon} \frac{\partial \mu_{Tj-1}^n}{\partial \epsilon_{vj-1}^n} a_{j-1}^n \right] \tag{C.100}$$

$$J_{9(j-1)+3}^{9(j-2)+8} = \frac{\Delta y^j}{64} (\rho_e^n T_e^n + \rho_e^{n-1} T_e^{n-1}) \sum v \sum \frac{1}{T} + \frac{1}{Re_{\delta o}} \left[\frac{\mu_{Tj-1}^n}{\sigma_\epsilon} + \mu_{j-1}^n \right] \tag{C.101}$$

$$J_{9(j-1)+3}^{9(j-2)+9} = -\frac{C_{\epsilon 1}}{128 Re_{\delta o}} \frac{\partial \mu_T byqsq_{j-1}^n}{\partial q_{j-1}^n} \sum \epsilon_v \left(\sum h \right)^2 \Delta y^j$$

$$+ \frac{C_{\epsilon 2}}{256} (\rho_e^n T_e^n + \rho_e^{n-1} T_e^{n-1}) \frac{\partial f_2 byqsq_{j-1}^n}{\partial q_{j-1}^n} \left(\sum \epsilon_v \right)^2 \sum \frac{1}{T} \Delta y^j$$

$$+ \frac{1}{Re_{\delta o}} \frac{\partial \mu_{Tj-1}^n}{\partial q_{j-1}^n} \frac{a_{j-1}^n}{\sigma_\epsilon} \tag{C.102}$$

$$J_{9(j-1)+3}^{9(j-2)+11} = -\frac{\alpha_j^n}{32} (\rho_e^n T_e^n + \rho_e^{n-1} T_e^{n-1}) \sum u(\epsilon_{vj}^n + \epsilon_{vj-1}^n - \epsilon_{vj}^{n-1} - \epsilon_{vj-1}^{n-1}) \frac{1}{T_{j-1}^{n2}}$$

$$- \frac{\Delta y^j}{64} (\rho_e^n T_e^n + \rho_e^{n-1} T_e^{n-1}) \sum v \sum a \frac{1}{T_{j-1}^{n2}}$$

$$- \frac{C_{\epsilon 1}}{128 Re_{\delta o}} \sum \epsilon_v \left(\sum h \right)^2 \Delta y^j \frac{\partial \mu_T byqsq_{j-1}^n}{\partial T_{j-1}^n}$$

$$+ \frac{C_{\epsilon 2}}{256} (\rho_e^n T_e^n + \rho_e^{n-1} T_e^{n-1}) \left(\sum \epsilon_v \right)^2$$

$$\times \left(- \sum f_2 byqsq \frac{1}{T_{j-1}^{n2}} + \frac{\partial f_2 byqsq_{j-1}^n}{\partial T_{j-1}^n} \sum \frac{1}{T} \right) \Delta y^j$$

$$- \frac{1}{Re_{\delta o}} \left[\left(\frac{\partial \mu_{Tj-1}^n}{\partial T_{j-1}^n} \frac{1}{\sigma_\epsilon} + \frac{d\mu_{j-1}^n}{dT_{j-1}^n} \right) a_{j-1}^n \right] \tag{C.103}$$

- Jacobian for Definition of $\partial \epsilon_v / \partial y$

$$J_{9(j-1)+4}^{9(j-1)+7} = 1.0 \tag{C.104}$$

$$J_{9(j-1)+4}^{9(j-1)+8} = -\frac{\Delta y^j}{2} \tag{C.105}$$

$$J_{9(j-1)+4}^{9(j-2)+7} = -1.0 \tag{C.106}$$

$$J_{9(j-1)+4}^{9(j-2)+8} = -\frac{\Delta y^j}{2} \tag{C.107}$$

- Jacobian for Turbulence Kinetic Energy Equation

$$J^{9(j-1)+4}_{9(j-1)+5} = \frac{1}{64}(\rho_e^n T_e^n + \rho_e^{n-1} T_e^{n-1})\alpha_j^n \sum \frac{1}{T} \sum q(q_j^n + q_{j-1}^n - q_j^{n-1} + q_{j-1}^{n-1}) \quad \text{(C.108)}$$

$$J^{9(j-1)+5}_{9(j-1)+5} = \frac{1}{128}(\rho_e^n T_e^n + \rho_e^{n-1} T_e^{n-1})\Delta y^j \sum \frac{1}{T} \sum q \sum b \quad \text{(C.109)}$$

$$J^{9(j-1)+6}_{9(j-1)+5} = -\frac{1}{16 Re_{\delta o}}\Delta y^j \sum \mu_T \sum h \quad \text{(C.110)}$$

$$
\begin{aligned}
J^{9(j-1)+7}_{9(j-1)+5} &= \frac{1}{16}(\rho_e^n T_e^n + \rho_e^{n-1} T_e^{n-1})\Delta y^j \sum \frac{1}{T}\left(1 + \frac{C_k}{4}\sum(M_t^2)\right) \\
&- \frac{1}{Re_{\delta o}}\frac{\partial B_j^n}{\partial \epsilon_{vj}^n} - \frac{1}{32 Re_{\delta o}}\Delta y^j \left(\sum h\right)^2 \frac{\partial \mu_{Tj}^n}{\partial \epsilon_{vj}^n}
\end{aligned}
\quad \text{(C.111)}
$$

$$
\begin{aligned}
J^{9(j-1)+9}_{9(j-1)+5} &= \frac{1}{64}(\rho_e^n T_e^n + \rho_e^{n-1} T_e^{n-1})\alpha_j^n \sum u \sum \frac{1}{T} \\
&\times \left(\sum q + q_j^n + q_{j-1}^n - q_j^{n-1} + q_{j-1}^{n-1}\right) \\
&+ \frac{1}{128}(\rho_e^n T_e^n + \rho_e^{n-1} T_e^{n-1})\Delta y^j \sum v \sum \frac{1}{T} \sum b \\
&- \frac{1}{32 Re_{\delta o}}\Delta y^j \left(\sum h\right)^2 \frac{\partial \mu_{Tj}^n}{\partial q_j^n} - \frac{1}{Re_{\delta o}}\frac{\partial B_j^n}{\partial q_j^n} \\
&+ \frac{1}{16}(\rho_e^n T_e^n + \rho_e^{n-1} T_e^{n-1})\Delta y^j \sum \epsilon_v \sum \frac{1}{T}\frac{C_k}{4}\frac{\partial(M_t^2)|_j^n}{\partial q_j^n}
\end{aligned}
\quad \text{(C.112)}
$$

$$J^{9(j-1)+10}_{9(j-1)+5} = \frac{1}{128}(\rho_e^n T_e^n + \rho_e^{n-1} T_e^{n-1})\Delta y^j \sum v \sum \frac{1}{T} \sum q - \frac{1}{Re_{\delta o}}\frac{\partial B_j^n}{\partial b_j^n} \quad \text{(C.113)}$$

$$
\begin{aligned}
J^{9(j-1)+11}_{9(j-1)+5} &= -\frac{1}{64}(\rho_e^n T_e^n + \rho_e^{n-1} T_e^{n-1})\alpha_j^n \sum u \sum q \\
&\times (q_j^n + q_{j-1}^n - q_j^{n-1} + q_{j-1}^{n-1})\frac{1}{T_j^{n2}} \\
&- \frac{1}{128}(\rho_e^n T_e^n + \rho_e^{n-1} T_e^{n-1})\Delta y^j \sum v \sum q \sum b \frac{1}{T_j^{n2}} \\
&- \frac{1}{32 Re_{\delta o}}\Delta y^j \left(\sum h\right)^2 \frac{\partial \mu_{Tj}^n}{\partial T_j^n} - \frac{1}{Re_{\delta o}}\frac{\partial B_j^n}{\partial T_j^n} \\
&+ \frac{1}{16}(\rho_e^n T_e^n + \rho_e^{n-1} T_e^{n-1})\Delta y^j \sum \epsilon_v \\
&\times \left(-\frac{1}{T_j^{n2}} + \frac{C_k}{4}\sum \frac{1}{T_j^n}\frac{\partial(M_t^2)|_j^n}{\partial T_j^n} - \frac{C_k}{4}\sum M_t^2 \frac{1}{T_j^{n2}}\right)
\end{aligned}
\quad \text{(C.114)}
$$

$$J^{9(j-1)+12}_{9(j-1)+5} = -\frac{1}{Re_{\delta o}}\frac{\partial B_j^n}{\partial c_j^n} \quad \text{(C.115)}$$

$$J^{9(j-2)+4}_{9(j-1)+5} = \frac{1}{64}(\rho_e^n T_e^n + \rho_e^{n-1} T_e^{n-1})\alpha_j^n \sum \frac{1}{T} \sum q(q_j^n + q_{j-1}^n - q_j^{n-1} + q_{j-1}^{n-1}) \quad \text{(C.116)}$$

$$J_{9(j-1)+5}^{9(j-2)+5} = \frac{1}{128}(\rho_e^n T_e^n + \rho_e^{n-1} T_e^{n-1})\Delta y^j \sum \frac{1}{T} \sum q \sum b \qquad (C.117)$$

$$J_{9(j-1)+5}^{9(j-2)+6} = -\frac{1}{16 Re_{\delta o}}\Delta y^j \sum \mu_T \sum h \qquad (C.118)$$

$$
\begin{aligned}
J_{9(j-1)+5}^{9(j-2)+7} &= \frac{1}{16}(\rho_e^n T_e^n + \rho_e^{n-1} T_e^{n-1})\Delta y^j \sum \frac{1}{T}\left(1 + \frac{C_k}{4}\sum(M_t^2)\right) \\
&+ \frac{1}{Re_{\delta o}}\frac{\partial B_{j-1}^n}{\partial \epsilon_{vj-1}^n} - \frac{1}{32 Re_{\delta o}}\Delta y^j \left(\sum h\right)^2 \frac{\partial \mu_{Tj-1}^n}{\partial \epsilon_{vj-1}^n} \qquad (C.119)
\end{aligned}
$$

$$
\begin{aligned}
J_{9(j-1)+5}^{9(j-2)+9} &= \frac{1}{64}(\rho_e^n T_e^n + \rho_e^{n-1} T_e^{n-1})\alpha_j^n \sum u \\
&\times \sum \frac{1}{T}(\sum q + q_j^n + q_{j-1}^n - q_j^{n-1} + q_{j-1}^{n-1}) \\
&- \frac{1}{32 Re_{\delta o}}\Delta y^j \left(\sum h\right)^2 \frac{\partial \mu_{Tj-1}^n}{\partial q_{j-1}^n} + \frac{1}{Re_{\delta o}}\frac{\partial B_{j-1}^n}{\partial q_{j-1}^n} \\
&+ \frac{1}{16}(\rho_e^n T_e^n + \rho_e^{n-1} T_e^{n-1})\Delta y^j \sum \epsilon_v \sum \frac{1}{T}\frac{C_k}{4}\frac{\partial(M_t^2)|_{j-1}^n}{\partial q_{j-1}^n} \\
&+ \frac{1}{128}(\rho_e^n T_e^n + \rho_e^{n-1} T_e^{n-1})\Delta y^j \sum v \sum \frac{1}{T}\sum b \qquad (C.120)
\end{aligned}
$$

$$J_{9(j-1)+5}^{9(j-2)+10} = \frac{1}{128}(\rho_e^n T_e^n + \rho_e^{n-1} T_e^{n-1})\Delta y^j \sum v \sum \frac{1}{T}\sum q + \frac{1}{Re_{\delta o}}\frac{\partial B_{j-1}^n}{\partial b_{j-1}^n} \quad (C.121)$$

$$
\begin{aligned}
J_{9(j-1)+5}^{9(j-2)+11} &= -\frac{1}{64}(\rho_e^n T_e^n + \rho_e^{n-1} T_e^{n-1})\alpha_j^n \sum u \sum q \\
&\times (q_j^n + q_{j-1}^n - q_j^{n-1} + q_{j-1}^{n-1})\frac{1}{T_{j-1}^{n2}} \\
&- \frac{1}{128}(\rho_e^n T_e^n + \rho_e^{n-1} T_e^{n-1})\Delta y^j \sum v \sum q \sum b \frac{1}{T_{j-1}^{n2}} \\
&+ \frac{1}{16}(\rho_e^n T_e^n + \rho_e^{n-1} T_e^{n-1})\Delta y^j \sum \epsilon_v \\
&\times \left(-\frac{1}{T_{j-1}^{n2}} + \frac{C_k}{4}\sum \frac{1}{T_j^n}\frac{\partial(M_t^2)|_{j-1}^n}{\partial T_{j-1}^n} - \frac{C_k}{4}\sum M_t^2 \frac{1}{T_{j-1}^{n2}}\right) \\
&- \frac{1}{32 Re_{\delta o}}\Delta y^j \left(\sum h\right)^2 \frac{\partial \mu_{Tj-1}^n}{\partial T_{j-1}^n} + \frac{1}{Re_{\delta o}}\frac{\partial B_{j-1}^n}{\partial T_{j-1}^n} \qquad (C.122)
\end{aligned}
$$

$$J_{9(j-1)+5}^{9(j-2)+12} = \frac{1}{Re_{\delta o}}\frac{\partial B_{j-1}^n}{\partial c_{j-1}^n} \qquad (C.123)$$

- Jacobian for Definition of $\partial q/\partial y$

$$J_{9(j-1)+6}^{9(j-1)+9} = 1.0 \qquad (C.124)$$

$$J_{9(j-1)+6}^{9(j-1)+10} = -\frac{\Delta y^j}{2} \qquad (C.125)$$

$$J^{9(j-2)+9}_{9(j-1)+6} = -1.0 \qquad (C.126)$$

$$J^{9(j-2)+10}_{9(j-1)+6} = -\frac{\Delta y^j}{2} \qquad (C.127)$$

- Jacobian for Energy Equation

$$
\begin{aligned}
J^{9(j-1)+4}_{9(j-1)+7} &= \frac{(\rho_e^n T_e^n + \rho_e^{n-1} T_e^{n-1})}{32 M_\infty^2 (\gamma - 1)} \left(\alpha_j^n \sum \frac{1}{T}(T_j^n + T_{j-1}^n - T_j^{n-1} - T_{j-1}^{n-1}) \right) \\
&+ \frac{(\rho_e^n T_e^n + \rho_e^{n-1} T_e^{n-1})}{64} \sum q \sum \frac{1}{T} \alpha_j^n (q_j^n + q_{j-1}^n - q_j^{n-1} - q_{j-1}^{n-1}) \\
&+ \frac{\Delta y^j}{4}(\beta^n + \beta^{n-1}) \qquad (C.128)
\end{aligned}
$$

$$
\begin{aligned}
J^{9(j-1)+5}_{9(j-1)+7} &= \frac{(\rho_e^n T_e^n + \rho_e^{n-1} T_e^{n-1})}{64 M_\infty^2 (\gamma - 1)} \Delta y^j \sum \frac{1}{T} \sum c \\
&+ \frac{(\rho_e^n T_e^n + \rho_e^{n-1} T_e^{n-1})}{128} \sum q \sum \frac{1}{T} \Delta y^j \sum b \qquad (C.129)
\end{aligned}
$$

$$J^{9(j-1)+6}_{9(j-1)+7} = -\frac{\Delta y^j}{16 Re_{\delta o}} \left(\sum \mu_T + \sum \mu \right) \sum h \qquad (C.130)$$

$$
\begin{aligned}
J^{9(j-1)+7}_{9(j-1)+7} &= -\frac{1}{M_\infty^2 (\gamma - 1) Re_{\delta o}} \left(\frac{c_j^n}{Pr_t} \frac{\partial \mu_{Tj}^n}{\partial \epsilon_{vj}^n} \right) \\
&- \frac{1}{32 Re_{\delta o}} \Delta y^j \left(\sum h \right)^2 \frac{\partial \mu_{Tj}^n}{\partial \epsilon_{vj}^n} \qquad (C.131)
\end{aligned}
$$

$$
\begin{aligned}
J^{9(j-1)+9}_{9(j-1)+7} &= \frac{(\rho_e^n T_e^n + \rho_e^{n-1} T_e^{n-1})}{64} \sum \frac{1}{T}(\sum u(q_j^n + q_{j-1}^n - q_j^{n-1} - q_{j-1}^{n-1}) \\
&+ \frac{\Delta y^j}{2} \sum v \sum b + \alpha_j^n \sum q \sum u) \\
&- \frac{1}{M_\infty^2 Re_{\delta o}} \left[\frac{c_j^n}{Pr_t} \frac{\partial \mu_{Tj}^n}{\partial q_j^n} \right] - \frac{\Delta y^j}{32 Re_{\delta o}} \frac{\partial \mu_{Tj}^n}{\partial q_j^n} \left(\sum h \right)^2 \qquad (C.132)
\end{aligned}
$$

$$J^{9(j-1)+10}_{9(j-1)+7} = \frac{(\rho_e^n T_e^n + \rho_e^{n-1} T_e^{n-1}) \Delta y^j}{128} \sum q \sum \frac{1}{T} \sum v \qquad (C.133)$$

$$
\begin{aligned}
J^{9(j-1)+11}_{9(j-1)+7} &= \frac{(\rho_e^n T_e^n + \rho_e^{n-1} T_e^{n-1})}{32 M_\infty^2 (\gamma - 1)} \\
&\times \left[\sum u \alpha_j^n \left(\sum \frac{1}{T} - \frac{T_j^n + T_{j-1}^n - T_j^{n-1} - T_{j-1}^{n-1}}{T_j^{n2}} \right) - \frac{\Delta y^j}{2} \frac{\sum v \sum c}{T_j^{n2}} \right] \\
&- \frac{(\rho_e^n T_e^n + \rho_e^{n-1} T_e^{n-1})}{64} \frac{\sum q}{T_j^{n2}} \\
&\times \left[\sum u \alpha_j^n (q_j^n + q_{j-1}^n - q_j^{n-1} - q_{j-1}^{n-1}) + \frac{\Delta y^j}{2} \sum v \sum b \right]
\end{aligned}
$$

$$- \frac{1}{Re_{\delta o} M_\infty^2 (\gamma - 1)} \left(\frac{1}{Pr_t} \frac{\partial \mu_{Tj}^n}{\partial T_j^n} + \frac{1}{Pr} \frac{d\mu_j^n}{dT_j^n} \right) c_j^n$$

$$- \frac{\Delta y^j}{32 M_\infty^2 (\gamma - 1) Re_{\delta o}} \left(\frac{\partial \mu_{Tj}^n}{\partial T_j^n} + \frac{d\mu_j^n}{dT_j^n} \right) \left(\sum h \right)^2 \qquad \text{(C.134)}$$

$$J^{9(j-1)+12}_{9(j-1)+7} = \frac{(\rho_e^n T_e^n + \rho_e^{n-1} T_e^{n-1})}{64 M_\infty^2 (\gamma - 1)} \Delta y^j \sum v \sum \frac{1}{T}$$

$$- \frac{1}{Re_{\delta o} M_\infty^2 (\gamma - 1)} \left(\frac{\mu_{Tj}^n}{Pr_t} + \frac{\mu_j^n}{Pr} \right) \qquad \text{(C.135)}$$

$$J^{9(j-2)+4}_{9(j-1)+7} = \frac{(\rho_e^n T_e^n + \rho_e^{n-1} T_e^{n-1})}{32 M_\infty^2 (\gamma - 1)} \left(\alpha_j^n \sum \frac{1}{T} (T_j^n + T_{j-1}^n - T_j^{n-1} - T_{j-1}^{n-1}) \right)$$

$$+ \frac{(\rho_e^n T_e^n + \rho_e^{n-1} T_e^{n-1})}{64} \sum q \sum \frac{1}{T} \alpha_j^n (q_j^n + q_{j-1}^n - q_j^{n-1} - q_{j-1}^{n-1})$$

$$+ \frac{\Delta y^j}{4} (\beta^n + \beta^{n-1}) \qquad \text{(C.136)}$$

$$J^{9(j-2)+5}_{9(j-1)+7} = \frac{(\rho_e^n T_e^n + \rho_e^{n-1} T_e^{n-1})}{64 M_\infty^2 (\gamma - 1)} \Delta y^j \sum \frac{1}{T} \sum c$$

$$+ \frac{(\rho_e^n T_e^n + \rho_e^{n-1} T_e^{n-1})}{128} \sum q \sum \frac{1}{T} \Delta y^j \sum b \qquad \text{(C.137)}$$

$$J^{9(j-2)+6}_{9(j-1)+7} = -\frac{\Delta y^j}{16 Re_{\delta o}} \left(\sum \mu_T + \sum \mu \right) \sum h \qquad \text{(C.138)}$$

$$J^{9(j-2)+7}_{9(j-1)+7} = \frac{1}{M_\infty^2 (\gamma - 1) Re_{\delta o}} \left(\frac{c_{j-1}^n}{Pr_t} \frac{\partial \mu_{Tj-1}^n}{\partial \epsilon_{vj-1}^n} \right)$$

$$- \frac{1}{32 Re_{\delta o}} \Delta y^j \left(\sum h \right)^2 \frac{\partial \mu_{Tj-1}^n}{\partial \epsilon_{vj-1}^n} \qquad \text{(C.139)}$$

$$J^{9(j-2)+9}_{9(j-1)+7} = \frac{(\rho_e^n T_e^n + \rho_e^{n-1} T_e^{n-1})}{64} \sum \frac{1}{T} (\sum u (q_j^n + q_{j-1}^n - q_j^{n-1} - q_{j-1}^{n-1}))$$

$$+ \frac{\Delta y^j}{2} \sum v \sum b + \alpha_j^n \sum q \sum u)$$

$$+ \frac{1}{M_\infty^2 Re_{\delta o}} \left[\frac{c_{j-1}^n}{Pr_t} \frac{\partial \mu_{Tj-1}^n}{\partial q_{j-1}^n} \right] - \frac{\Delta y^j}{32 Re_{\delta o}} \frac{\partial \mu_{Tj-1}^n}{\partial q_{j-1}^n} \left(\sum h \right)^2 \qquad \text{(C.140)}$$

$$J^{9(j-2)+10}_{9(j-1)+7} = \frac{(\rho_e^n T_e^n + \rho_e^{n-1} T_e^{n-1}) \Delta y^j}{128} \sum q \sum \frac{1}{T} \sum v \qquad \text{(C.141)}$$

$$J^{9(j-2)+11}_{9(j-1)+7} = \frac{(\rho_e^n T_e^n + \rho_e^{n-1} T_e^{n-1})}{32 M_\infty^2 (\gamma - 1)}$$

$$\times \left[\sum u \alpha_j^n \left(\sum \frac{1}{T} - \frac{T_j^n + T_{j-1}^n - T_j^{n-1} - T_{j-1}^{n-1}}{T_{j-1}^{n2}} \right) - \frac{\Delta y^j}{2} \frac{\sum v \sum c}{T_{j-1}^{n2}} \right]$$

$$- \frac{(\rho_e^n T_e^n + \rho_e^{n-1} T_e^{n-1})}{64} \frac{\sum q}{T_{j-1}^{n2}}$$

$$\times \left[\sum u \alpha_j^n (q_j^n + q_{j-1}^n - q_j^{n-1} - q_{j-1}^{n-1}) + \frac{\Delta y^j}{2} \sum v \sum b \right]$$

$$- \frac{1}{Re_{\delta o} M_\infty^2 (\gamma - 1)} \left(\frac{1}{Pr_t} \frac{\partial \mu_{Tj-1}^n}{\partial T_{j-1}^n} + \frac{1}{Pr} \frac{d\mu_{j-1}^n}{dT_{j-1}^n} \right) c_{j-1}^n$$

$$- \frac{\Delta y^j}{32 M_\infty^2 (\gamma - 1) Re_{\delta o}} \left(\frac{\partial \mu_{Tj-1}^n}{\partial T_{j-1}^n} + \frac{d\mu_{j-1}^n}{dT_{j-1}^n} \right) \left(\sum h \right)^2 \qquad \text{(C.142)}$$

$$J_{9(j-1)+7}^{9(j-2)+12} = \frac{(\rho_e^n T_e^n + \rho_e^{n-1} T_e^{n-1})}{64 M_\infty^2 (\gamma - 1)} \Delta y^j \sum v \sum \frac{1}{T}$$

$$- \frac{1}{Re_{\delta o} M_\infty^2 (\gamma - 1)} \left(\frac{\mu_{Tj-1}^n}{Pr_t} + \frac{\mu_{j-1}^n}{Pr} \right) \qquad \text{(C.143)}$$

- Jacobian for Definition of $\partial T / \partial y$

$$J_{9(j-1)+8}^{9(j-1)+11} = 1.0 \qquad \text{(C.144)}$$

$$J_{9(j-1)+8}^{9(j-1)+12} = -\frac{\Delta y^j}{2} \qquad \text{(C.145)}$$

$$J_{9(j-1)+8}^{9(j-2)+11} = -1.0 \qquad \text{(C.146)}$$

$$J_{9(j-1)+8}^{9(j-2)+12} = -\frac{\Delta y^j}{2} \qquad \text{(C.147)}$$

C.2.4 Portion of the Jacobian Associated with the Boundary Conditions at the Edge of the Computational Domain

- Jacobian for Boundary Condition on u

$$J_{9jl}^{9jl-8} = 1.0 \qquad \text{(C.148)}$$

- Jacobian for Boundary Condition on ϵ

$$J_{9jl+1}^{9jl-5} = 1.0 - kgrad \qquad \text{(C.149)}$$

$$J_{9jl+1}^{9jl-4} = kgrad \qquad \text{(C.150)}$$

- Jacobian for Boundary Condition on q

$$J_{9jl+2}^{9jl-3} = 1.0 - kgrad \qquad \text{(C.151)}$$

$$J_{9jl+2}^{9jl-2} = kgrad \qquad \text{(C.152)}$$

- Jacobian for Boundary Condition on T

$$J_{9jl+2}^{9jl-1} = 1.0 \qquad\qquad (C.153)$$

Where $kgrad = 0$ indicates a dirichlet boundary condition and $kgrad = 1$ indicates a Neumann boundary condition for q and ϵ_v.

$$\vec{J} = \begin{bmatrix} B_1 & C_1 & & & & & \\ A_2 & B_2 & C_2 & & & & \\ \cdot & \cdot & \cdot & & & & \\ & \cdot & \cdot & \cdot & & & \\ & & A_j & B_j & C_j & & \\ & & \cdot & \cdot & \cdot & & \\ & & & \cdot & & \cdot & \\ & & & & A_{jl-1} & B_{jl-1} & C_{jl-1} \\ & & & & & B_{jl} & C_{jl} \end{bmatrix}$$

where

$$A_i = \begin{bmatrix} a_1^1 & a_1^2 & a_1^3 & a_1^4 & a_1^5 & a_1^6 & a_1^7 & a_1^8 & a_1^9 \\ a_2^1 & a_2^2 & a_2^3 & a_2^4 & a_2^5 & a_2^6 & a_2^7 & a_2^8 & a_2^9 \\ a_3^1 & a_3^2 & a_3^7 & a_3^3 & a_3^4 & a_3^6 & a_3^7 & a_3^8 & a_3^9 \\ a_4^1 & a_4^2 & a_4^3 & a_4^4 & a_4^5 & a_4^6 & a_4^7 & a_4^8 & a_4^9 \\ a_5^1 & a_5^2 & a_5^3 & a_5^4 & a_5^5 & a_5^6 & a_5^7 & a_5^8 & a_5^9 \\ a_6^1 & a_6^2 & a_6^3 & a_6^4 & a_6^5 & a_6^8 & a_6^7 & a_6^8 & a_6^9 \\ a_7^1 & a_7^2 & a_7^3 & a_7^4 & a_7^5 & a_7^6 & a_7^7 & a_7^8 & a_7^9 \\ a_8^1 & a_8^2 & a_8^3 & a_8^4 & a_8^5 & a_8^6 & a_8^7 & a_8^8 & a_8^9 \\ a_9^1 & a_9^2 & a_9^3 & a_9^4 & a_9^5 & a_9^6 & a_9^7 & a_9^8 & a_9^9 \end{bmatrix}$$

$$B_i = \begin{bmatrix} b_1^1 & b_1^2 & b_1^3 & b_1^4 & b_1^5 & b_1^6 & b_1^7 & b_1^8 & b_1^9 \\ b_2^1 & b_2^2 & b_2^3 & b_2^4 & b_2^5 & b_2^6 & b_2^7 & b_2^8 & b_2^9 \\ b_3^1 & b_3^2 & b_3^3 & b_3^4 & b_3^5 & b_3^6 & b_3^7 & b_3^8 & b_3^9 \\ b_4^1 & b_4^2 & b_4^3 & b_4^4 & b_4^5 & b_4^6 & b_4^7 & b_4^8 & b_4^9 \\ b_5^1 & b_5^2 & b_5^3 & b_5^4 & b_5^5 & b_5^6 & b_5^7 & b_5^8 & b_5^9 \\ b_6^1 & b_6^2 & b_6^3 & b_6^4 & b_6^5 & b_6^6 & b_6^7 & b_6^8 & b_6^9 \\ b_7^1 & b_7^2 & b_7^3 & b_7^4 & b_7^5 & b_7^6 & b_7^7 & b_7^8 & b_7^9 \\ b_8^1 & b_8^2 & b_8^3 & b_8^4 & b_8^5 & b_8^6 & b_8^7 & b_8^8 & b_8^9 \\ b_9^1 & b_9^2 & b_9^3 & b_9^4 & b_9^5 & b_9^6 & b_9^7 & b_9^8 & b_9^9 \end{bmatrix}$$

$$C_i = \begin{bmatrix} c_1^1 & c_1^2 & c_1^3 & c_1^4 & c_1^5 & c_1^6 & c_1^7 & c_1^8 & c_1^9 \\ c_2^1 & c_2^2 & c_2^3 & c_2^4 & c_2^5 & c_2^6 & c_2^7 & c_2^8 & c_2^9 \\ c_3^1 & c_3^2 & c_3^3 & c_3^4 & c_3^5 & c_3^6 & c_3^7 & c_3^8 & c_3^9 \\ c_4^1 & c_4^2 & c_4^3 & c_4^4 & c_4^5 & c_4^6 & c_4^7 & c_4^8 & c_4^9 \\ c_5^1 & c_5^2 & c_5^3 & c_5^4 & c_5^5 & c_5^6 & c_5^7 & c_5^8 & c_5^9 \\ c_6^1 & c_6^2 & c_6^3 & c_6^4 & c_6^5 & c_6^6 & c_6^7 & c_6^8 & c_6^9 \\ c_7^1 & c_7^2 & c_7^3 & c_7^4 & c_7^5 & c_7^6 & c_7^7 & c_7^8 & c_7^9 \\ c_8^1 & c_8^2 & c_8^3 & c_8^4 & c_8^5 & c_8^6 & c_8^7 & c_8^8 & c_8^9 \\ c_9^1 & c_9^2 & c_9^3 & c_9^4 & c_9^5 & c_9^6 & c_9^7 & c_9^8 & c_9^9 \end{bmatrix}$$

Figure C.1: Form of the Resulting Jacobian

Appendix D

Convergence Criteritia

D.1 Convergence Criteria

The convergence criteria for Newton's method employed is to test if the average of the absolute value of the relative change of each of the independent variables is less than some specified tolerance. If this tolerance is met for each of the independent variables, then convergence is assumed and the iterating at that spatial location stops. Table D.1 gives the tolerances typically employed. The algorithm used to test for convergence

Variable	Lowest Value for Test	Tolerance
u_{tau}	1×10^{-6}	1×10^{-5}
T_{wall}	1×10^{-6}	1×10^{-5}
Q_{wall}	1×10^{-6}	1×10^{-5}
u	1×10^{-6}	1×10^{-5}
v	1×10^{-6}	1×10^{-5}
h	1×10^{-6}	1×10^{-5}
ϵ_v	1×10^{-9}	1×10^{-6}
a	1×10^{-9}	1×10^{-6}
q	1×10^{-9}	1×10^{-6}
b	1×10^{-9}	1×10^{-6}
T	1×10^{-6}	1×10^{-5}
c	1×10^{-6}	1×10^{-5}

Table D.1: Tolerances Employed in Iterating by Newton's Method

of the solution at each iteration works by summing the absolute value of the relative change of each indepedent variable at each grid location. The sum of the relative change at iteration i is defined by equation D.1

$$\vec{\sigma}^i = \sum_{j=1}^{jl} \left| \frac{\delta \vec{w}^i}{\vec{w}^i} \right| \tag{D.1}$$

The relative change at each grid location is only added if the absolute value of the variable at that grid location is above sum specified "Test" value. This is to prevent the code from computing the relative change when the value of the independent variable is zero. For cases in which the heat transfer at the wall is adiabatic the code tests for only the absolute value of the change in Q_{wall} and compares this value to the tolerance. Once the sum of the relative changes of each of the independent variables is known, an average value is found by dividing the sum of each independent variable by the number of grid locations in which the calculation of the relative change is made. This yields the average relative change of each of the indpendent variables. When this value is less than the tolerance the solution is said to be converged. A decrease in the tolerances by a factor of ten is seen to have a very minimal effect on the solution, such that the solution obtained by the specified tolerances in Table D.1 may be assumed to be the converged solution.

In a typical calculation it is the variables a,b,c and h which take the highest number of iterations to converge. These variables correspond to the derivatives with respect to y of ϵ_v, q, T and u. A typical converged solution results in the tolerance of the primary variables u,v,ϵ_v,q and T being of the order 10^{-8} for the criteria given in Table D.1.

Appendix E

Favre Averaged vs. Conventional Averaged Reynolds Shear Stress

In compressible flow fields the Reynolds shear stress is given by

$$\tau_{xy}^{turb} = -\overline{\rho u'' v''} \tag{E.1}$$

where u'' and v'' are the mass averaged fluctuations in the velocity as described in Chapter 2, ρ is the instantaneous density and $^-$ signifies Reynolds averaging. In conventional Reynolds averaged notation the compressible Reynolds shear stress is given by

$$\tau_{xy}^{turb} = - \left(\bar{\rho} \overline{u' v'} + \overline{\rho' u' v'} - \frac{\overline{(\rho' u')}\overline{(\rho' v')}}{\bar{\rho}} \right) \tag{E.2}$$

where u', v', and ρ' are the fluctuating components of the instantaneous velocity and density, such that $\overline{u'} = 0$.

Equations E.1 and E.2 are equivalent. However, in the experimental measurement of compressible flow fields it is the fluctuating mass flux, $\rho' u_i'$, which is measured with either single or crossed wire anemomenters [11]. Using these measurements and the "strong Reynolds analogy" the parameter $\bar{\rho} \overline{u' v'}$ may be calculated. This is the experimental shear stress given by Fernando *et al* for the calculation of a supersonic, turbulent boundary layer in an adverse pressure gradient [10], [11], [43] which is compared to the present model. It may be shown that the shear stress given by Fernando *et al* is fundamentally equivalent to the shear stress calculated by the present model.

The Fernando *et al* experimental data is for a $M_\infty = 2.92$ adiabatic boundary layer experiencing a mild pressure gradient. Since the flow is adiabatic the stagnation temperature may be assumed to be constant throughout the boundary layer. The data of Fernando shows this to be true across the boundary layer within 4% with the

experimental uncertainty being $\pm 1\%$. The definition of total temperature is given by

$$T_0 \equiv T + \frac{1}{2C_p}(u^2 + v^2 + w^2) \qquad \text{(E.3)}$$

where T_0 is the dimensional stagnation temperature, T is the dimensional static temperature, C_p is the coefficient of specific heat at constant pressure and $u,v,$ and w are the dimensional, instaneous, local components of the velocity. Using Reynolds averaging, equation E.3 may be rewritten in the form

$$\bar{T}_0 + T_0' = \bar{T} + T' + \frac{1}{2C_p}(\bar{u}\bar{u} + 2\bar{u}u' + u'u' + \bar{v}\bar{v} + 2\bar{v}v' + v'v' + \bar{w}\bar{w} + 2\bar{w}w' + w'w') \qquad \text{(E.4)}$$

In a two dimensional boundary layer $\bar{w} = 0$, $\bar{u} >> \bar{v}$, and, except for very close to the wall, $u' \sim v'$. If the stagnation temperature is constant then its time fluctuating component must be equal to 0, and the stagnation temperature must be independent of the turbulent (time dependent) variables. Since the fluctuating component of the velocity is typically at least an order of magnitude less than the the mean component the second order turbulent parameters are signifigantly less than the first order parameters. The data of Fernando et al shows $u'/\bar{u} < .15$. Therefore, grouping first order turbulent terms and using the above approximations for the relative contribution yields

$$T' \approx -\frac{1}{C_p}\bar{u}u' \qquad \text{(E.5)}$$

According to Bradshaw [1] in a non-hypersonic boundary layer ($M_e < 5.0$) Morkovin's hypothesis shows that the acoustic mode of turbulence is negligible

$$p'/\bar{p} << 1 \qquad \text{(E.6)}$$

Therefore from the equation of state

$$p = \rho R T \qquad \text{(E.7)}$$

$$\bar{p} + p' = (\bar{\rho} + \rho')R(\bar{T} + T') \qquad \text{(E.8)}$$

and similar arguements as proposed above for the stagnation temperature it may be shown that

$$\rho' \approx -\bar{\rho}\frac{T'}{\bar{T}} \qquad \text{(E.9)}$$

The purpose of arguing equations E.5 and E.9 is to show that the triple density velocity correlation of the conventional Reynolds averaged shear stress is signifigantly less than mean density, double velocity correlation. Using the approximations given by equations E.5 and E.9 and the fact that $u' \sim v'$ it may be assumed that

$$\overline{\rho'u'v'} \approx \frac{\bar{\rho}\bar{u}}{C_p\bar{T}}\overline{u'^3} \tag{E.10}$$

and

$$\bar{\rho}\overline{u'v'} \approx \bar{\rho}\overline{u'^2} \tag{E.11}$$

The ratio of equation E.10 to E.11 is

$$\frac{\overline{\rho'u'v'}}{\bar{\rho}\overline{u'v'}} \approx (\gamma - 1)M^2\sqrt{\frac{\overline{u'^2}}{\bar{u}^2}} \tag{E.12}$$

where M is the local Mach number. According to the experimental data of Fernando *et al* the quantity $(\gamma - 1)M^2\sqrt{\frac{\overline{u'^2}}{\bar{u}^2}}$ is less than 0.1 everywhere.

Similar arguments may be used for comparing the third and second terms of equation E.2. The second term may be approximated by equation E.10, and the third term may be approximated by

$$\frac{(\overline{\rho'u'})(\overline{\rho'v'})}{\bar{\rho}} \approx \left(\frac{\bar{u}}{C_p\bar{T}}\right)^2\overline{u'^2} \tag{E.13}$$

The ratio of equation E.10 to E.13 is

$$\frac{\overline{\rho'u'v'}}{\frac{(\overline{\rho'u'})(\overline{\rho'v'})}{\bar{\rho}}} \approx (\gamma - 1)M^2\sqrt{\frac{\overline{u'^2}}{\bar{u}^2}} \tag{E.14}$$

Therefore the third term of equation E.2 is less than 10% of the second term and less than 1% of the first term.

According to Fernando *et al* [10] there is a very signifigant, -5% to $+30\%$, uncertainty associated with measuring the kinemtaic Reynolds shear stress, $\overline{u'v'}$. Therefore the maximum uncertainty of 10% introduced in ignoring the additional contribution to the Reynolds shear stress by the triple velocity correlation falls within the experimental uncertainty and is justified.

Appendix F

Low Reynolds Number $k - \epsilon$ Two Equation Compressible Turbulence Code

A copy of the utilized $k - \epsilon$ code and tabulated function f_μ may be obtained from Professor Doyle D. Knight at

Address:

Professor Doyle D. Knight

Rutgers University

Department of Mechanical and Aerospace Eningeering

P.O. Box 909

Piscataway, NJ 08855-0909

Phone Number:

(908) 445-4464

email address:

knight@jove.rutgers.edu

References

[1] Bradshaw, P. (1977) "Compressible Turbulent Shear Layers," *Annual Review of Fluid Mechanics,* Vol. 9, pp. 33-54.

[2] Bradshaw, P. and Unsworth, K. (1974) "Comment on 'Evaluation of Preston Tube Calibration Equations in Supersonic Flow,"' *AIAA Journal,* Vol. 15, No. 12., pp. 1293-1295.

[3] Carvin, C., Devieve, J.F. and Smits, A.J. (1988) "The Near Wall Temperature Profile of Turbulent Boundary Layers," *AIAA Paper 88-0136.*

[4] Cebeci, T. and Smith, A.M.0. (1974) <u>Analysis of Turbulent Boundary Layers</u>, Academic Press, New York.

[5] Chien, K.Y. (1982) "Prediction of Channel and Boundary Layer Flows with a Low Reynolds Number Turbulence Model," *AIAA Journal,* Vol. 20, No. 1, pp. 33-38.

[6] Coles, D. (1968) "The Young Persons Guide to the Data," a Survey Lecture Prepared for the 1968 AFOSR-IFP-Stanford Conference on Computation of Turbulent Boundary Layers, The Rand Corporation.

[7] Comte-Bellot G., and Corrsin, S. (1971) "Simple Eulerian Time Correlation of Full- and Narrow- Band Velocity Signals in Grid-Generated 'Isotropic' Turbulence," *Journal of Fluids Mechanics,* Vol. 48, pp. 273-337.

[8] Dailey, L. D., and Jennions, I. K. (1994) "Simulating Laminar-Turbulent Transition with a Low Reynolds Number $k - \epsilon$ Turbulence Model in a Navier-Stokes Flow Solver," *AIAA Paper 94-0189.*

[9] Dutoya, D., and Michard, P. (1981) "A Program for Calculating Boundary Layers along Compressor and Turbine Blades," <u>Numerical Methods in Heat Transfer</u>, edited by R. Lewis, K. Morgan and O. Zienkiewicz, John Wiley and Sons, New York.

[10] Fernando, E. M., and Smits, A.J. (1990) "A Supersonic Turbulent Boundary Layer in an Adverse Pressure Gradient," *Journal of Fluid Mechanics,* Vol. 211, pp. 285-307.

[11] Fernando, E. M., (1988) "Supersonic Turbulent Boundary Layer in an Adverse Pressure Gradient," Ph.D. Thesis, Mechanical and Aerospace Engineering Department, Princeton University.

[12] Garrison, T.J., Settles, G.S., Narayanswami, N. and Knight, D. D. (1993) "Structure of Crossing-Shock-Wave/Turbulent-Boundary-Layer Interactions," *AIAA Journal,* Vol. 31, No. 12, pp. 2204-2211.

[13] Hassid, S. and Poreh, M. (1978) "A Turbulent Energy Dissipation Model for Flows with Drag Reduction," *Journal of Fluids Engineering*, Vol. 100, pp. 107-112.

[14] Hayes, W.D. , Probstein, R.F. (1959) Hypersonic Flow Theory, Academic Press, New York.

[15] Hoffman, G. (1975) "Improved Form of the Low Reynolds Number $k - \epsilon$ Turbulence Model," *Physics of Fluids*, Vol. 18, pp. 309-312.

[16] Hopkins, E. J., and Inouye M. (1971) "An Evaluation of Theories for Predicting Turbulent Skin Friction and Heat Transfer on Flat Plates at Supersonic and Hypersonic Mach Numbers," *AIAA Journal*, Vol. 9, No. 6, pp. 993-1003.

[17] Huang, P.G., Bradshaw, P. and Coakley, T.J. (1994) "Turbulence Models for Compressible Boundary Layers," *AIAA Journal*, Vol. 32, No. 4, pp. 735-740.

[18] Jaluria, Y. (1988) Computer Methods for Engineering, Allyn and Bacon, Inc., Boston.

[19] Jayaram, M., Taylor, M.W., and Smits, A.J. (1987) "The Response of a Compressible Turbulent Boundary Layer to Short Regions of Concave Surface Curvature," *Journal of Fluid Mechanics*, Vol. 175, pp. 343-362.

[20] Jones, W.P. and Launder, B.E. (1972) "The Prediction of Laminarization with a Two-Equation Model of Turbulence," *International Journal of Heat and Mass Transfer*, Vol. 15, pp. 301-314.

[21] Jones, W.P. and Launder, B.E. (1973) "The Calculation of Low-Reynolds-Number Phenomena with a Two-Equation Model of Turbulence," *International Journal of Heat and Mass Transfer,*, Vol. 16, pp. 1119-1130.

[22] Keller, H.B. (1970) "A New Difference Scheme for Parabolic Problems," Numerical Solutions of Parital Differential Equations, Vol. II, B. Hubbard, Ed., Academic Press, New York.

[23] Keller, H.B., and Cebeci, T., (1971) "Accurate Numerical Methods for Boundary Layer Flows - I. Two Dimensional Laminar Flows," *Lecture Notes in Physics, Vol. 8, Proceedings of the Second International Conference on Numerical Methods in Fluid Dynamics*, Springer-Verlag, New York.

[24] Keller, H. B. and Cebeci, T. (1972) "Accurate Numerical Methods for Boundary-Layer Flows - II. Two Dimensional Turbulent Flows," *AIAA Journal*, Vol. 13 , No. 10, pp. 1193.

[25] Knight, D. D. (1992) "Development of a Two-Equation Turbulence Model for Hypersonic Flows," Proposal to NASA, March.

[26] Knight, D. D. (1993) "On the Decay of Isotropic Turbulence - Reynolds Stress Equation Model,", Internal Report No. 4, Department of Mechanical and Aerospace Engineering, Rutgers University.

[27] Knight, D. D. (1993) "Notes on Finding the Low Reynolds Number Corrections to the $k - \epsilon$ Turbulence Model," Unpublished Work, Department of Mechanical and Aerospace Engineering, Rutgers University.

[28] Knight, D. D. (1993) "Compressible Wall Layer for $k - \epsilon$ Model," Tech. Rep. Internal Report B-4, Dept of Mech and Aero Engr, Rutgers University, June.

[29] Knight, D. D., Horstman, C. C., Shapey, B. and Bogdonoff, S. (1987) "Structure of Supersonic Turbulent Flow Past a Sharp Fin," *AIAA Journal*, Vol. 25, No. 10, pp. 1331 - 1337.

[30] Knight, D. D., Garrison, T.J., Settles, G.S., Zheltovodov, A.A., Maksimov, A.I., Shevchenko, A.M. and Vorontsov, S.S. (1995) "Asymmetric Crossing Shock Wave Turbulent Boundary Layer Interaction," *AIAA Paper 95-0231*, January

[31] Knight, D.D., and Becht, R. (1992) "Boundary Layer Program," Private Communication, August.

[32] Ladd, J. A., and Kral, L. D. (1992) "Development and Application of a Zonal $k - \epsilon$ Turbulence Model for Complex 3-D Flowfields," *AIAA Paper 92-3176*.

[33] Lam, C. and Bremhorst, K. (1981) "Modified Form of the $k-\epsilon$ Model for Predicting Wall Turbulence," *Journal of Fluids Engineering*, Vol. 103, pp. 456-460.

[34] Launder, B. and Sharma, B. (1974) "Application of the Energy Dissipation Model of Turbulence to the Calculation of Flow Near a Spinning Disk," *Letters in Heat and Mass Transfer*, Vol. 1, pp 131-138.

[35] Launder, B. and Spalding, D. (1974) "The Numerical Computation of Turbulent Flow," *Computer Methods in Applied Mechanics and Engineering*, Vol. 3, pp. 269-289.

[36] Moler, C. (1978) "Linpack, Version 8/14/78", University of New Mexico, Argonne National Laboratory.

[37] Morkovin, M. V. (1962) "Effects of Compressibility on Turbulent Flow," The Mechanics of Turbulence, A. Favre, Ed., Gordon and Breach, p. 367.

[38] Myong, H. and Kasagi, N. (1990) "A New Approach to the Improvement of the $k-\epsilon$ Turbulence Model for Wall-Bounded Shear Flows," *JSME International Journal*, Vol. 33, pp. 63-72.

[39] Patel, V.C., Wolfgang, R., and Scheuerer, G. (1985) "Turbulence Models for Near-Wall and Low Reynolds Number Flows: A Review," *AIAA Journal*, Vol. 23, No. 9, pp. 1308-1319.

[40] Reynolds, W.C. (1976) "Computation of Turbulent Flows," *Annual Review of Fluid Mechanics*, Vol. 8, pp. 183-208.

[41] Sarkar, S., Erlebacher, G., Hussaini, M., and Kreis, H. (1991) "The Analysis and Modelling of Dilatational Terms in Compressible Turbulence," *Journal of Fluid Mechanics*, Vol. 227, pp. 473-493.

[42] Schlichting H. (1979) Boundary-Layer Theory, 7th Edition, McGraw-Hill, Inc., New York, New York.

[43] Settles, G., and Dodson, L. (1992) "Hypersonic Turbulent Boundary-Layer and Free Shear Layer Database," Gas Dynamics Laboratory, Department of Mechanical Engineering, Penn State University, December, Ref. 10., pp. 53-63.

[44] So, R. M. C., Zhang, H. S., and Speziale, C. G. (1991) "Near-Wall Modeling of the Dissipative Rate Equation," *AIAA Journal*, Vol. 29, No. 12., pp. 2069-2076.

[45] Sommer, T.P., So, R.M.C., and Zhang, H.S. (1993) "On the Assumption of Vanishing Temperature Fluctuations at the Wall for Heat Transfer Modeling," *AIAA Paper 93-0088*.

[46] Spalart, P. (1988) "Direct Simulation of a Turbulent Boundary Layer up to $Re_\theta = 1410$", *Journal of Fluid Mechanics*, Vol. 187, pp. 61-98.

[47] Speziale, C. G., Abid, R., and Anderson, E. C. (1990) "A Critical Evaluation of Two-Equation Models for Near Wall Turbulence," *AIAA Paper 90-1481*.

[48] Speziale, C. G., Abid, R., and Anderson, E. C. (1992) "Critical Evaluation of Two-Equation Models for Near-Wall Turbulence," *AIAA Journal*, Vol. 30, No. 2., pp. 324-331.

[49] Shih, T. H. and Hsu, A. T. (1991) "An Improved $k - \epsilon$ Model for Near-Wall Turbulence," *AIAA Paper 91-611*, Renvo, NV.

[50] Taylor, M.W. (1984) "A Supersonic Turbulent Boundary Layer on concavely Curved Surfaces," Princeton University, Mechanical and Aerospace Engineering Dept., Report MAE-1684.

[51] Tennekes, H. and Lumley, J.L. (1972) A First Course in Turbulence, The MIT Press, Cambridge Massachusetts.

[52] Weighardt, K. and Tillman, W. (1951) "On the Turbulent Friction Layer for Rising Pressure," Tech. Rep. TM 1314, NACA.

[53] White, F.M. (1974) Viscous Fluid Flow, McGraw-Hill, Inc., New York.

[54] Wilcox, D. (1993) Turbulence Modeling for CFD, DCW Industries, Inc., La Canada, CA.

[55] Yang, Z. and Shih, T.H. (1993) "A Galilean and Tensorial Invariant $k - \epsilon$ Model for Near Wall Turbulence," *AIAA Paper 93-3105*.

[56] Zeman, O. (1990) "Dilatational Dissipation: The Concept and Application in Modeling Compressible Mixing Layers," *Physics of Fluids A.*, pp. 178-188.

[57] Zhang, H.S., So, R.M.C., Speziale, C.G. and Lai,Y.G. (1992) "A Near-Wall Two-Equation Model for Compressible Turbulent Flows," *AIAA Paper 92-0442*.

[58] Zheltovodov, A.A., Trofimov, V.M., Shilein, E.H., and Yakovlev, V.N., (1990) "An Experimental Documentation of Supersonic Turbulent Flows in the Vicinity of Forward and Backward Facing Ramps," Inst. of Theoretical and Applied Mechanics Report 2013, Siberian Division, USSR Academy of Sciences, April.